Arch. Rational Mech. Anal. 130 (1995) 25–101 © Springer-Verlag 1995

N-Pulse Homoclinic Orbits in Perturbations of Resonant Hamiltonian Systems

G. HALLER & S. WIGGINS

Communicated by P. HOLMES

Abstract

In this paper we develop an analytical method to detect orbits doubly asymptotic to slow manifolds in perturbations of integrable, two-degree-of-freedom resonant Hamiltonian systems. Our *energy-phase method* applies to both Hamiltonian and dissipative perturbations and reveals families of multi-pulse solutions which are not amenable to Melnikov-type methods. As an example, we study a two-mode approximation of the nonlinear, nonplanar oscillations of a parametrically forced inextensional beam. In this problem we find unusually complicated mechanisms for chaotic motions and verify their existence numerically.

Contents

1. Introduction

1.1. Motivation

Hamiltonian systems with slow variables arise in many problems of physics and engineering. In most cases the slow evolution of a particular variable in these systems is a consequence of one of the two phenomena: near-integrability or near-resonance.

In the case of near-integrability the Hamiltonian system is close to another one which admits nontrivial invariants besides the underlying Hamiltonian itself. Using these invariants as new coordinates, one finds their time variation slow in the near-integrable system. In the case of near-resonance, some of the variables in the system are necessarily angular variables. We usually speak about a resonance in such a system when the corresponding angular frequencies admit a nontrivial integer combination which vanishes on some domain of the phase space. As is well known (see, e.g., ARNOLD, KOZLOV, & NEISHTADT [4]), in such cases one can apply a symplectic change of variables which transforms the resonant combination of the phase variables into a new phase variable. As a result, this new phase is slowly varying in a neighborhood of the resonant domain.

Thus one can expect to find several slow variables in near-integrable systems when the equations are localized near a resonant domain of the phase space. Frequently, these domains contain invariant manifolds of solutions, which therefore all have slow evolution in some but not all coordinate directions. We refer to such structures as *partially slow manifolds.* The presence of two different time scales makes the study of these localized problems quite subtle, and in most cases singular perturbation techniques are needed to analyze the partially slow manifolds.

The most interesting and important partially slow manifolds are hyperbolic. These structures are distinguished since they admit global stable and unstable manifolds which "transmit" the singular nature of the manifolds to other parts of the phase space. Well-known examples of hyperbolic partially slow manifolds are the manifolds containing lower-dimensional hyperbolic tori (or *whiskered tori*) created in the destruction of resonant KAM tori in nearly integrable Hamiltonian systems (see e.g., ARNOLD [3] and TRESHCHEV [44]). A general global perturbation theory for such structures does not currently exist; the lack of such a theory is the main obstacle in studying the details of diffusion and transport near resonances in multi-degree-of-freedom Hamiltonian systems.

The goal of this paper is to make one step towards the understanding of hyperbolic partially slow invariant structures in Hamiltonian systems and their dissipative perturbations. We address the simplest possible case, in which the Hamiltonian admits one slowly varying action variable (as a consequence of near-integrability), and, in certain domains of the phase space, one slowly varying angle variable (as a consequence of near resonance). Because of the presence of a single angle, such problems, in fact, admit a *slow manifold* instead of a partially slow one. As mentioned above, we are particularly interested in hyperbolic slow manifolds, which require at least two more coordinate directions transversal to the slow manifold in the integrable Hamiltonian limit. Hence, the simplest possible case is that of a near-integrable, two-degree-of-freedom Hamiltonian system with a slow, hyperbolic 2-manifold of solutions.

1.2. The main example: oscillations of a parametrically forced beam

Although the analysis of this paper is a first step in the development of a general theory for hyperbolic partially slow manifolds, it highlights many of the issues arising in higher dimensions. Most remarkably, even the two-degree-of-freedom case treated here has many immediate applications to resonance problems arising in engineering and physics. In particular, our main example is related to the nonplanar, nonlinear dynamics of a vertical, elastic beam fixed to a horizontal base which oscillates sinusoidally. This problem was first studied by NAYFEH & PAI [38], who argued that for typical motions of the beam, most modes die out under the effect of internal damping. The surviving modes are exactly those with natural frequencies in strong resonance with the frequency of the parametric forcing. Under this assumption the method of multiple scales combined with Galerkin's method yields a set of two complex amplitude equations, which approximate slow frequency and phase modulations on the normal modes of the linearized problem. A fixed point of this system therefore represents a nonlinear normal mode, a periodic solution represents a quasiperiodic oscillation, etc. Recently FENG & LEAL [11] showed that these equations can be simplified due to the presence of a symmetry. In the case of a beam with a uniform square cross section, for small excitations, and for excitation frequencies approximately twice the first natural frequency of the lateral vibrations of the beam, the mode equations can be transformed to the form

$$\begin{aligned}
\dot{x}_1 &= 2(2I-b)x_2 - 2x_1^2x_2 - 4x_2^3 - \varepsilon[\Gamma(2x_2\cos 2\phi - x_1\sin 2\phi) + dx_1],\\
\dot{x}_2 &= 2x_1(b+x_2^2) - \varepsilon[\Gamma x_2 \sin 2\phi + dx_2],\\
\dot{I} &= \varepsilon[2\Gamma((I-x_2^2)\sin 2\phi - x_1x_2\cos 2\phi) - 2dI],\\
\dot{\phi} &= b + s - 2\delta I + 2x_2^2 + \varepsilon\Gamma\cos 2\phi.
\end{aligned} \tag{1.1}$$

To obtain this system, we used a change of variables from FENG & SETHNA [14], where similar mode equations for parametrically excited thin plates were studied. In (1.1) the parameters b and s are related to detunings from the exact internal 1:1 resonance arising from the nearly square cross section, and from the exact external

1:2 resonance between the two principal lateral models and the excitation (see FENG & LEAL [11] for details). The structural constant $\delta = 4.8118$ can be computed from the numerical values listed in NAYFEH & PAI [38] (for the case of $n = 1, m = 1$ in their notation). The internal viscous damping coefficient $d > 0$ and the forcing amplitude Γ appear in the perturbation terms multiplied by a small parameter $\varepsilon \geqq 0$ (for comparison with FENG & LEAL [15], we have $\varepsilon\Gamma = 2\alpha_7 g\omega_{2n}^2$, $\varepsilon d = 2\mu\omega_{2n}$). All parameters are nondimensionalized. For $\varepsilon = 0$ and $x_1 = x_2 = 0$ the action-angle-type variables, I and ϕ, describe amplitude and phase-modulated quasiperiodic oscillations of the tip of the unforced, undamped beam in the plane of one of the two first normal modes. Roughly speaking, the x_1 and x_2 variables measure position and momentum deviations, respectively, from these purely one-mode motions. Note that for $\varepsilon = 0$ system (1.1) is integrable.

Our motivation to consider the case of this internal-external 1:1:2 resonance is that the numerical study of NAYFEH & PAI [38] showed an apparently continuous Fourier spectrum for this resonance, while the spectrum remained characteristically discrete for other resonances they considered. We use the theory developed in the forthcoming sections to rigorously prove the existence of chaotic dynamics in this two-mode model, which we believe to be a good approximation of the actual motion of the beam. We focus on the fate of the family of nonlinear normal modes $x_1 = x_2 = 0, I = (b + s)/2\delta, \phi = \text{const}$, which form a circle of equilibria for system (1.1). As a result of near-resonance ($\dot{\phi} \approx 0$ near the circle) and near-integrability ($\varepsilon \ll 1$), our model system possesses a "thin" slow manifold created in the break-up of the circle of equilibria. This manifold contains motions with slow phase and amplitude modulations and will be shown to have a prominent role in creating chaotic dynamics near some surviving nonlinear normal modes.

1.3. General formulation

In addition to the above example, the theory developed in this paper applies to a number of other problems, such as the study of parametrically excited plates and shells, surface waves, and shallow arches (see HOLMES [27], FENG & SETHNA [12–14], FENG & WIGGINS [15], YANG & SETHNA [47], and TIEN & NAMACHCHIVAYA [42]), a model of the driven nonlinear Schrödinger equation (BISHOP, FOREST, MCLAUGHLIN, & OVERMAN [5]), the analysis of magnetic spin waves (CASCON & KOILLER [7]), and a wide class of three-degree-of-freedom Hamiltonian resonances (HALLER & WIGGINS [23]). All these problems can be transformed to the same "normal form" which can be written succinctly as

$$\begin{aligned}
\dot{x} &= JD_x H_0(x, I) + \varepsilon[JD_x H_1(x, I, \phi; \varepsilon) + g_x(x, I, \phi; \varepsilon)], \\
\dot{I} &= \varepsilon[-D_\phi H_1(x, I, \phi; \varepsilon) + g_I(x, I, \phi; \varepsilon)], \\
\dot{\phi} &= D_I H_0(x, I) + \varepsilon[D_I H_1(x, I, \phi; \varepsilon) + g_\phi(x, I, \phi; \varepsilon)],
\end{aligned} \tag{1.2}$$

with $(x, I, \phi) \in \mathscr{P} \subset \mathbb{R}^2 \times \mathbb{R} \times S^1$ and

$$J = \begin{pmatrix} 0 & 1 \\ -1 & 0 \end{pmatrix}.$$

The unperturbed system $(1.2)_{\varepsilon=0}$ derives from the Hamiltonian H_0, and the perturbaton also has a Hamiltonian part deriving from εH_1, which is 2π-periodic in the variable ϕ. The corresponding perturbation terms usually describe forcing, while other dissipative terms are listed in g_x, g_I and g_ϕ, which are all 2π-periodic in ϕ. The Hamiltonians H_0 and H_1 are C^{r+1} functions, and g_x, g_I and g_ϕ are C^r functions with $r \geqq 3$. The Hamiltonian part of the vector field is defined on the symplectic manifold $(\mathscr{P}, \omega)$ with the symplectic form

$$\omega = dx_1 \wedge dx_2 + d\phi \wedge dI. \tag{1.3}$$

As we shall see shortly, the variable I plays the role of the slowly varying action-type variable, ϕ is the slowly varying angle near resonance, and (x_1, x_2) are the transversal coordinates responsible for the hyperbolicity of a slow manifold parametrized by I and ϕ.

In our forced beam example, as well as in all the other applications mentioned above, the existence of a hyperbolic slow manifold for small $\varepsilon > 0$ follows from the following two features of system (1.2):

(H1) *There exists $I_1 < I_2$ such that for any $I \in [I_1, I_2]$, $(1.2)^x_{\varepsilon=0}$ (i.e., the x-component of (1.2) with $\varepsilon = 0$) has a hyperbolic fixed point $\bar{x}_0(I)$ connected to itself by a homoclinic trajectory $x^h(t, I)$.*

(H2) *Exactly* one *of the following two conditions hold*:

(H2a) *There exists $I_r \in (I_1, I_2)$ such that*

$$D_I H_0(\bar{x}_0(I_r), I_r) = 0,$$

$$m(I_r) = D_I^2[H_0(\bar{x}_0(I), I)]|_{I=I_r} \neq 0.$$

(H2b) *For every $I \in [I_1, I_2]$*

$$D_I H_0(\bar{x}_0(I), I) = 0.$$

We now discuss how these two features lead to the existence of a *normally hyperbolic slow manifold* (see. e.g., Hirsch, Pugh, & Shub [25] for a definition of normal hyperbolicity). First, note that (H1) implies the existence of a normally hyperbolic invariant 2-manifold $\mathscr{A}_0$ for system $(1.2)_{\varepsilon=0}$ in the form

$$\mathscr{A}_0 = \{(x, I, \phi) \in \mathscr{P} | x = \bar{x}^0(I), I \in [I_1, I_2], \phi \in S^1\}, \tag{1.4}$$

which can be considered to be the image of the annulus $A = [I_1, I_2] \times S^1$ under the embedding

$$\begin{aligned} g_0 &: A \to \mathscr{P}, \\ (I, \phi) &\mapsto (\bar{x}^0(I), I, \phi). \end{aligned} \tag{1.5}$$

It is easy to see that $\mathscr{A}_0$ has a three-dimensional stable manifold $W^s(\mathscr{A}_0)$ and a three-dimensional unstable manifold $W^u(\mathscr{A}_0)$, which coincide in the homoclinic

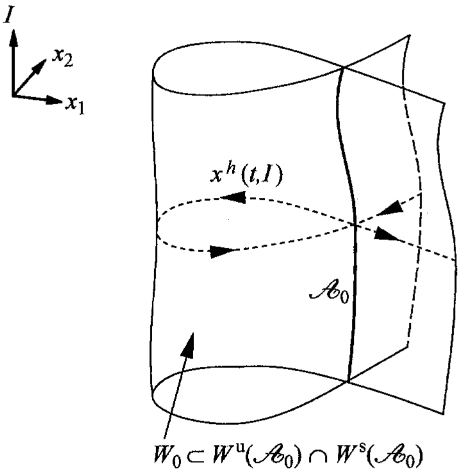

Fig. 1. The manifolds $\mathscr{A}_0$ and W_0 with the ϕ coordinate suppressed.

manifold W_0 (see Fig. 1). The solutions of $(1.2)_{\varepsilon=0}$ on W_0 can be written in the form

$$y_0(t, I, \phi_0) = \left(x^h(t, I), I, \phi_0 + \int_0^t D_I H_0(x^h(\tau, I), I)\, d\tau \right). \tag{1.6}$$

By classic results (see, e.g., FENICHEL [16]) for small $\varepsilon > 0$, system (1.2) has a two-dimensional invariant manifold $\mathscr{A}_\varepsilon$ which is (ε, C^r)-close to $\mathscr{A}_0$. (Throughout this paper two manifolds are said to be (ε, C^r)-close if there exists a C^r diffeomorphism between them whose norm is $\mathscr{O}(\varepsilon)$ in the C^r topology.) As a result, $\mathscr{A}_\varepsilon$ is still a C^r embedding of the annulus A through a map

$$\begin{aligned} &g_\varepsilon\colon A \to \mathscr{P}, \\ &(I, \phi) \mapsto (\bar{x}^\varepsilon(I, \phi), I, \phi) = (\bar{x}^0(I) + \varepsilon x^1(I, \phi, \varepsilon), I, \phi). \end{aligned} \tag{1.7}$$

Let $i_\varepsilon\colon \mathscr{A}_\varepsilon \hookrightarrow \mathscr{P}$ be the inclusion map of $\mathscr{A}_\varepsilon$ with $\varepsilon \geqq 0$. Then it can be shown (see HALLER & WIGGINS [19]) that for small $\varepsilon \geqq 0$, $(\mathscr{A}_\varepsilon, i_\varepsilon^*\omega)$ is a symplectic 2-manifold with

$$i_\varepsilon^*\omega = (1 + \mathscr{O}(\varepsilon))\, d\phi \wedge dI, \tag{1.8}$$

on which the Hamiltonian part of the vector field in (1.2) derives from the *restricted Hamiltonian*

$$\mathscr{H}_\varepsilon = H \,|\, \mathscr{A}_\varepsilon = i_\varepsilon^* H. \tag{1.9}$$

For small nonzero ε we also have two persisting locally invariant 3-manifolds, $W^s_{\mathrm{loc}}(\mathscr{A}_\varepsilon)$ and $W^u_{\mathrm{loc}}(\mathscr{A}_\varepsilon)$, (ε, C^r)-close to $W^s_{\mathrm{loc}}(\mathscr{A}_\varepsilon)$ and $W^u_{\mathrm{loc}}(\mathscr{A}_\varepsilon)$, respectively.

Systems of the form (1.2) with assumption (H1) have been studied by HOLMES & MARSDEN [26] and WIGGINS [45]. Using a version of Melnikov's method they

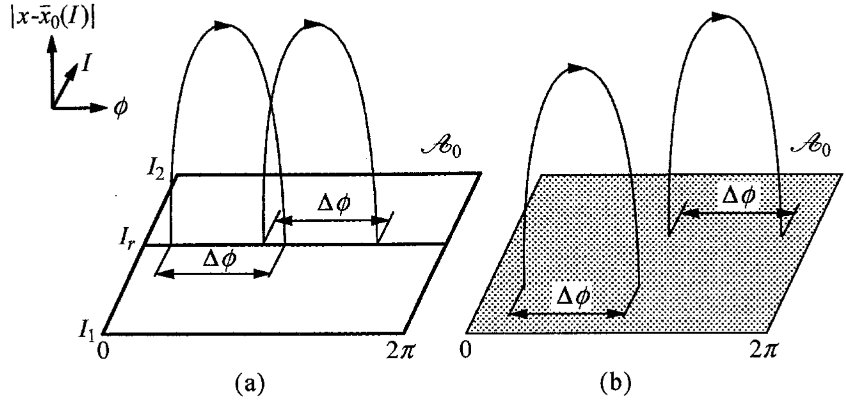

Fig. 2. The geometric meaning of the phase shift $\Delta\phi$ in the case of hypothesis (H2a) and (H2b), respectively.

showed *for purely Hamiltonian perturbations* the generic existence of Smale horseshoes near $\mathscr{A}_\varepsilon$ on every level set

$$E_\varepsilon(h) = \{(x, I, \phi) \in \mathscr{P} \,|\, H(x, I, \phi; \varepsilon) = h\} \tag{1.10}$$

of H intersecting $\mathscr{A}_\varepsilon$. This, by a result of MOSER [37], implies chaotic dynamics and non-integrability for system (1.2). In the case of general dissipative perturbations, isolated horseshoes may exist provided there is a balance between forcing and damping terms in the perturbation. However, the methods of HOLMES & MARSDEN [26] and WIGGINS [45] do not apply when hypothesis (H2) holds. This hypothesis ensures the existence of a resonance on the manifold $\mathscr{A}_0$ and it implies that either a submanifold of $\mathscr{A}_0$ or $\mathscr{A}_0$ itself is a *resonant manifold* for the angular variable ϕ. In particular, (H2) assumes that the frequency $D_I H$ vanishes either on isolated circles in $\mathscr{A}_0$ or on all of $\mathscr{A}_0$. An immediate consequence of this resonance is that the *phase shift*, i.e., the net change of ϕ along orbits on W_0 given by

$$\Delta\phi(I) = \int_{-\infty}^{+\infty} D_I H_0(x^h(t, I), I)\, dt \tag{1.11}$$

is finite either for $I = I_r$ (assumption (H2a)) or for every $I \in [I_1, I_2]$ (assumption (H2b)), as shown in Figs. 2a,b. For small $\varepsilon > 0$, hypothesis (H2) implies that either a subset or all of $\mathscr{A}_\varepsilon$ is a *slow manifold* for system (1.2).

As we indicated earlier, hypothesis (H2a) is satisfied for our beam example as well as in BISHOP, FOREST, MCLAUGHLIN, & OVERMAN [5], FENG & SETHNA [12–14], FENG & WIGGINS [15], TIEN & NAMACHCHIVAYA [42], YANG & SETHNA [47], and hypothesis (H2b) holds in HOLMES [27] and HALLER & WIGGINS [21, 23]. It turns out that it is more advantageous to adapt (H2b) as a working hypothesis, since by applying a blow-up transformation (see KOVAČIČ & WIGGINS [33]) of the form

$$(I, \phi) \mapsto (I_r + \sqrt{\varepsilon}\eta, \phi), \tag{1.12}$$

one can transform resonant circles into "thin" two-dimensional resonant manifolds which put the problem in the framework of assumption (H2b). Motivated by this fact, we work here assuming that hypothesis (H2b) holds, but we also apply the results to the case of (H2a).

1.4. The main results

Under hypothesis (H2b) we study the global aspects of the creation of the hyperbolic slow manifold $\mathscr{A}_\varepsilon$. We establish a global perturbation technique, the *energy-phase method*, which generalizes the energy-phase criterion of HALLER & WIGGINS [19] for simple one-pulse orbits homoclinic to slow manifolds. Detecting multi-pulse orbits requires machinery more involved than the Melnikov-type argument in HALLER & WIGGINS [19]. Surprisingly, the result is a technique which is usually much simpler to use than the Melnikov method and yet detects more sophisticated families of solutions. In particular, it can be used to prove the existence of *N-pulse homoclinic orbits* to $\mathscr{A}_\varepsilon$: these are orbits negatively asymptotic to some invariant set in $\mathscr{A}_\varepsilon$ which enter and leave a small neighborhood of $\mathscr{A}_\varepsilon$ N times, then finally return and approach an invariant set of $\mathscr{A}_\varepsilon$ asymptotically.

For purely Hamiltonian perturbations, the usual Melnikov function is replaced by the nth *order energy-difference function* (denoted by $\Delta^n \mathscr{H}(I, \phi)$) which is directly computable from the perturbation and is defined on the annulus A. The transverse zero set Z^n_- of $\Delta^n \mathscr{H}(I, \phi)$ is used to associate *pulse numbers* with orbits on the slow manifold $\mathscr{A}_\varepsilon$. To find the pulse numbers of slow orbits, it suffices to compute them for the orbits of a *reduced Hamiltonian* $\mathscr{H}$ which approximates the actual Hamiltonian dynamics on $\mathscr{A}_\varepsilon$. It turns out that if the pulse number of an approximate orbit γ_0^- is N, then there exists a nearby slow orbit γ_ε^- and an N-pulse orbit y_ε^N homoclinic to the slow manifold $\mathscr{A}_\varepsilon$, such that y_ε^N is negatively asymptotic exactly to γ_ε^-. One also obtains the positive limit set of y_ε^N by using a set Z^N_+ which can be obtained from Z^N_- through a rotation by $N\Delta\phi$ (see (1.11)). We also study the effects of the presence of an additional homoclinic manifold in the unperturbed problem. In this case our method can be used to construct *jumping N-pulse homoclinic orbits* which stay near one of the homoclinic manifolds during some of their pulses, then switch to the other one for a while, etc. To describe this complicated motion we can determine a *jump sequence* of two symbols based on the analysis of the reduced Hamiltonian $\mathscr{H}$.

For dissipative perturbations we have to perform similar steps to apply the method, but the energy-difference function now contains an additional term which accounts for the loss of energy that occurs between the first and last pulses of multi-pulse orbits. Also, the asymptotics of multi-pulse connections detected this way are different from those for the Hamiltonian case.

In both the Hamiltonian and the dissipative cases, the multi-pulse orbits we construct spend an amount of time of $\mathcal{O}(\log(1/\varepsilon))$ during their intermediate passages near the slow manifold. This is to be compared with the passage time $\mathcal{O}(1/\sqrt{\varepsilon})$ in the work of KAPER & KOVAČIČ [30], who used the exchange lemma of JONES, KAPER, & KOPELL [29] and its generalization by TIN [43] to construct multi-pulse orbits under hypothesis (H2a) in a neighborhood of single-pulse orbits amenable to a Melnikov-type method. The longer the passage time, the more one has to be concerned with large error in numerical experiments. Our experience is that following orbits numerically in a "boundary layer" near a hyperbolic slow manifold on times scales of order $\mathcal{O}(1/\sqrt{\varepsilon})$ is extremely difficult (see Section 5.2.6). We believe that numerical and physical observability are strongly related, which suggests that the multi-pulse behavior observed near slow manifolds in near-integrable systems is primarily due to the presence of orbits detected by the energy-phase method. This is supported by the numerical experiments performed on our beam model (see Sections 5.1.5 and 5.2.6), as well as by those appearing in HALLER & WIGGINS [22].

In Section 5 of this paper we describe the application of the above results to the system (1.1). For zero damping we show the existence of transverse multi-pulse homoclinic and heteroclinic orbits connecting slow periodic solutions. This implies the existence of multi-pulse motions in the two-mode beam model which connect small quasiperiodic oscillations near nonlinear normal modes surviving the effect of forcing. These orbits turn out to form a complicated spatial structure which approaches a self-similar structure as the perturbation vanishes. This homoclinic "tree" can be constructed explicitly by our method and without numerical simulation. In the presence of damping, different types of structurally stable N-pulse orbits homoclinic to $\mathcal{A}_\varepsilon$ are created. We can compute the gradual break-up of the homoclinic tree as the dissipation increases relative to the forcing. We also construct *multi-pulse Šilnikov orbits* and *cycles* which connect the normal modes, and exist on an intricate set of the parameter space (see ŠILNIKOV [40] or WIGGINS [45] for the description of Šilnikov orbits, and KOVAČIČ & WIGGINS [33] for the construction of single-pulse Šilnikov orbits near resonance bands). This establishes the existence of multi-pulse Smale horseshoes for a fairly large open set of parameter values in the damped-forced beam model.

2. Dynamics within and near the invariant manifolds

From this point on we assume that hypothesis (H2b) is satisfied. We first establish our results for the purely Hamiltonian system

$$\begin{aligned}
\dot{x} &= JD_xH_0(x, I) + \varepsilon JD_xH_1(x, I, \phi; \varepsilon),\\
\dot{I} &= -\varepsilon D_\phi H_1(x, I, \phi; \varepsilon),\\
\dot{\phi} &= D_IH_0(x, I) + \varepsilon D_1 H_1(x, I, \phi; \varepsilon),
\end{aligned} \tag{2.1}$$

then extend them to the case of hypothesis (H2a) in Section 3.3, and to the original dissipative system (1.2) in Section 4.

First, we list some features of the invariant manifolds $\mathcal{A}_\varepsilon$, $W^s(\mathcal{A}_\varepsilon)$, and $W^u(\mathcal{A}_\varepsilon)$ introduced in the previous section. We do not deal with their existence, only refer the reader to the well-known persistence and smoothness results of FENICHEL [16] as spelled out for system (2.1) in HALLER & WIGGINS [19]. We do, however, discuss the dynamics on $\mathcal{A}_\varepsilon$ and the internal structure of $W^s(\mathcal{A}_\varepsilon)$ and $W^u(\mathcal{A}_\varepsilon)$. We also study the nature of the flow $F_t^\varepsilon(\cdot)$ of (2.1) in a neighborhood of $\mathscr{A}_\varepsilon$, which is crucial in tracking the repeated passages of multi-pulse orbits near the slow manifold.

2.1. *Dynamics in $\mathscr{A}_\varepsilon$, $W^s(\mathscr{A}_\varepsilon)$, and $W^u(\mathscr{A}_\varepsilon)$*

As we noted in the previous section, for small ε, $\mathscr{A}_\varepsilon$ is a symplectic manifold on which the *restricted Hamiltonion* $\mathscr{H}_\varepsilon = H|\mathscr{A}_\varepsilon$ generates a vector field satisfying

$$\begin{pmatrix} \dot{\phi} \\ \dot{I} \end{pmatrix} = i_\varepsilon^* \omega^\# (D_{(\phi, I)} \mathscr{H}_\varepsilon) = \varepsilon J D_{(\phi, I)} \mathscr{H} + \mathcal{O}(\varepsilon^2), \tag{2.2}$$

with $i_\varepsilon^* \omega^\#: T\mathscr{A}_\varepsilon^* \to T\mathscr{A}_\varepsilon$, $\langle (i_\varepsilon^* \omega^\#)^{-1}[p](u), v \rangle = i_\varepsilon^* \omega[p](u, v)$ for all $p \in \mathscr{A}_\varepsilon$, $u, v \in T_p \mathscr{A}_\varepsilon$. (Here $\langle\, ,\rangle$ denotes the usual pairing between the elements of a vector space and its dual.) The *reduced Hamiltonian* $\mathscr{H}$ in (2.2) can be written as

$$\mathscr{H}(I, \phi) = H_1(\bar{x}^0(I), I, \phi; 0), \tag{2.3}$$

as shown in HALLER & WIGGINS [19]. It is related to the restricted Hamiltonian $\mathscr{H}_\varepsilon$ through

$$\mathscr{H}_\varepsilon = h_0 + \varepsilon \mathscr{H} + \mathcal{O}(\varepsilon), \tag{2.4}$$

with $h_0 = H_0|\mathscr{A}_0 = \text{const}$. By a slight abuse of notation we consider $\mathscr{H}(I, \phi)$ to be defined on the annulus $A = [\mathrm{I}_1, I_2] \times S^1$. Equation (2.4) shows that a structurally stable orbit $\gamma \subset A$ of $\mathscr{H}$ gives rise to an orbit $\gamma_\varepsilon \subset \mathscr{A}_\varepsilon$ of $\mathscr{H}_\varepsilon$ such that $g_\varepsilon^{-1}(\gamma_\varepsilon)$ and γ_0 are (ε, C^r)-close in A. One of our goals is to find out about the orbits of $\mathscr{H}_\varepsilon$ based on our knowledge of $\mathscr{H}$.

Definition 2.1. We say that an orbit $\gamma \subset A$ of some Hamiltonian defined on A is an *internal orbit* if it is structurally stable with respect to small Hamiltonian perturbations *and* if it is bounded away from ∂A. Similarly, an orbit $\gamma_\varepsilon \in \mathscr{A}_\varepsilon$ of the restricted Hamiltonian $\mathscr{H}_\varepsilon$ is called an internal orbit if $g_\varepsilon^{-1}(\gamma_\varepsilon)$ is an internal orbit of the Hamiltonian $g_\varepsilon^* \mathscr{H}_\varepsilon$ on $(A, g_\varepsilon^* \omega)$.

By definition, internal orbits are either periodic orbits, homoclinic orbits, or structurally stable heteroclinic orbits (this last case imposes restrictions on H_1). In what follows we are interested in orbits of (1.2) in $\mathscr{P}$ which are asympotic to internal orbits in $\mathscr{A}_\varepsilon$. The sets of orbits positively and negatively asymptotic to an internal orbit $\gamma_\varepsilon \subset \mathscr{A}_\varepsilon$ are denoted by $W^s(\gamma_\varepsilon)$ and $W^u(\gamma_\varepsilon)$. In the case when γ_ε is periodic, this yields the usual definition of stable and unstable manifolds for periodic orbits. If γ_ε is an orbit homoclinic to a fixed point p_ε, we obtain $W^s(\gamma_\varepsilon) = W^s(p_\varepsilon)$ and $W^u(\gamma_\varepsilon) = W^u(p_\varepsilon)$, where $W^s(p_\varepsilon)$ and $W^u(p_\varepsilon)$ are the two-dimensional "full" stable and unstable manifolds of p_ε lying in the phase space $\mathscr{P}$. We use a similar definition for the case of structurally stable heteroclinic orbits.

Our next proposition is a reformulation of the results of FENICHEL [17] on the foliation of stable and unstable manifolds (see also HALLER & WIGGINS [19]).

FENICHEL was able to relate orbits in $W^s(\mathscr{A}_\varepsilon)$ to their ω-limit set in $\mathscr{A}_\varepsilon$ by showing the existence and persistence of a smooth family of curves, called *fibers*, which foliate $W^s_{\text{loc}}(\mathscr{A}_\varepsilon)$. The fibers of the family are usually not individually invariant under the flow, but the family itself is invariant, i.e., fibers are mapped into fibers by the underlying flow. Each fiber intersects $\mathscr{A}_\varepsilon$ in a unique point, which we call the *base point of the fiber*, and fibers of the unperturbed problem deform smoothly into fibers of the perturbed problem. Most importantly, a solution starting on a fiber of $W^s_{\text{loc}}(\mathscr{A}_\varepsilon)$ is asymptotic to the trajectory in $\mathscr{A}_\varepsilon$ which runs through the base point of the fiber, as long as that trajectory stays in $\mathscr{A}_\varepsilon$. Similar statements hold for $W^u_{\text{loc}}(\mathscr{A}_\varepsilon)$ but, for brevity, we do not list them. To formulate the results precisely, we fix some δ with $\varepsilon \ll \delta \ll 1$ and define a closed tubular set U_δ around $\mathscr{A}_0$ by

$$U_\delta = \{(x, I, \phi) \in \mathscr{P} \,|\, |x - \bar{x}^0(I)| \leqq \delta, (I, \phi) \in A\}. \tag{2.5}$$

We then have the following result which is a direct application of the general results of FENICHEL [17] to system (1.2) (see also WIGGINS [46] regarding the statement (ii).

Proposition 2.1. *There exist ε_0 and δ_0 with $0 < \varepsilon_0 \ll \delta_0 \ll 1$ such that for every $\varepsilon \in [0, \varepsilon_0]$ there exists a two-parameter family $\mathscr{F}^s_\varepsilon = \bigcup_{p \in \mathscr{A}_\varepsilon} f^s_\varepsilon(p)$ of C^r smooth curves $f^s_\varepsilon(p)$ for which*

(i) *$\mathscr{F}^s_\varepsilon = (W^s_{\text{loc}}(\mathscr{A}_\varepsilon) \cup \mathscr{A}_\varepsilon) \cap U_{\delta_0}$ and $f^s_\varepsilon(p) \cap \mathscr{A}_\varepsilon = p$.*

(ii) *$\mathscr{F}^s_\varepsilon$ is in class C^r in p and in ε.*

(iii) *$\mathscr{F}^s_\varepsilon$ is a positively invariant family, i.e., $F^\varepsilon_t(f^s_\varepsilon(p)) \subset f^s_\varepsilon(F^\varepsilon_t(p))$ for any $t \geqq 0$ and $p \in \mathscr{A}_\varepsilon$ with $F^\varepsilon_t(p) \in \mathscr{A}_\varepsilon$.*

(iv) *There exist C_s, $\lambda_s > 0$ such that if $y \in f^s_\varepsilon(p)$, then*

$$|F^\varepsilon_t(y) - F^\varepsilon_t(p)| < C_s e^{-\lambda_s t}$$

for any $t \geqq 0$ with $F^\varepsilon_t(p) \in \mathscr{A}_\varepsilon$.

(v) *For any $p \neq p'$, $f^s_\varepsilon(p) \cap f^s_\varepsilon(p') = \emptyset$.*

(vi) *For any $p \neq p'$ and $y \in f^s_\varepsilon(p)$, $y' \in f^s_\varepsilon(p')$,*

$$\lim_{t \to \infty} \frac{|F^\varepsilon_t(y) - F^\varepsilon_t(p)|}{|F^\varepsilon_t(y') - F^\varepsilon_t(p)|} = 0.$$

2.2. Dynamics near the slow manifold $\mathscr{A}_\varepsilon$

The next lemma provides a normal form of system (2.1) in a neighborhood of the perturbed manifold, following the basic idea of local normalization sketched in FENICHEL [17]. Similar normal forms also appeared in the general singular perturbation context of JONES & KOPELL [28].

Lemma 2.2. *There exist ε_0 and δ_0 with $0 < \varepsilon_0 \ll \delta_0 \ll 1$ such that for $\varepsilon \leqq \varepsilon_0$ there is a C^{r-2} change of coordinates T^ε: $U_{\delta_0} \to \mathbb{R}^2 \times A$, $(x, I, \phi) \mapsto (z, I, \phi)$ with $\varepsilon \mapsto T^\varepsilon$ in*

C^{r-2}. *In the* (z, I, ϕ) *coordinates the flow of* (1.2) *satisfies the equations*

$$\begin{aligned} \dot{z} &= A(z, I, \phi; \varepsilon)z, \\ \dot{I} &= \varepsilon k_I(z, I, \phi; \varepsilon), \\ \dot{\phi} &= z^T B(z, I, \phi; \varepsilon)z + \varepsilon k_\phi(z, I, \phi; \varepsilon), \end{aligned} \tag{2.6}$$

with

$$A = \begin{pmatrix} \lambda + \langle q_1, z\rangle + \varepsilon k_1 & 0 \\ 0 & -\lambda + \langle q_2, z\rangle + \varepsilon k_2 \end{pmatrix}, \tag{2.7}$$

where $\lambda\colon \mathbb{R} \to \mathbb{R}^+$ *is in* C^{r-1}, $k_1, k_2, k_I, k_\phi\colon \mathbb{R}^2 \times A \times [0, \varepsilon_0] \to \mathbb{R}$ *are in* C^{r-2}, $B\colon \mathbb{R}^2 \times A \times [0, \varepsilon_0] \to \mathbb{R}^{2\times 2}$ *is symmetric and is in* C^{r-2}, *and* $q_1, q_2\colon \mathbb{R}^2 \times A \times [0, \varepsilon_0] \to \mathbb{R}^2$ *are* C^{r-3} *functions of their arguments.*

Proof. The proof follows that of FENICHEL [17] for the analytic case, but we keep track of the loss of smoothness at each change of coordinates that he applies. Another difference is that we do not perform FENICHEL's last step in the construction since it would impose more stringent smoothness hypotheses on system (2.1) without a substantial improvement on the normal form. Also, for our specific system (2.1) we are able to perform the normalization globally, i.e., in a neighborhood of the whole manifold $\mathscr{A}_\varepsilon$. For details see HALLER [20]. □

The significance of this lemma is that it smoothly "linearizes" the local dynamics around $\mathscr{A}_\varepsilon$. In particular, $\mathscr{A}_\varepsilon$ is described by the equation $z = 0$, and its local stable and unstable manifolds satisfy $z_1 = 0$ and $z_2 = 0$, respectively. This simple geometry enables us to study trajectories that will have a great significance later in our analysis. These trajectories pass near the slow manifold $\mathscr{A}_\varepsilon$ in a very special way: they stay between two $\mathcal{O}(\sqrt{\varepsilon})$-tubes around $\mathscr{A}_\varepsilon$ during their passage, and the time they spend in this tubular neighborhood is of order $\mathcal{O}(1)$. As a result, they are not subject to the intense stretching present in a "boundary layer" near $\mathscr{A}_\varepsilon$, but their (I, ϕ) coordinates still have a time evolution similar to that of the slow orbits on $\mathscr{A}_\varepsilon$. In the following, (x_p, I_p, ϕ_p) refers to the coordinates of a point $p \in \mathscr{P}$ and $T^\varepsilon_\rho(p)$ denotes the (dummy) ρ coordinates of the image of p under the transformation T^ε constructed in Lemma 2.2. We also use the notation

$$\partial_1 U_\delta = \{p \in \partial U_\delta | I_p \in (I_1, I_2)\}.$$

Lemma 2.3. *Let* $w_\varepsilon(t) = (x(t), I(t), \phi(t))$ *with* $t \in \mathbb{R}$ *be a trajectory of* (1.2). *Assume that for* $\varepsilon < \tilde{\varepsilon}_0$, *fixed* $\vartheta > 0$, *and* $\delta(\varepsilon) = \vartheta\sqrt{\varepsilon}$, $w_\varepsilon(t)$ *enters* $U_{\delta(\varepsilon)}$ *(as defined in* (2.5)) *at a point* $p_\varepsilon \in \partial_1 U_{\delta(\varepsilon)}$ *and leaves it at* $q_\varepsilon \in \partial_1 U_{\delta(\varepsilon)}$. *Let the distance of the point* p_ε *from the local stable manifold* $W^s_{\text{loc}}(\mathscr{A}_\varepsilon)$ *obey the estimate*

$$d(p_\varepsilon, W^s_{\text{loc}}(\mathscr{A}_\varepsilon)) > K\sqrt{\varepsilon} \tag{2.8}$$

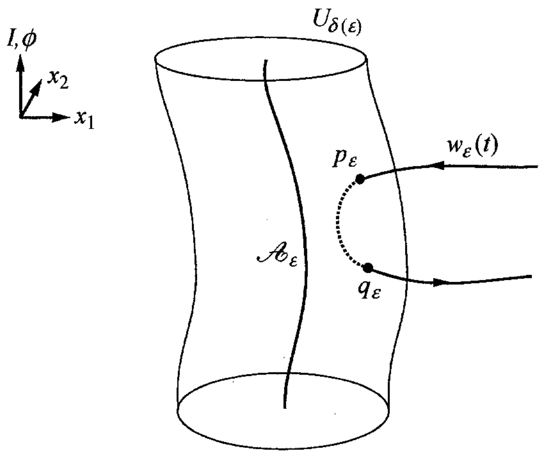

Fig. 3. Geometry for Lemma 2.3.

for some $0 < K < \vartheta$. *Then there exists an* $\bar{\varepsilon}_0$ *with* $0 < \bar{\varepsilon}_0 \leqq \hat{\varepsilon}_0$ *such that for* $0 < \varepsilon \leqq \bar{\varepsilon}_0$,

$$|I_{q_\varepsilon} - I_{p_\varepsilon}| \leqq K_I \varepsilon, \quad |\phi_{q_\varepsilon} - \phi_{p_\varepsilon}| \leqq K_\phi \varepsilon, \tag{2.9}$$

where I_I *and* K_ϕ *are positive constants (see Fig. 3 for geometry).*

Proof. We first let

$$\hat{\varepsilon}_0 = \min\left(\varepsilon_0, \tilde{\varepsilon}_0, \frac{\delta_0^2}{\vartheta^2}\right),$$

where ε_0, $\delta_0 > 0$ are as in the statement of Lemma 2.2. Then for $\varepsilon < \hat{\varepsilon}_0$ we know that $w_\varepsilon(t)$ enters $U_{\delta(\varepsilon)}$ within which, according to Lemma 2.2, system (1.2) is C^{r-2} conjugate to system (2.6). The subspace $z_2 = \text{const.}$, $z_1 = 0$ in the phase space of (2.6) is a graph over the (I, ϕ) variables; hence there exists $s_\varepsilon \in W^s_{\text{loc}}(\mathscr{A}_\varepsilon)$ such that

$$I_{p_\varepsilon} = I_{s_\varepsilon}, \quad \phi_{p_\varepsilon} = \phi_{s_\varepsilon}, \quad T^\varepsilon_{z_2}(p_\varepsilon) = T^\varepsilon_{z_2}(s_\varepsilon), \quad |T^\varepsilon_{z_1}(p_\varepsilon)| > |T^\varepsilon_{z_1}(s_\varepsilon)| = 0, \tag{2.10}$$

where T^ε is the transformation constructed in Lemma 2.2 (T^ε is the identity map for the (I, ϕ) coordinates). Furthermore, since T^ε is a C^{r-2} diffeomorphism, we can select $L > 0$ such that

$$\|D(T^\varepsilon)^{-1}\| \leqq L \tag{2.11}$$

in some open set $\tilde{U}(\hat{\varepsilon}_0) \subset \mathbb{R}^2 \times A$. Then (2.8), (2.10), (2.11), and the mean value inequality imply that

$$\text{if} \quad K\sqrt{\varepsilon} < |p_\varepsilon - s_\varepsilon| \leqq L|T^\varepsilon(p_\varepsilon) - T^\varepsilon(s_\varepsilon)| = L|T^\varepsilon_{z_1}(p_\varepsilon)|, \quad \text{then } |T^\varepsilon_{z_1}(p_\varepsilon)| > \frac{K}{L}\sqrt{\varepsilon}. \tag{2.12}$$

We now let $r_\varepsilon = g_\varepsilon(I_{q_\varepsilon}, \phi_{q_\varepsilon}) \in \mathscr{A}_\varepsilon$ (see (1.7)) and, under the assumptions of the lemma, obtain

$$|T_z^\varepsilon(q_\varepsilon)| = |T^\varepsilon(q_\varepsilon) - T^\varepsilon(r_\varepsilon)| \leqq \frac{1}{L}|q_\varepsilon - r_\varepsilon| = \frac{1}{L}\delta(\varepsilon). \tag{2.13}$$

Let t_ε denote the time the trajectory $w_\varepsilon(t)$ spends between the points p_ε and q_ε. For simplicity, we assume that $T_{z_1}^\varepsilon(p_\varepsilon) > 0$, which implies that $T_{z_1}^\varepsilon(q_\varepsilon) > 0$ by the invariance of the $z_1 = 0$ hyperplane under the dynamics of system (2.6). Then, using our normal form (2.6) and equation (2.7), for any $t \leqq t_\varepsilon$ we can write

$$\begin{aligned} T_{z_1}^\varepsilon(w_\varepsilon(t)) &= T_{z_1}^\varepsilon(p_\varepsilon) + \int_0^t (\lambda + \langle q_1, z\rangle + \varepsilon k_1) z_1 |_{T^\varepsilon(w_\varepsilon(\tau))} d\tau \\ &\geqq T_{z_1}^\varepsilon(p_\varepsilon) + \int_0^t (c_1 - c_2 |T_z^\varepsilon(w_\varepsilon(\tau))| - c_3\varepsilon) T_{z_1}^\varepsilon(w_\varepsilon(\tau)) d\tau \\ &\geqq T_{z_1}^\varepsilon(p_\varepsilon) + \int_0^t \left(c_1 - c_2 \frac{\delta(\varepsilon)}{L} - \varepsilon c_3\right) T_{z_1}^\varepsilon(w_\varepsilon(\tau)) d\tau, \end{aligned} \tag{2.14}$$

where, within $\tilde{U}(\hat{\varepsilon}_0)$, $c_1 > 0$ is a lower bound for λ, and $c_2, c_3 > 0$ are upper bounds for $|q_1|$ and $|k_1|$, respectively. Fixing some $0 < \nu < 1$ and setting

$$\bar{\varepsilon}_0 = \min\left(\hat{\varepsilon}_0, \left[\frac{c_1(1-\nu)L}{2c_2\vartheta}\right]^2, \left[\frac{c_2\vartheta}{Lc_3}\right]^2\right), \tag{2.15}$$

we obtain that, for $\varepsilon \leqq \bar{\varepsilon}_0$, $c_1\nu > 0$ is a lower bound for the first factor in the integrand of (2.14). Then, using a reverse Gronwall inequality and substituting $t = t_\varepsilon$, we arrive at the expression

$$T_{z_1}^\varepsilon(q_\varepsilon) \geqq T_{z_1}^\varepsilon(p_\varepsilon) e^{c_1\nu t_\varepsilon},$$

from which we obtain the estimate

$$t_\varepsilon \leqq \frac{1}{c_1\nu} \log \frac{T_{z_1}^\varepsilon(q_\varepsilon)}{T_{z_1}^\varepsilon(p_\varepsilon)} \leqq \frac{1}{c_1\nu} \log \frac{\vartheta}{K}, \tag{2.16}$$

where we have also used (2.12) and (2.13).

We now estimate the change of the I coordinate while the trajectory $w_\varepsilon(t)$ passes from p_ε to q_ε. Using $(2.6)^I$ and (2.16) we have

$$|I_{q_\varepsilon} - I_{p_\varepsilon}| \leqq \varepsilon \int_0^{t_\varepsilon} |k_I|_{T^\varepsilon(w_\varepsilon(\tau))} d\tau \leqq \varepsilon c_4 t_\varepsilon \leqq \varepsilon \frac{c_4}{c_1\nu} \log \frac{\vartheta}{K}, \tag{2.17}$$

where $c_4 > 0$ is an upper bound for $|k_I|$ in $\tilde{U}(\bar{\varepsilon}_0)$. This proves the first inequality in (2.9). As for the second inequality of (2.9), equation $(2.6)^\phi$ gives rise to the estimate

$$\begin{aligned} |\phi_{q_\varepsilon} - \phi_{p_\varepsilon}| &\leqq \int_0^{t_\varepsilon} |z^T B z + \varepsilon k_\phi|_{T^\varepsilon(w_\varepsilon(\tau))} d\tau \\ &\leqq \varepsilon\left(\frac{\vartheta^2}{L^2} c_5 + c_6\right) t_\varepsilon \leqq \varepsilon \frac{1}{c_1\nu}\left(\frac{\vartheta^2}{L^2} c_5 + c_6\right) \log \frac{\vartheta}{K}, \end{aligned} \tag{2.18}$$

where c_5, $c_6 > 0$ are upper bounds for $\|B\|$ and $|k_\phi|$ in $\tilde{U}(\bar{\varepsilon}_0)$, respectively. Again, this shows that for $0 < \varepsilon < \bar{\varepsilon}_0$ we can choose $K_\phi^{\cdot} > 0$ to satisfy the second inequality in (2.9). $\square$

We now construct two-dimensional Poincaré sections within the three-dimensional level surfaces of H. These sections will be used to follow trajectories as long as they keep a minimal distance from the slow manifold $\mathscr{A}_\varepsilon$, or more precisely, obey the distance condition (2.8) of Lemma 2.3. We want to capture them by smooth Poincaré sections which are graphs over the annulus A. This turns out to be possible if the trajectories of interest are within a certain maximal distance from the slow manifold. This maximal distance condition is most conveniently expressed in terms of a maximal energy deviation from the energy h_0 of $\mathscr{A}_0$ (see (2.4) and the statement of Lemma 2.4 below).

From now on $\tilde{W}^{\mathrm{s}}_{\mathrm{loc}}(\mathscr{A}_\varepsilon)$ and $\tilde{W}^{\mathrm{u}}_{\mathrm{loc}}(\mathscr{A}_\varepsilon)$ denote the connected components of $W^{\mathrm{s}}_{\mathrm{loc}}(\mathscr{A}_\varepsilon)$ and $W^{\mathrm{u}}_{\mathrm{loc}}(\mathscr{A}_\varepsilon)$, respectively, which are (ε, C^r)-close to appropriate subsets of W_0. By the normal hyperbolicity of $\mathscr{A}_\varepsilon$, both $W^{\mathrm{s}}_{\mathrm{loc}}(\mathscr{A}_\varepsilon)$ and $W^{\mathrm{u}}_{\mathrm{loc}}(\mathscr{A}_\varepsilon)$ have precisely one more connected component, but hypothesis (H1) tells nothing about the geometry of the corresponding global invariant manifolds. In Section 3 we include these other components in our analysis under supplementary assumptions.

Let us first define a family of Poincaré sections for system (1.2) in the vicinity of $\mathscr{A}_\varepsilon$. We fix some (yet undetermined) $\vartheta > 0$ and on every energy surface $E_\varepsilon(h)$ (see (1.10)) introduce the set

$$\Sigma_\varepsilon(h) = \partial_1 U_{\delta(\varepsilon)} \cap E_\varepsilon(h),$$

where $\delta(\varepsilon)$ is defined as in Lemma 2.3. Note that for $\varepsilon = 0$, $\Sigma_\varepsilon(h_0)$ becomes singular. We now give conditions under which the Poincaré sections defined above are smooth symplectic manifolds.

Lemma 2.4. *Let a constant $\kappa > 0$ be fixed. Then there exist positive constants $\bar{\varepsilon}_0$ and ϑ_0 such that for $0 < \varepsilon < \bar{\varepsilon}_0$, $\vartheta > \vartheta_0$, and $|h - h_0| < \kappa\varepsilon$,*

(i) *$E_\varepsilon(h)$ and $E_0(h_0)$ are $(\sqrt{\varepsilon}, C^1)$-close within the three-dimensional tube $\bar{U}(\vartheta, \varepsilon) = \overline{U_{\delta_0} - U_{\delta(\varepsilon)/2}}$, where δ_0 is that of Lemma 2.2.*

(ii) *Two of the connected components of $\Sigma_\varepsilon(h)$, $\Sigma^{\mathrm{s}}_\varepsilon(h)$ and $\Sigma^{\mathrm{u}}_\varepsilon(h)$, are $(\sqrt{\varepsilon}, C^1)$-close to $\Pi^{\mathrm{s}}_\varepsilon = \partial_1 U_{\delta(\varepsilon)} \cap \tilde{W}^{\mathrm{s}}_{\mathrm{loc}}(\mathscr{A}_0)$ and $\Pi^{\mathrm{u}}_\varepsilon = \partial_1 U_{\delta(\varepsilon)} \cap \tilde{W}^{\mathrm{u}}_{\mathrm{loc}}(\mathscr{A}_0)$, respectively (see Fig. 4). Moreover, $(\Sigma^{\mathrm{s}}_\varepsilon(h), \bar{\omega})$ and $(\Sigma^{\mathrm{u}}_\varepsilon(h), \bar{\omega})$ with $\bar{\omega} = d\phi \wedge dI$ are symplectic 2-manifolds and embeddings of the annulus A through two C^1 maps $e^{\mathrm{s}}_\varepsilon \colon A \to \mathscr{P}$ and $e^{\mathrm{u}}_\varepsilon \colon A \to P$, respectively.*

Proof. First note that $E_0(h_0) \cap U_{\delta_0} \supset W_0 \cap U_{\delta_0} \neq \emptyset$ and that the intersection is transversal; hence for $\varepsilon > 0$ small enough, $E_\varepsilon(h) \cap U_{\delta_0} \neq \emptyset$. We decrease $\bar{\varepsilon}_0$ of Lemma 2.3 to achieve this and select $p_0 \in E_0(h_0) \cap \bar{U}(\vartheta, \varepsilon)$ and $p_\varepsilon \in E_\varepsilon(h) \cap \bar{U}(\vartheta, \varepsilon)$, both from a fixed submanifold $I = I_0$, $\phi = \phi_0$. Such a choice is possible since $|D_x H_0|$ (as well as $|D_x H|$) is at least of order $\mathcal{O}(\sqrt{\varepsilon})$ (i.e., strictly nonzero for $\varepsilon > 0$) in $\bar{U}(\vartheta, \varepsilon)$ (hypothesis (H1)); hence any energy surface can locally be written in the

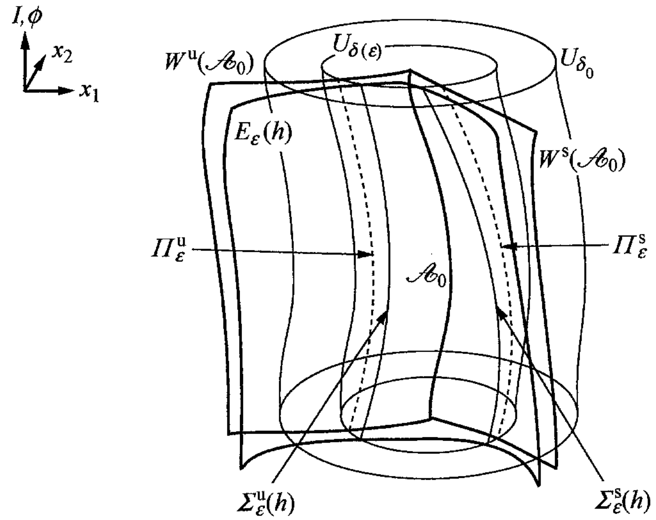

Fig. 4. Statement (ii) of Lemma 2.4.

form $x_i = f(x_j, I, \phi; \varepsilon)$. From hypothesis (H1) we also have

$$D_x H(\bar{x}^0(I_0), I_0, \phi_0; 0) = 0,$$

from which we obtain

$$D_x H(x. I, \phi; \varepsilon) = M_1(x, I, \phi; \varepsilon)(x - \bar{x}^0(I_0)) + m_2(x, I, \phi; \varepsilon)(I - I_0)$$
$$+ m_3(x, I, \phi; \varepsilon)(\phi - \phi_0) + \varepsilon m_4(x, I, \phi; \varepsilon), \tag{2.19}$$

where the matrix M_1 and the functions m_2, m_3, and m_4 are of class C^{r-1} in their arguments (see HALLER [20] for more details). Now note that on the line $l_{p_0, p_\varepsilon} \subset \bar{U}(\vartheta, \varepsilon)$ connecting p_ε and p_0, (2.19) simplifies to

$$D_x H(x, I_0, \phi_0; \varepsilon) = M_1(x, I_0, \phi_0; \varepsilon)(x - \bar{x}^0(I_0)) + \varepsilon m_4(x, I_0, \phi_0; \varepsilon). \tag{2.20}$$

Since, for small $\varepsilon > 0$ and appropriate p_ε, l_{p_0, p_ε}, *does not intersect* $U_{\delta(\varepsilon)/2}$, (2.20) gives rise to the estimate

$$|DH||_{l_{p_0, p_\varepsilon}} \geqq |D_x H||_{l_{p_0, p_\varepsilon}} > c_7 \frac{\vartheta\sqrt{\varepsilon}}{2} - c_8 \varepsilon > c_7 \frac{\vartheta\sqrt{\varepsilon}}{4}, \tag{2.21}$$

where $c_7 > 0$ is a lower bound within U_{δ_0} for the positive eigenvalue of

$$M_1(x, I_0, \phi_0; \varepsilon) = \int_0^1 D_x^2 H(\bar{x}^0(I_0) + s(x - \bar{x}^0(I_0)), I_0, \phi_0; \varepsilon)\, ds,$$

and $c_8 > 0$ is an upper bound for $|m_4|$ in U_{δ_0}. By assumption, we also have

$$\kappa\varepsilon > |H_0|_{p_0} - H|_{p_\varepsilon}| > \left|H_0|_{p_0} - H_0|_{p_\varepsilon}\right| - \left|H_0|_{p_\varepsilon} - H|_{p_\varepsilon}\right| = \left|H_0|_{p_0} - H_0|_{p_\varepsilon}\right| - \varepsilon\left|H_1|_{p_\varepsilon}\right|$$

$$> c_7 \frac{\vartheta\sqrt{\varepsilon}}{4} |p_0 - p_\varepsilon| - c_9 \varepsilon > c_7 \frac{\vartheta\sqrt{\varepsilon}}{8} |p_0 - p_\varepsilon|, \tag{2.22}$$

where we have used the mean value theorem together with (2.21), and further diminished $\bar{\varepsilon}_0$, if necessary ($c_9 > 0$ is an upper bound for $|H_1|$ in U_{δ_0}). Thus, based on (2.22), we have

$$|p_0 - p_\varepsilon| < \frac{8\kappa}{c_7 \vartheta} \sqrt{\varepsilon}. \tag{2.23}$$

Similarly, we obtain that

$$|DH_0|_{p_0} - DH|_{p_\varepsilon}| \leqq |DH_0|_{p_0} - DH_0|_{p_\varepsilon}| + \varepsilon |DH_1|_{p_\varepsilon}|$$

$$< c_{10} |p_0 - p_\varepsilon| + c_{11}\varepsilon < \frac{16\kappa c_{10}}{c_7 \vartheta} \sqrt{\varepsilon}, \tag{2.24}$$

where $c_{10}, c_{11} > 0$ are upper bounds within U_{δ_0} for $\|D^2 H\|$ and $|DH_1|$, respectively. But (2.23) and (2.24) together prove the first statement of the lemma.

Let us now make the specific choice $p_0 \in \partial U_{\delta(\varepsilon)/2}$. Then

$$|p_0 - p_\varepsilon| < \frac{\vartheta}{2} \sqrt{\varepsilon} \tag{2.25}$$

would ensure that $E_\varepsilon(h)$ intersects $\partial_1 U_{\delta(\varepsilon)}$. Inequality (2.23) implies that (2.25) is satisfied if we choose

$$\vartheta \geqq \vartheta_0 = 4 \sqrt{\frac{\kappa}{c_7}}. \tag{2.26}$$

Furthermore, the intersection of $E_\varepsilon(h)$ and $\partial_1 U_{\delta(\varepsilon)}$ is transversal for $\varepsilon > 0$ small enough, since $E_0(h_0)$ and $\partial_1 U_{\delta(\varepsilon)}$ intersect transversally and $E_\varepsilon(h)$ and $E_0(h_0)$ are $(\sqrt{\varepsilon}, C^1)$-close. Hence $\Sigma_\varepsilon(h) = E_\varepsilon(h) \cap \partial_1 U_{\delta(\varepsilon)}$ has two connected components which are manifolds and are $(\sqrt{\varepsilon}, C^1)$-close to Π_ε^s and Π_ε^u, respectively. In that case they are graphs over the annulus A as asserted in statement (ii) of the lemma. Since on $\partial_1 U_{\delta(\varepsilon)}$ locally either x_1 is a function of x_2 or vice versa, the symplectic form ω of $\mathscr{P}$ restricts to the closed two-form $\bar{\omega}$ on $\partial_1 U_{\delta(\varepsilon)}$. Let us introduce the inclusions i_ε^s: $\Sigma_\varepsilon^s(h) \subsetneq \mathscr{P}$ and i_ε^u: $\Sigma_\varepsilon^u(h) \subsetneq \mathscr{P}$. (Both the embeddings and the inclusions of $\Sigma_\varepsilon^s(h)$ and $\Sigma_\varepsilon^u(h)$ do depend on the energy h.) Since both e_ε^s and e_ε^u are diffeomorphisms, $i_\varepsilon^{u*}\omega = \bar{\omega}$ and $i_\varepsilon^{s*}\omega = \bar{\omega}$ are nondegenerate; hence $(\Sigma_\varepsilon^s(h), \bar{\omega})$ and $(\Sigma_\varepsilon^u(h), \bar{\omega})$ are symplectic manifolds (with boundary). This concludes the proof of the lemma. □

We now introduce Poincaré maps between the sections $\Sigma_\varepsilon^s(h)$ and $\Sigma_\varepsilon^u(h)$ to track trajectories obeying both the minimal distance condition (2.8) and the maximal distance condition of Lemma 2.4 on some time interval. On appropriate open sets $R^s_\varepsilon(h) \subset \Sigma^s_\varepsilon(h)$ and $R^u_\varepsilon(h) \subset \Sigma^u_\varepsilon(h)$ we define the *local map* L^h_ε and the *global map* G^h_ε, respectively, by

$$L^h_\varepsilon\colon R^s_\varepsilon(h) \to \Sigma^u_\varepsilon(h), \quad G^h_\varepsilon\colon R^u_\varepsilon(h) \to \Sigma^s_\varepsilon(h),$$
$$p \mapsto F^\varepsilon_{t^\varepsilon_L(p)}(p), \qquad p \mapsto F^\varepsilon_{t^\varepsilon_G(p)}(p),$$

with

$$t^\varepsilon_L(p) = \inf\{t > 0 \mid F^\varepsilon_t(p) \in \Sigma^u_\varepsilon(h)\}, \quad t^\varepsilon_G(p) = \inf\{t > 0 \mid F^\varepsilon_t(p) \in \Sigma^s_\varepsilon(h)\}.$$

Since the domains of definitions of these maps are graphs over the annulus A, they induce two conjugate maps, $\mathscr{G}^h_\varepsilon$ and $\mathscr{L}^h_\varepsilon$, on A which are defined through the commutative diagrams

$$\begin{array}{ccccccc} R^s_\varepsilon(h) & \xrightarrow{L^h_\varepsilon} & \Sigma^u_\varepsilon(h) & \qquad & R^u_\varepsilon(h) & \xrightarrow{G^h_\varepsilon} & \Sigma^s_\varepsilon(h) \\ e^s_\varepsilon \uparrow & & \uparrow e^u_\varepsilon & & e^u_\varepsilon \uparrow & & \uparrow e^s_\varepsilon \\ (e^s_\varepsilon)^{-1}(R^s_\varepsilon(h)) & \xrightarrow[\mathscr{L}^h_\varepsilon]{} & A & & (e^u_\varepsilon)^{-1}(R^u_\varepsilon(h)) & \xrightarrow[\mathscr{G}^h_\varepsilon]{} & A \end{array} \tag{2.27}$$

Instead of following trajectories though the local and global maps directly, it is more convenient to study these conjugate maps acting on the annulus. The following step is crucial in our construction: we give universal (i.e., system-independent) C^1 approximations for $\mathscr{G}^h_\varepsilon$ and $\mathscr{L}^h_\varepsilon$ in terms of the unperturbed geometry.

Lemma 2.5. *Let a constant $\kappa > 0$ be fixed and let $\vartheta_0 > 0$ be selected as in the statement of Lemma 2.4. Then there exists $\vartheta^* \geqq \vartheta_0$ such that for $0 < \varepsilon < \bar{\varepsilon}_0$, $\vartheta > \vartheta^*$, and $|h - h_0| < \kappa_\varepsilon$,*

(i) *The two-dimensional maps L^h_ε, G^h_ε, $\mathscr{L}^h_\varepsilon$, and $\mathscr{G}^h_\varepsilon$ are symplectic.*

(ii) *Under condition* (2.26) *the global map G^h_ε can be defined on $R^u_\varepsilon(h) = \Sigma^u_\varepsilon(h)$, and its conjugate map $\mathscr{G}^h_\varepsilon$ are $(\sqrt{\varepsilon}, C^1)$-close to the rotation map*

$$\mathscr{R}\colon A \to A,$$
$$(I, \phi) \mapsto (I, \phi + \Delta\phi(I)),$$

where the phase shift $\Delta\phi(I)$ is defined in (1.11).

(iii) *For any compact set $S^s_\varepsilon(h) \subset R^s_\varepsilon(h) \subset \Sigma^s_\varepsilon(h)$ satisfying*

$$d(S^s_\varepsilon(h), W^s_{\mathrm{loc}}(\mathscr{A}_\varepsilon)) > K\sqrt{\varepsilon}, \tag{2.28}$$

with some $0 < K < \vartheta$, the map $\mathscr{L}^h_\varepsilon$ is $(\sqrt{\varepsilon}, C^1)$-close on $(e^u_\varepsilon)^{-1}(S^s_\varepsilon(h))$ to the identity map of A.

Proof. Throughout the proof we use the notation of the earlier lemmas without explicit reference. It is enough to prove (i) for the maps G^h_ε and $\mathscr{G}^h_\varepsilon$, since the same argument works for L^h_ε and $\mathscr{L}^h_\varepsilon$. That G^h_ε is symplectic is a standard result (see, e.g., ARNOLD & AVEZ [2] and HALLER [20] for details). But then $\mathscr{G}^h_\varepsilon$ is symplectic, since we have

$$\mathscr{G}^h_{\varepsilon *}\bar{\omega} = (e^s_\varepsilon)^{-1}_* G^h_{\varepsilon *} e^u_{\varepsilon *}\bar{\omega}(e^s_\varepsilon)^{-1}_* G^h_{\varepsilon *}\bar{\omega} = (e^s_\varepsilon)^{-1}_*\bar{\omega} = \bar{\omega}.$$

We now proceed with the proof of (ii) of the lemma. As we noted in Lemma 2.4, the energy surface $E_\varepsilon(h)$ intersects $\partial_1 U_{\delta(\varepsilon)}$ transversally in two components. By the nature of the perturbed flow F^ε_t near W_0 and the continuity of $E_\varepsilon(h)$, every trajectory starting from the first component $\Sigma^u_\varepsilon(h)$ is guided to the second component $\Sigma^s_\varepsilon(h)$. This proves the first statement on the global map in (ii). We now turn to the proof of the statement on the map $\mathscr{G}^h_\varepsilon$.

Let us introduce the map

$$G_\varepsilon\colon \Pi^u_\varepsilon \to \Pi^s_\varepsilon,$$
$$p \mapsto F^0_{\tau_\varepsilon(p)}(p).$$

with

$$\tau_\varepsilon(p) = \inf\{t > 0 \,|\, F^0_t(p) \in \Pi^s_\varepsilon\}.$$

Note that for ε sufficiently small and $\vartheta > \vartheta^* \geqq \vartheta_0$, G_ε is a Poincaré map with a "finite time of flight". (For instance, for $\varepsilon = 0.01$ and $\vartheta = 5$, G_ε follows trajectories as they leave a tube of radius $\delta = 0.5 = 50\varepsilon$ around $\mathscr{A}_0$ and then return to the same tube.) By the smooth dependence of Poincaré maps on parameters (here ε and the energy h) it follows that G^h_ε and G_ε are $(\sqrt{\varepsilon}, C^1)$-close for ε sufficiently small. Let us introduce the map $\mathscr{G}_\varepsilon\colon A \to A$ which is C^r conjugate to G_ε and is defined analogously to $\mathscr{G}^h_\varepsilon$ (see (2.27)). As a consequence, $\mathscr{G}_\varepsilon$ is $(\sqrt{\varepsilon}, C^1)$-close to $\mathscr{G}^h_\varepsilon$. Now observe that $\bar{G}_0 = g_0 \circ \mathscr{R} \circ g_0^{-1}$ (see (1.5)) maps α-limit points of unperturbed homoclinic trajectories to their ω-limit points; hence $\bar{G}_0$ is a smooth "geometric" extension of the map G_ε at $\sqrt{\varepsilon} = 0$. It follows from (ii) of Proposition 2.1 that $\bar{\mathscr{G}}_0 \equiv \mathscr{R}$ is a smooth extension of $\mathscr{G}_\varepsilon$ at $\sqrt{\varepsilon} = 0$. Therefore, $\mathscr{G}_\varepsilon$ and $\mathscr{R}$ are $(\sqrt{\varepsilon}, C^1)$-close. Since $\mathscr{G}_\varepsilon$ and $\mathscr{G}^h_\varepsilon$ are $(\sqrt{\varepsilon}, C^1)$-close, this completes the proof of (ii).

Statement (iii) does not allow a similar geometric argument, because one cannot define in this way a $(\sqrt{\varepsilon}, C^1)$-close conjugate map $\mathscr{L}_\varepsilon$ which would extend smoothly to $\sqrt{\varepsilon} = 0$. Instead, we make use of the normal form of Lemma 2.2 and the estimates of Lemma 2.3. First note that the initial conditions of trajectories starting from $S^s_\varepsilon(h)$ satisfy the distance condition (2.8); hence the (ε, C^0)-closeness of $\mathscr{L}^h_\varepsilon$ to the identity follows immediately from Lemma 2.3. Therefore, using the notation of that lemma, we only have to show that for some constant $\bar{K} > 0$,

$$\left\| \frac{\partial(I_{q_\varepsilon}, \phi_{q_\varepsilon})}{\partial(I_{p_\varepsilon}, \phi_{p_\varepsilon})} - \mathrm{Id}_2 \right\| < \bar{K}\sqrt{\varepsilon}, \tag{2.29}$$

where $\mathrm{Id}_2 \in \mathbb{R}^{2\times 2}$ is the identity matrix. Let $C^* > 0$ be a uniform Lipshitz constant in $T^\varepsilon(U_{\delta(\varepsilon)})$ for the right-hand side of system (2.6), with T^ε constructed in Lemma 2.2. For the deviation of two trajectories $w_\varepsilon(t)$ and $w'_\varepsilon(t)$ of (2.6) (satisfying the conditions of Lemma 2.3) we have the usual Gronwall estimate

$$|I_\varepsilon(t) - I'_\varepsilon(t)| \leqq |w_\varepsilon(t) - w'_\varepsilon(t)| \leqq |w_0 - w'_0| e^{C^* t}, \tag{2.30}$$

where $w_\varepsilon(0) = w_0 \neq w'_\varepsilon(0) = w'_0$, $I_\varepsilon(t)$ and $I'_\varepsilon(t)$ denote the I coordinate of the corresponding solutions. Dividing both sides of (2.30) by $|w_0 - w'_0|$ and taking the limit as $w'_0 \to w_0$, we obtain that

$$|D_{w_0} I_\varepsilon(t)| \leqq 2e^{C^* t}. \tag{2.31}$$

Since estimates similar to (2.31) hold for the time evolution of the other three coordinates of $w_\varepsilon(t)$ and $w'_\varepsilon(t)$, we can also write

$$|D_{w_0} z_{1\varepsilon}(t)|, |D_{w_0} z_{2\varepsilon}(t)|, |D_{w_0} \phi_\varepsilon(t)| \leqq 2e^{C^* t}. \tag{2.32}$$

Then (2.31) and (2.32) give rise to the inequality

$$\| D_{w_0} w_\varepsilon(t) \| \leqq 4e^{C^* t}, \tag{2.33}$$

where, as before, $\| \cdot \|$ denotes the Euclidean matrix norm.

Consider now the I coordinate of the solution $w_\varepsilon(t)$ of (2.6) given by

$$I_\varepsilon(t) = I_{p_\varepsilon} + \varepsilon \int_0^t k_I|_{w_\varepsilon(\tau)} d\tau, \tag{2.34}$$

the differentiation of which with respect to I_{p_ε} yields

$$\frac{dI_\varepsilon(t)}{dI_{p_\varepsilon}} = 1 + \varepsilon \int_0^t \langle Dk_I|_{w_\varepsilon(\tau)}, D_{I_{p_\varepsilon}} w_\varepsilon(\tau) \rangle d\tau. \tag{2.35}$$

Since $w_0 = T^\varepsilon(p_\varepsilon)$, (2.32) and (2.35) lead to the estimate

$$\left| \frac{dI_\varepsilon(t)}{dI_{p_\varepsilon}} - 1 \right| \leqq \varepsilon \int_0^t 4c_{15} e^{C^* \tau} d\tau = \varepsilon \frac{4c_{15}}{C^*} e^{C^* t}, \tag{2.36}$$

where $c_{15} > 0$ is an upper bound for $|Dk_I|$ on $\tilde{U}(\bar{\varepsilon}_0)$. Substituting $t = t_\varepsilon$ and using (2.16) gives

$$\left| \frac{dI_{q_\varepsilon}}{dI_{p_\varepsilon}} - 1 \right| = \left| \frac{dI_\varepsilon(t_\varepsilon)}{dI_{p_\varepsilon}} - 1 \right| \leqq \varepsilon \frac{4c_{15}}{C^*} \left(\frac{\vartheta}{K} \right)^{C^*/c_1 \nu} < K_1 \varepsilon, \tag{2.37}$$

with appropriate $K_1 > 0$. Starting from (2.34) we obtain in the same way that

$$\left| \frac{dI_{q_\varepsilon}}{d\phi_{p_\varepsilon}} \right| \leqq K_1 \varepsilon. \tag{2.38}$$

Also, applying the same argument to

$$\phi_\varepsilon(t) = \phi_{p_\varepsilon} + \int_0^t [z^T B(z, I, \phi; \varepsilon) z + \varepsilon k_\phi(z, I, \phi; \varepsilon)]|_{w_\varepsilon(\tau)} d\tau,$$

we arrive at the expressions

$$\left| \frac{d\phi_{q_\varepsilon}}{d\phi_{p_\varepsilon}} - 1 \right|, \quad \left| \frac{d\phi_{q_\varepsilon}}{dI_{p_\varepsilon}} \right| \leqq K_2 \sqrt{\varepsilon} + K_3 \varepsilon, \tag{2.39}$$

with $K_2, K_3 > 0$. But (2.37), (2.38), and (2.39) imply (2.29) with $\bar{K} = \sqrt{2K_1^2 + K_2^2 + K_3^2}$, which concludes the proof of the lemma. □

3. The energy-phase method: Hamiltonian perturbations

3.1. Main construction

With the estimates and construction of the previous section at hand, we now formulate our main results for the case of purely Hamiltonian perturbations (system (2.1)) under the hypothesis (H2b). First, for any integer $n \geqq 1$ we define the *nth order energy-difference function* $\Delta^n \mathscr{H}: A \to \mathbb{R}$ as

$$\begin{aligned}\Delta^n \mathscr{H}(I, \phi) &= \mathscr{H}(I, \phi + n\Delta\phi(I)) - \mathscr{H}(I, \phi) \\ &= H_1(\bar{x}^0(I), I, \phi + n\Delta\phi(I); 0) - H_1(\bar{x}^0(I), I, \phi; 0). \end{aligned} \tag{3.1}$$

We recall that $\mathscr{H}$ is the reduced Hamiltonian defined in (2.3) and that $\Delta\phi$ is the phase shift defined in (1.11). Note that $\Delta^n \mathscr{H}$ contains *energy*-type information from the perturbed problem and *phase*-type information from the unperturbed problem. The zero set of $\Delta^n \mathscr{H}$ is

$$V_-^n = \{(I, \phi) \in A \,|\, \Delta^n \mathscr{H}(I, \phi) = 0\}. \tag{3.2}$$

We are particularly interested in the transverse zeros of $\Delta^n \mathscr{H}$, which are contained in the set

$$Z_-^n = \{(I, \phi) \in V_-^n \,|\, D\Delta^n \mathscr{H}(I, \phi) \neq (0, 0)\}, \tag{3.3}$$

where D denotes the gradient operator with respect to the (I, ϕ) variables. We also need the $n\,\Delta\phi(I)$ translate of these sets in the ϕ coordinate direction, so we define

$$V_+^n = \mathscr{R}^n(V_-^n), \quad Z_+^n = \mathscr{R}^n(Z_-^n), \tag{3.4}$$

where the map $\mathscr{R}$ is defined in Lemma 2.5. For later convenience we also define

$$V_-^0 = \emptyset. \tag{3.5}$$

In the following we introduce a tool to describe the intersections of the zero sets above with the internal orbits introduced in Definition 2.1.

Definition 3.1. For an internal orbit $\gamma \subset A$ of $\mathscr{H}$ let N denote the minimal nonnegative integer for which γ has no intersection with V_-^k, $k = 0, \ldots, N-1$, but has a nonempty transversal intersection with Z_-^N. If such an N exists, then we call it the *pulse number* of γ and denote it by $N(\gamma)$. In short,

$$N(\gamma) = \min\{n \geqq 1 \,|\, V_-^k \cap \gamma = \emptyset, k = 0, \ldots, n-1, Z_-^n \pitchfork \gamma\}, \tag{3.6}$$

where the symbol $\pitchfork$ refers to nonempty transversal intersection.

Remark 3.1. If, say, γ is tangent to Z_-^n and if $V_-^k \cap \gamma = \emptyset$, $k = 0, \ldots, n-1$, then $N(\gamma)$ is clearly not defined. As we shall see in our beam example in Section 5, this class of internal orbits is distinguished because its members separate orbits with different pulse numbers. Another frequent situation when $N(\gamma)$ may not be defined occurs when the phase shift $\Delta\phi$ is constant and "resonates" with 2π, i.e., there exist relatively prime positive integers N and k such that $N\Delta\phi(I) \equiv 2k\pi$. This case will be discussed separately in the study of resonance bands in Section 3.3, where the appropriate phase shift is always independent of I.

The main result of this section is the following: Suppose that $N(\gamma_0^-) = N$ for an internal orbit γ_0^- of the reduced Hamiltonian. Then γ_0^- approximates a slow orbit γ_ε^- on $\mathscr{A}_\varepsilon$ such that γ_ε^- is the backward limit set of an N-pulse transverse orbit homoclinic to $\mathscr{A}_\varepsilon$. The homoclinic orbit leaves a neighborhood of $\mathscr{A}_\varepsilon$ near the point $g_0(b_-)$ and finally returns to $\mathscr{A}_\varepsilon$ near the point $g_0(b_+)$, where g_0 is defined in (1.5) and

$$b_- = \gamma_0^- \cap Z_-^N, \quad b_+ = \mathscr{R}^N(b_-). \tag{3.7}$$

Furthermore, the positive limit set, γ_ε^+, of the homoclinic orbit can be approximated by an internal orbit γ_0^+ of $\mathscr{H}$ which passes through b_+. During its pulses the homoclinic orbit is "shadowed" by a set Y^N of unperturbed orbits homoclinic to $\mathscr{A}_0$. Y^N is defined as

$$Y^N = \bigcup_{i=1}^{N} y_0^i, \tag{3.8}$$

where $y_0^i \subset W_0$ is an unperturbed orbit of $(1.2)_{\varepsilon=0}$ asymptotic to the points $g_0 \circ \mathscr{R}^{i-1}(b_-)$ and $g_0 \circ \mathscr{R}^i(b_-)$ in negative and positive time, respectively, with $\mathscr{R}^0 \equiv \mathrm{Id}$. The following theorem states all this in precise terms.

Theorem 3.1. *Assume that hypotheses* (H1) *and* (H2b) *hold. Suppose that for an internal orbit* $\gamma_0^- \subset A$ *of the reduced Hamiltonian* $\mathscr{H}$,

(A1) $N \equiv N(\gamma_0^-)$ *is defined.*

(A2) *Let* b_- *and* b_+ *be defined as in* (3.7). *Assume that the orbit* $\gamma_0^+ \subset A$ *of the reduced Hamiltonian* $\mathscr{H}$ *which contains* b_+ *is an internal orbit with* $Z_+^N \pitchfork \gamma_0^+$ *(see Fig. 5).*

(A3) *If* $N > 1$ *and* $D_x H_0$ *points outward on* W_0, *then*

$$\Delta^k \mathscr{H}(b_-) > 0, \quad k = 1, \ldots, N-1.$$

If $N > 1$ *and* $D_x H_0$ *points inward on* W_0, *then*

$$\Delta^k \mathscr{H}(b_-) < 0, \quad k = 1, \ldots, N-1.$$

Then there exists $\varepsilon_0 > 0$ *such that for* $0 < \varepsilon < \varepsilon_0$ *the following hold:*

(i) $\mathscr{A}_\varepsilon$ *has an* N*-pulse homoclinic orbit* y_ε^N *which is positively asymptotic to an internal orbit* $\gamma_\varepsilon^+ \subset \mathscr{A}_\varepsilon$ *and negatively asymptotic to an internal orbit* $\gamma_\varepsilon^- \subset \mathscr{A}_\varepsilon$. *Moreover,* $g_\varepsilon^{-1}(\gamma_\varepsilon^+)$ *and* γ_0^+, *as well as* $g_\varepsilon^{-1}(\gamma_\varepsilon^+)$ *and* γ_0^+, *are* (ε, C^0)*-close. If* γ_0^+ *is periodic, then* C^0 *can be replaced by* C^r *in this last statement.*

(ii) y_ε^N *lies in the intersection of* $W^u(\gamma_\varepsilon^-)$ *and* $W^s(\gamma_\varepsilon^+)$, *which is transversal within the energy surface* $E_\varepsilon(h)$, *where* $h = H|\gamma_\varepsilon^+ = H|\gamma_\varepsilon^-$.

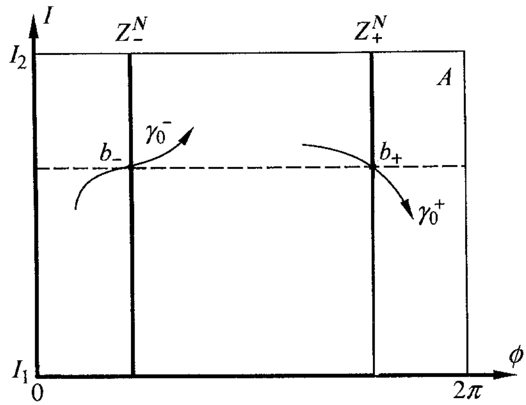

Fig. 5. Assumption (A2) of Theorem 3.1.

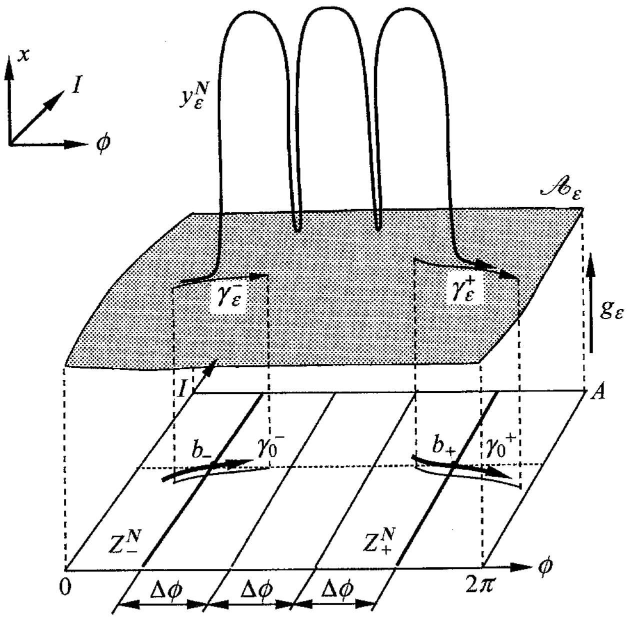

Fig. 6. An example of the statement (iii) of Theorem 3.1 for $N = 3$.

(iii) *Outside a neighborhood of* $\mathscr{A}_\varepsilon$, y_ε^N *is* $(\sqrt{\varepsilon}, C^1)$*-close to the set* Y^N *defined in* (3.8) (*see Fig.* 6 *for an example*).

Proof. For convenience, throughout the proof we use the symbol $\overset{s,\varepsilon^\beta}{\sim}$ for (ε^β, C^s)-closeness of sets and maps.

Let us start by letting $h_0^- = \mathscr{H}|\gamma_0^-$. Note that by the compactness of A and the smoothness of the reduced Hamiltonian $\mathscr{H}$ (see (2.3)) there exists $\kappa > 0$

such that

$$\|h_0^-\| < \frac{\kappa}{2}. \tag{3.9}$$

For this κ we select some $\vartheta > \vartheta^{(0)} \equiv \vartheta^*$ to ensure the applicability of Lemmas 2.4 and 2.5 (see the statements of these lemmas).

Our second observation, following from Definition 3.1, is that if $\gamma_0^- \pitchfork Z_-^N$, then

$$\mathscr{R}^k(\gamma_0^-) \cap \gamma_0^+ = \emptyset, \quad k = 1, \ldots, N-1, \quad \mathscr{R}^N(\gamma_0^-) \pitchfork \gamma_0^+, \quad \mathscr{H}|\gamma_0^+ = h_0^-. \tag{3.10}$$

(The first part of this statement is vacuous for $N = 1$.) Since γ_0^- is an internal orbit, for small ε, $\mathscr{A}_\varepsilon$ contains an internal orbit γ_ε^- of $\mathscr{H}_\varepsilon$ such that

$$g_\varepsilon^{-1}(\gamma_\varepsilon^-) \overset{r,\varepsilon}{\sim} \gamma_0^-, \tag{3.11}$$

where the embedding g_ε of $\mathscr{A}_\varepsilon$ is defined in (1.7). Let

$$h = H|\gamma_\varepsilon^- = \mathscr{H}_\varepsilon|\gamma_\varepsilon^- = h_0 + \varepsilon h_0^- + \mathcal{O}(\varepsilon^2), \tag{3.12}$$

with h_0 defined in (2.4). Since γ_0^+ is also an internal orbit, $D\mathscr{H}|\gamma_0^+ \neq 0$. (If γ_0^+ is a homoclinic or heteroclinic orbit in A, this statement is not true on its closure.) If γ_0^+ is a periodic orbit (i.e., a member of a family of periodic orbits of $\mathscr{H}$), by the implicit function theorem there exists a periodic internal orbit γ_ε^+ such that $g_\varepsilon^{-1}(\gamma_\varepsilon^+) \overset{r,\varepsilon}{\sim} \gamma_0^+$ and

$$H|\gamma_\varepsilon^+ = \mathscr{H}_\varepsilon|\gamma_\varepsilon^+ = h. \tag{3.13}$$

If γ_0^+ is not periodic, then it is a homoclinic or heteroclinic orbit (see Definition 2.1). In that case it perturbs to a nearby homoclinic or heteroclinic orbit, but one that does not necessarily have energy h. However, since there are internal periodic orbits arbitrarily close to γ_0^+, we can guarantee that there exists an internal orbit γ_ε^+ such that

$$g_\varepsilon^{-1}(\gamma_\varepsilon^+) \overset{1,\varepsilon}{\sim} \gamma_0^+ \tag{3.14}$$

inside a fixed neighborhood of Z_+^N, and (3.13) still holds. Then, for ε small enough, (3.10), (3.11), and (3.14) imply that

$$\mathscr{R}^k(g_\varepsilon^{-1}(\gamma_\varepsilon^-)) \cap g_\varepsilon^{-1}(\gamma_\varepsilon^+) = \emptyset, \quad k = 1, \ldots, N-1, \quad \mathscr{R}^N(g_\varepsilon^{-1}(\gamma_\varepsilon^-)) \pitchfork g_\varepsilon^{-1}(\gamma_\varepsilon^+). \tag{3.15}$$

Furthermore, we see from (3.9), (3.12), and (3.13) that for small $\varepsilon > 0$,

$$\|h - h_0\| = \|H|\gamma_\varepsilon^+ - h_0\| = \|H|\gamma_\varepsilon^- - h_0\| = \varepsilon\|h_0^- + \mathcal{O}(\varepsilon)\| < \varepsilon\kappa. \tag{3.16}$$

Hence the trajectories in $W^{\mathrm{u}}(\gamma_\varepsilon^-)$ obey the maximal distance condition required for the application of Lemmas 2.4 and 2.5.

By Proposition 2.1, γ_ε^- has a C^r local unstable manifold $W_{\mathrm{loc}}^{\mathrm{u}}(\gamma_\varepsilon^-) \subset W_{\mathrm{loc}}^{\mathrm{u}}(\mathscr{A}_\varepsilon)$, which consists of a subfamily of unstable fibers $f_\varepsilon^{\mathrm{u}}$ (i.e., a smooth subset of the family $\mathscr{F}_\varepsilon^{\mathrm{s}}$) with their basepoints contained in γ_ε^-. In the usual way $W_{\mathrm{loc}}^{\mathrm{u}}(\gamma_\varepsilon^-)$ can be

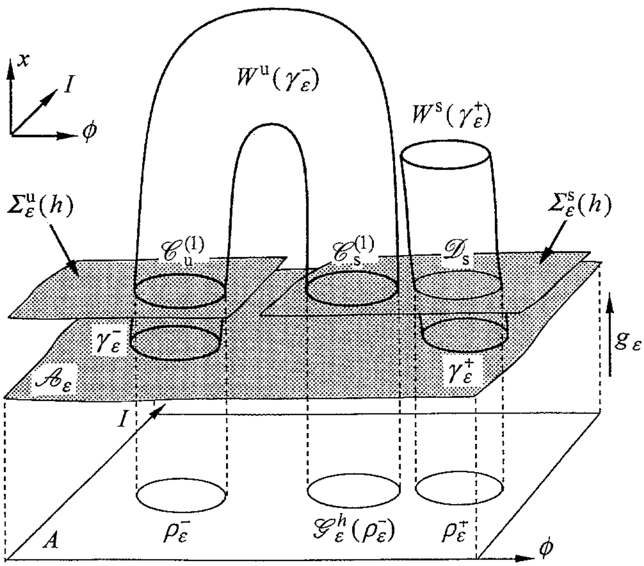

Fig. 7. The main construction in the proof of Theorem 3.1.

extended to an injectively immersed global manifold $W^{\mathrm{u}}(\gamma_\varepsilon^-) \subset E_\varepsilon(h)$. Now by (3.16) and (ii) of Lemma 2.4, for small $\varepsilon > 0$, the Poincaré section $\Sigma_\varepsilon^{\mathrm{u}}(h)$ is a two-dimensional graph over A. Since it is also a local transversal to the flow in the energy surface $E_\varepsilon(h)$, it is intersected transversally (within $E_\varepsilon(h)$) by $W_{\mathrm{loc}}^{\mathrm{u}}(\gamma_\varepsilon^-)$ in a curve $\mathscr{C}_{\mathrm{u}}^{(1)} \subset \Sigma_\varepsilon^{\mathrm{u}}(h)$ (see Fig. 7). By Proposition 2.1,

$$\rho_\varepsilon^- = (e_\varepsilon^{\mathrm{u}})^{-1}(\mathscr{C}_{\mathrm{u}}^{(1)}) \overset{1,\sqrt{\varepsilon}}{\sim} g_\varepsilon^{-1}(\gamma_\varepsilon^{-1}). \tag{3.17}$$

By (ii) of Lemma 2.5, the global map G_ε^h is defined on $\mathscr{C}_{\mathrm{u}}^{(1)}$. Let us define $\mathscr{C}_{\mathrm{s}}^{(1)} = G_\varepsilon^h(\mathscr{C}_{\mathrm{u}}^{(1)})$ (see Fig. 7) and note that from (2.27) and (3.17) we have $(e_\varepsilon^{\mathrm{s}})^{-1}(\mathscr{C}_{\mathrm{s}}^{(1)}) = \mathscr{G}_\varepsilon^h(\rho_\varepsilon^-)$.

Similarly, $W_{\mathrm{loc}}^{\mathrm{s}}(\gamma_\varepsilon^+)$ intersects the Poincaré section $\Sigma_\varepsilon^{\mathrm{s}}(h)$ in a curve $\mathscr{D}_{\mathrm{s}} \subset \Sigma_\varepsilon^{\mathrm{s}}(h)$. As shown in Fig. 7, we define $\rho_\varepsilon^+ = (e_\varepsilon^{\mathrm{s}})^{-1}(\mathscr{D}_{\mathrm{s}})$ and conclude from Proposition 2.1 that

$$\rho_\varepsilon^+ \overset{1,\sqrt{\varepsilon}}{\sim} g_\varepsilon^{-1}(\gamma_\varepsilon^+). \tag{3.18}$$

Then (3.10), (3.17), and (3.18) imply that

$$\mathscr{R}^k(\rho_\varepsilon^-) \cap \rho_\varepsilon^+ = \emptyset, \quad k = 1, \ldots, N-1, \quad \mathscr{R}^N(\rho_\varepsilon^-) \pitchfork \rho_\varepsilon^+. \tag{3.19}$$

(As we noted after (3.10), for $N = 1$ only the second part of this statement is meaningful.) For future reference we now introduce the tracking map $\mathscr{T}_{\varepsilon,N}^h \colon A \to A$ by

$$\mathscr{T}_{\varepsilon,N}^h = \mathscr{G}_\varepsilon^h \circ \underbrace{(\mathscr{L}_\varepsilon^h \circ \mathscr{G}_\varepsilon^h) \circ \cdots \circ (\mathscr{L}_\varepsilon^h \circ \mathscr{G}_\varepsilon^h)}_{N-1}, \tag{3.20}$$

which (if well-defined) will be used to track the graph-projections of subsequent intersections of $W^{\mathrm{u}}(\gamma_\varepsilon^-)$ with the Poincaré section $\Sigma_\varepsilon^{\mathrm{s}}(h)$.

We first consider the case of one-pulse orbits, i.e., we assume that $N = 1$. Then for small $\varepsilon > 0$, (3.19), (3.20), and (ii), (iii) of Lemma 2.5 imply

$$\mathscr{T}^h_{\varepsilon,1}(\rho_\varepsilon^-) \pitchfork \rho_\varepsilon^+, \tag{3.21}$$

which, by the commutative diagrams of (2.27) proves that $\mathscr{C}_{\mathrm{s}}^{(1)} \pitchfork \mathscr{D}_{\mathrm{s}}$ within $\Sigma_\varepsilon^{\mathrm{s}}(h)$. ($e_\varepsilon^{\mathrm{s}}$ is a diffeomorphism). But this in turn implies that $W^{\mathrm{u}}(\gamma_\varepsilon^-) \pitchfork W^{\mathrm{s}}(\gamma_\varepsilon^+)$ within $E_\varepsilon(h)$, as asserted in (ii) of the lemma. Also, (iii) follows from the size of $U_{\delta(\varepsilon)}$ and the fact that $g_0 \circ \mathscr{R} \circ g_0^{-1}$ maps α-limit points of unperturbed homoclinic trajectories to their ω-limit points.

Let us now suppose that $N = 2$. From what we have discussed up till now it follows that in this case, for small ε, $\mathscr{C}_{\mathrm{s}}^{(1)} \cap \mathscr{D}_{\mathrm{s}} = \emptyset$. (Hence the trajectories of (1.2) enter $U_{\delta(\varepsilon)}$ without intersecting $\tilde{W}^{\mathrm{s}}_{\mathrm{loc}}(\mathscr{A}_\varepsilon)$.) Using (2.11) we know that for small ε, $T^\varepsilon(U_{\delta(\varepsilon)})$ is contained in a tubular neighborhood of the manifold $z = 0$ in the phase space of (2.6), which is a subset of $\tilde{U}(\bar{\varepsilon}_0)$. This means that the trajectories described above that miss $\mathscr{D}_{\mathrm{s}}$ enter a neighborhood of $\mathscr{A}_\varepsilon$ in which their behavior is described by the normal form (2.6). Consequently, in compliance with the normal hyperbolicity of $\mathscr{A}_\varepsilon$, they make a near-saddle passage and leave a neighborhood of $\mathscr{A}_\varepsilon$.

The hypersurface $W^{\mathrm{s}}_{\mathrm{loc}}(\mathscr{A}_\varepsilon)$ locally divides the phase space into two disjoint components. Since we have only assumed the existence of one homoclinic structure, we are only able to use our tracking construction for solutions which again travel in a neighborhood of the homoclinic structure W_0 after their near-saddle type passage. In other words, we have to make sure that solutions in $W^{\mathrm{u}}(\gamma_\varepsilon^-)$ leave a neighborhood of $\mathscr{A}_\varepsilon$ near the component $\tilde{W}^{\mathrm{u}}_{\mathrm{loc}}(\mathscr{A}_\varepsilon)$ of $W^{\mathrm{u}}_{\mathrm{loc}}(\mathscr{A}_\varepsilon)$ (see the discussion after Lemma 2.3).

Suppose that the first of the two cases in assumption (A3) holds. Then for small ε, $D_x H$ points in a direction away from the interior of W_0. Consequently, if a solution arriving in a neighborhood of $\mathscr{A}_\varepsilon$ has a lower energy than nearby orbits in $W^{\mathrm{s}}_{\mathrm{loc}}(\mathscr{A}_\varepsilon)$, then it passes $\mathscr{A}_\varepsilon$ and exists near $\tilde{W}^{\mathrm{u}}_{\mathrm{loc}}(\mathscr{A}_\varepsilon)$, as required. But condition (A3) with $k = 1$ ensures exactly this since it requires the leading-order term in the energy of γ_ε^- to be smaller than the leading-order terms in the energies of slow orbits whose local unstable manifolds foliate $W^{\mathrm{s}}_{\mathrm{loc}}(\mathscr{A}_\varepsilon)$ near the entry of $W^{\mathrm{u}}(\mathscr{A}_\varepsilon)$. Here we used the fact that the intersections of the local stable manifolds of slow orbits with $\Pi_\varepsilon^{\mathrm{s}}$ project down to curves in A which are $(\sqrt{\varepsilon}, C^1)$-close to the projections of slow orbits themselves under g_ε^{-1}. This follows from the fibering of the local stable manifold (Proposition 2.1) and the properties of the Pointcaré in Lemma 2.4. A similar argument gives the correct exit direction when the second case in assumption (A3) holds, i.e., when $D_x H_0$ points in a direction away from the interior of W_0. Furthermore, for $k = 1, \ldots, N-1$, assumption (A3) guarantees an exit in the correct direction for the kth passage.

Knowing the basic character of passage near $\mathscr{A}_\varepsilon$ of the trajectories starting from $\mathscr{C}_{\mathrm{s}}^{(1)}$, we expect to be able to track them via the local map L_ε^h. By Lemma 2.5, we have a good approximation for the conjugate map $\mathscr{L}_\varepsilon^h$, provided the minimal distance condition (2.28) is satisfied for an appropriate $0 < K < \vartheta$. The next step in our construction is to verify this, i.e., to ensure that the incoming trajectories do not enter $U_{\delta(\varepsilon)}$ too close to $W^{s}_{\text{loc}}(\mathscr{A}_\varepsilon)$.

Since $\text{cl}(\gamma_0^-)$ is compact and, by assumption (A1), is separated from Z^1_-, assumption (A3) implies the existence of a positive number $K^{(1)} > 0$ such that

$$\| h_0^- - \mathscr{H} | \mathscr{R}(\gamma_0^-) \| > 2K^{(1)}. \tag{3.22}$$

Based on the nature of the foliation of $\tilde{W}^{s}_{\text{loc}}(\mathscr{A}_\varepsilon) \cap \partial_1 U_{\delta(\varepsilon)}$ by local stable manifolds of slow orbits (Proposition 2.1) and on the $(\sqrt{\varepsilon},\ C^1)$-closeness of the objects involved, we conclude from (3.12) and (3.22) that if $p_c \in \mathscr{C}^{(1)}_{\text{s}}$ and $p_w \in \tilde{W}^{s}_{\text{loc}}(\mathscr{A}_\varepsilon)$ are two points with the same (I, ϕ) coordinates, then

$$\begin{aligned} \| H|_{p_c} - H|_{p_w} \| &= \| h - [h_0 + \varepsilon \mathscr{H} [g_{W^s}^{-1}(p_w) + \mathscr{O}(\varepsilon \sqrt{\varepsilon})] \| \\ &= \| h_0 + \varepsilon h_0^- + \mathscr{O}(\varepsilon\sqrt{\varepsilon}) - [h_0 + \varepsilon \mathscr{H}|_{p_w^0} + \mathscr{O}(\varepsilon\sqrt{\varepsilon})] \| \\ &= \varepsilon \| h_0^- - \mathscr{H}|_{p_w^0} + \mathscr{O}(\sqrt{\varepsilon}) \| > K^{(1)}\varepsilon, \end{aligned} \tag{3.23}$$

where $p_w^0 \in \mathscr{R}(\gamma_0^-)$ is a point $\sqrt{\varepsilon}$-close to $g_{W^s}^{-1}(p_w)$ with $g_{W^s}: A \to \mathscr{P}$ being the embedding of $\tilde{W}^{s}_{\text{loc}}(\mathscr{A}_\varepsilon) \cap \partial_1 U_{\delta(\varepsilon)}$. For an appropriate $c_{16} > 0$ let $c_{16} \vartheta \sqrt{\varepsilon}$ be an upper bound for $\| DH \|$ in $U_{\delta(\varepsilon)}$ (see (2.20) and compare (2.21)). Then the mean value theorem and (3.23) imply that

$$\varepsilon K^{(1)} < \| H|_{p_c} - H|_{p_w} \| \leqq c_{16} \vartheta \sqrt{\varepsilon} \| p_c - p_w \|,$$

which yields

$$\| p_c - p_w \| \geqq \frac{K^{(1)}}{c_{16} \vartheta} \sqrt{\varepsilon}. \tag{3.24}$$

If we set $S^{s}_{\varepsilon}(h) \equiv \text{cl}(\mathscr{C}^{(1)}_{\text{s}})$, then the minimal distance condition (2.28) of Lemma 2.5 is satisfied provided we choose

$$0 < \frac{K^{(1)}}{c_{16} \vartheta} < \vartheta \ \Rightarrow \ \vartheta > \vartheta^{(1)} = \max\left(\vartheta^0, \sqrt{\frac{K^{(1)}}{c_{16}}} \right).$$

In this case, by (iii) of Lemma 2.5, for $\varepsilon > 0$ sufficiently small, the trajectories starting from $\mathscr{C}^{(1)}_{\text{s}}$ intersect $\Sigma^{\text{u}}_{\varepsilon}(h)$ in a curve $\mathscr{C}^2_{\text{u}} = L^h_\varepsilon(\mathscr{C}^{(1)}_{\text{s}})$. Moreover, by (ii) of Lemma 2.5 they later reintersect $\Sigma^{s}_{\varepsilon}(h)$ in a curve $\mathscr{C}^{(2)}_{\text{s}}$ with

$$\mathscr{C}^{(2)}_{\text{s}} = G^h_\varepsilon(\mathscr{C}^{(2)}_{\text{u}}) = G^h_\varepsilon \circ L^h_\varepsilon \circ G^h_\varepsilon(\mathscr{C}^{(1)}_{\text{u}}). \tag{3.25}$$

Also, by Lemma 2.5, the commutative diagrams of (2.27), (3.20), and (3.25) show that

$$\mathscr{T}^{h}_{\varepsilon, 2}(\rho_\varepsilon^-) \overset{1,\sqrt{\varepsilon}}{\sim} \mathscr{R}^2(\rho_\varepsilon^-). \tag{3.26}$$

Then, as in the case of $N = 1$, (3.19), (3.18) and (3.26) imply that

$$\mathscr{T}^{h}_{\varepsilon, 2}(\rho_\varepsilon^-) \pitchfork \rho_\varepsilon^+.$$

From this, by the same argument as in the case $N = 1$, we conclude statements (i)–(iii) of the theorem for $N = 2$ and for some ε_0 bound on ε.

One can now repeat the above construction for any $N > 2$. Assumption (A3) ensures a repeated "nice" passage of the orbits in $W^u(\gamma_\varepsilon^-)$ near $\mathscr{A}_\varepsilon$. At the jth passage ($j < N$) we find an appropriate constant $K^{(j)} \geqq K^{(j-1)} > 0$ (see (3.23)) to describe the energy difference between orbits in $W^u(\gamma_\varepsilon^-)$ and nearby orbits in $\tilde{W}^s(\mathscr{A}_\varepsilon)$. This provides us with an estimate of the form (3.24) for the local distance of the two manifolds. To follow the passage via the local map L_ε^h, we select the size of $U_{\delta(\varepsilon)}$ by setting

$$\vartheta = \vartheta^{(j)} = \max\left(\vartheta^{(j-1)}, \sqrt{\frac{K^{(j)}}{c_{15}}}\right).$$

We define $\mathscr{C}_u^{(j+1)} = L_\varepsilon^h(\mathscr{C}_s^{(j)})$ and apply the global map G_ε^h to $\mathscr{C}_u^{(j+1)}$. We define the curve

$$\mathscr{C}_s^{(j+1)} = G_\varepsilon^h(\mathscr{C}_u^{(j)}),$$

which is the $(j+1)$st intersection (in forward time) of $W^u(\gamma_\varepsilon^-)$ with $\Sigma_\varepsilon^s(h)$. Note that by Lemma 2.5

$$\mathscr{T}_{\varepsilon, j+1}^h(\rho_\varepsilon^-) = (e_\varepsilon^s)^{-1}(\mathscr{C}_s^{(j+1)}) \overset{1,\sqrt{\varepsilon}}{\sim} \mathscr{R}^{j+1}(\rho_\varepsilon^-). \tag{3.27}$$

If $j + 1 = N$, then (3.19), (3.18), and (3.27) imply that

$$\mathscr{T}_{\varepsilon, N}^h(\rho_\varepsilon^-) \pitchfork \rho_\varepsilon^+,$$

which proves the theorem the same way as in the case $N = 2$. If $j + 1 < N$ we repeat the above construction recursively until we reach N. At every step we possibly need to decrease the current bound $\varepsilon_0^{(j)} > 0$ on ε to be able to proceed further. Since N is finite, we can finally select $\varepsilon_0 \equiv \varepsilon_0^{(N)} > 0$ so that the statements of the theorem hold. □

An immediate consequence of Theorem 3.1 is

Theorem 3.2. *Assume that hypotheses* (H1) *and* (H2b) *are satisfied and assumptions* (A1)–(A3) *of Theorem 3.1 hold. Assume further that $\gamma_0^+ = \gamma_0^-$ of Theorem 3.1 is a periodic orbit in A. Then*

(i) *The statements of Theorem 3.1 hold with $\gamma_\varepsilon = \gamma_\varepsilon^+ = \gamma_\varepsilon^-$, i.e., the N-pulse orbit y_ε^N is homoclinic to a slow periodic orbit γ_ε.*

(ii) *System* (1.2) *has Smale horseshoes near γ_ε on energy surfaces sufficiently close to $E_\varepsilon(h)$.*

Proof. Statement (i) follows from the fact that internal orbits are locally energetically unique, so $\gamma_\varepsilon^+ = \gamma_\varepsilon^-$ must hold. Statement (iii) follows from the Smale-Birkhoff homoclinic theorem (see SMALE [41]) and the structural stability of horseshoes. □

The statement of Theorem 3.2 is sketched in Fig. 8 for the case $N = 3$.

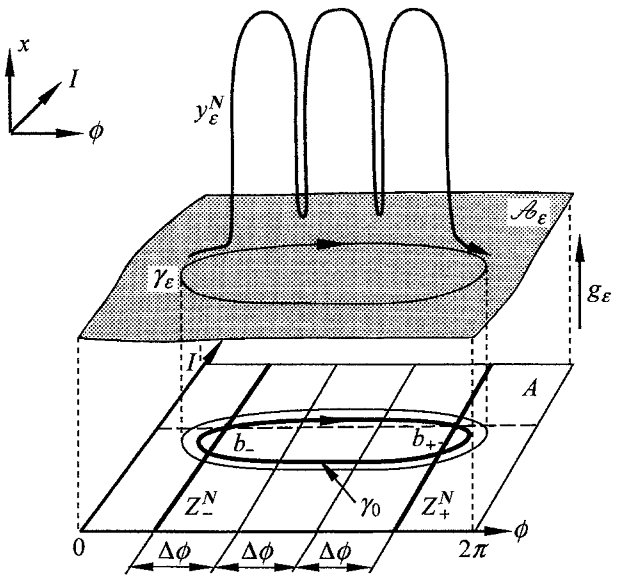

Fig. 8. The statement of Theorem 3.2 for $N = 3$.

Remark 3.2. In the case $N = 1$, Theorem 3.1 gives a result similar to that of HALLER & WIGGINS [19]. In that reference, however, we obtained better smoothness results for the distance of y_ε^1 and the set Y^1. The reason is that to detect simple (i.e., one-pulse) orbits homoclinic to the manifold $\mathscr{A}_\varepsilon$ one does not have to deal with the complications related to the passage near $\mathscr{A}_\varepsilon$ and can select a fixed tubular neighborhood U_{δ_0} around $\mathscr{A}_\varepsilon$ to work with.

Remark 3.3. It follows from the proof of Theorem 3.1 that the first intersections of N-pulse orbits with the sections $\Sigma_\varepsilon^{\mathrm{u}}(h)$ form a smooth curve. Each point on this curve lies on an unstable fiber, so by Proposition 2.1 the basepoints of these fibers from a C^r curve $B_{\mathrm{u},\varepsilon}^N \subset \mathscr{A}_\varepsilon$, which depends smoothly on ε and other parameters in the system. We refer to $B_{\mathrm{u},s}^N \subset \mathscr{A}_\varepsilon$ as the *N-take-off curve*, because the N-pulse orbits leave the immediate vicinity of $\mathscr{A}_\varepsilon$ near this curve. We also define the *take-off point* p_ε of an N-pulse orbit y_ε^N to be

$$p_\varepsilon = B_{\mathrm{u},\varepsilon}^N \cap \gamma_\varepsilon^-,$$

where γ_ε^- is the orbit on the slow manifold to which y_ε^N asymptotes in backward time (see Fig. 9). Note that $g_\varepsilon^{-1}(B_{\mathrm{u},\varepsilon}^N)$ can be smoothly approximated with an error of $\mathcal{O}(\sqrt{\varepsilon})$ by a subset z_-^N of the transverse zero set Z_-^N. This subset is defined as

$$z_-^N = \{p \in Z_-^N \mid \exists \gamma\colon N(\gamma) = N, \gamma \pitchfork Z_-^N, p \in \gamma \cap Z_-^N\}. \tag{3.28}$$

Similarly, upon their final return the N-pulse orbits homoclinic to $\mathscr{A}_\varepsilon$ intersect a one-parameter family of stable fibers whose basepoints form the *N-landing curve*

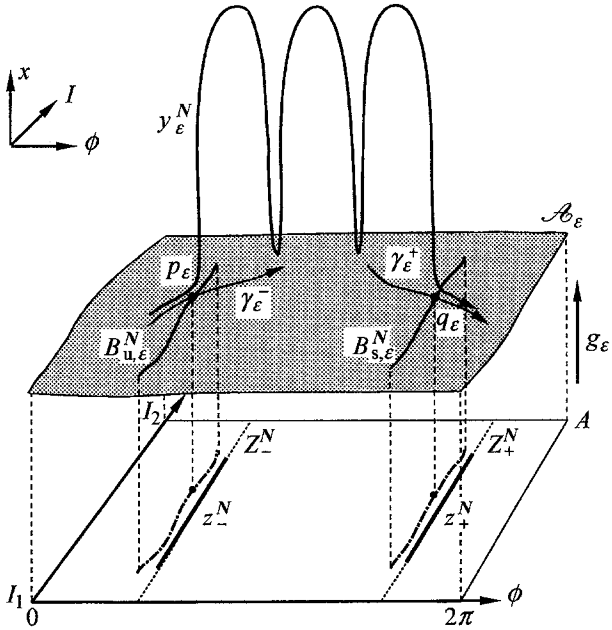

Fig. 9. The take-off and landing points and curves.

$B_{s,\varepsilon}^N \subset \mathscr{A}_\varepsilon$. We define the *landing point* of the N-pulse orbit y_ε^N as

$$q_\varepsilon = B_{s,\varepsilon}^N \cap \gamma_\varepsilon^+,$$

where γ_ε^+ is the orbit on the slow manifold to which y_ε^N asymptotes in forward time (see Fig. 9). Again, the set $g_\varepsilon^{-1}(B_{N,\varepsilon}^u)$ is $(\sqrt{\varepsilon}, C^1)$-close to

$$z_+^N = \mathscr{R}^N(z_-^N). \tag{3.29}$$

It follows from Theorem 3.1 that the I coordinates of the take-off and landing points of a given N-pulse orbit y_ε^N differ by $\mathscr{O}(\sqrt{\varepsilon})$. The landing and take-off points and curves prove especially useful in Section 4 when we discuss how the families of Hamiltonian multi-pulse orbits change under dissipative perturbations.

3.2. *Jumping N-pulse orbits*

Theorem 3.1 contains the basic construction of N-pulse homoclinic orbits to the manifold $\mathscr{A}_\varepsilon$ in the case of purely Hamiltonian perturbations in system (1.2). In this subsection we give an important extension of the results to the case when the unperturbed system admits two homoclinic manifolds, i.e.,

(H1′) There exist $I_1 < I_2$ such that for any $I \in [I_1, I_2]$, $(1.2)_{\varepsilon=0}^x$ has a hyperbolic fixed point $\bar{x}_0(I)$ connected to itself by two homoclinic trajectories, $x^{h+}(t, I)$ and $x^{h-}(t, I)$.

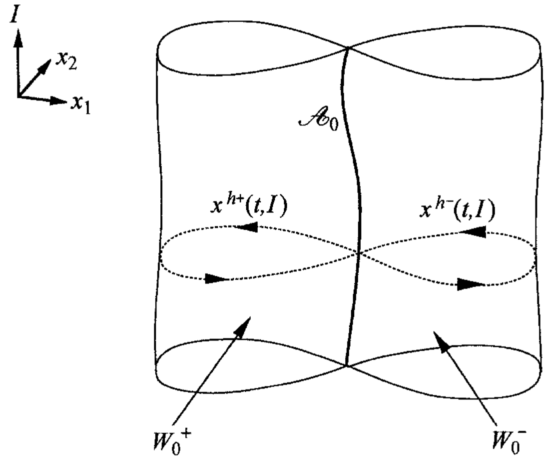

Fig. 10. The geometry of hypothesis (H1′).

This hypothesis implies the existence of two homoclinic manifolds W_0^+ and W_0^- (see Fig. 10). which contain solutions $y_0^+(t, I, \phi_0)$ and $y_0^-(t, I, \phi_0)$ of $(1.2)_{\varepsilon=0}$ (compare (1.6) and substitute $x^{h+}(t, I)$ and $x^{h-}(t, I)$, respectively). Hypothesis (H1′) is satisfied in our main example described in Section 1.2 as well as in many other applications. Here we restrict the discussion to the case when both homoclinic manifolds admit the same phase shift, i.e.,

$$\textbf{(H3)} \qquad \Delta\phi(I) = \int_{-\infty}^{+\infty} D_I H_0(x^{h+}(t, I), I)\, dt \equiv \int_{-\infty}^{+\infty} D_I H_0(x^{h-}(t, I), I)\, dt.$$

This assumption is not essential but greatly simplifies the formulation of the results. Moreover, in most applications the existence of *two* manifolds homoclinic to $\mathscr{A}_\varepsilon$ is the result of a discrete symmetry in the problem, which also ensures that hypothesis (H3) holds. For the case of unequal phase shifts the reader is referred to HALLER & WIGGINS [23].

In Theorem 3.3 we give conditions for the existence of *jumping N-pulse homoclinic orbits* to the manifold $\mathscr{A}_\varepsilon$. These orbits make N departures and returns, as do the N-pulse homoclinic orbits of Theorem 3.1, but they may change the unperturbed homoclinic manifold they temporarily follow. This behavior is described by a sequence of two symbols:

Definition 3.2. Let $j = \{j_i\}_{i=1}^N, j_i \in \{+1, -1\}$ be a finite sequence. We say that an N-pulse orbit y_ε^N homoclinic to the slow manifold $\mathscr{A}_\varepsilon$ of system (2.1) is *a jumping orbit with jump sequence* $j \equiv j(y_\varepsilon^N)$ if there exists a point $b_- \in A$ and a constant $\varepsilon_0 > 0$ such that for $0 < \varepsilon < \varepsilon_0$, outside a fixed, small neighborhood of $\mathscr{A}_\varepsilon$, y_ε^N is $(\sqrt{\varepsilon}, C^1)$-close to the set

$$Y_j^N = \bigcup_{i=1}^N y_0^i, \tag{3.30}$$

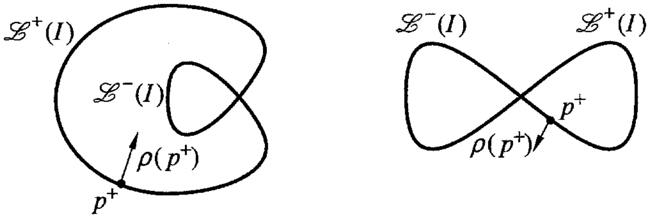

Fig. 11. The definition of the normal $\rho(p^+)$ in two cases.

where

$$y_0^i \subset \begin{cases} W_0^+ & \text{if } j_i = +1, \\ W_0^- & \text{if } j_i = -1, \end{cases} \tag{3.31}$$

is an unperturbed orbit of $(1.2)_{\varepsilon=0}$ asymptotic to the points $g_0(\mathscr{R}^{i-1}(b_-))$ and $g_0(\mathscr{R}^i(b_-))$ in negative and positive time, respectively ($\mathscr{R}^0 \equiv \mathrm{Id}$).

Consider now the homoclinic loops

$$\mathscr{L}^+(I) = \{x^{h+}(t;I)\}_{t=-\infty}^{+\infty}, \quad \mathscr{L}^-(I) = \{x^{h-}(t;I)\}_{t=-\infty}^{+\infty}. \tag{3.32}$$

The loop $\mathscr{L}^+(I)$ divides the (x_1, x_2)-plane into two disjoint open sets, the exterior $\mathrm{Ext}(\mathscr{L}^+(I))$ and the interior $\mathrm{Int}(\mathscr{L}^+(I))$ of $\mathscr{L}^+(I)$. Let us pick a point $p^+ \in \mathscr{L}^+(I)$ and let $\rho(\rho^+)$ denote the unit normal to $\mathscr{L}^+(I)$ at the point p^+ pointing in the direction of the other homoclinic loop $\mathscr{L}^-(I)$. In other words, $\rho(p^+)$ points to $\mathrm{Ext}(\mathscr{L}^+(I))$ if $\mathscr{L}^-(I) \subset \mathrm{Ext}(\mathscr{L}^+(I))$, and $\rho(p^+)$ points to $\mathrm{Int}(\mathscr{L}^+(I))$ if $\mathscr{L}^-(I) \subset \mathrm{Int}(\mathscr{L}^+(I))$, as shown in Fig. 11. We define the sign constant

$$\sigma = \mathrm{sign}\langle D_x H_0|_{p^+}, \rho(p^+)\rangle. \tag{3.33}$$

Note that σ is independent of I and of the choice of p^+ because of the normal hyperbolicity of the unperturbed manifold $\mathscr{A}_0$. The sign constant σ also remains the same if we interchange the roles of $\mathscr{L}^+(I)$ and $\mathscr{L}^-(I)$.

Remark 3.4. Notice that σ gives information about the local unperturbed flow near $\mathscr{A}_0$. Namely, σ identifies the later exit direction of trajectories entering a neighborhood U_{δ_0} of $\mathscr{A}_0$ close to $W^{s+} \equiv W^s_{\mathrm{loc}}(\mathscr{A}_0) \cap W_0^+$. If $\sigma = +1$, then trajectories with energies higher than $H_0 | W^s_{\mathrm{loc}}(\mathscr{A}_0)$ exit in the direction of $W^{u-} \equiv W^u_{\mathrm{loc}}(\mathscr{A}_0) \cap W_0^-$ and trajectories with energies lower than $H_0 | W^s_{\mathrm{loc}}(\mathscr{A}_0)$ exit in the direction of $W^{u+} \equiv W^u_{\mathrm{loc}}(\mathscr{A}_0) \cap W_0^+$. Similarly, if $\sigma = -1$, then trajectories with energies higher than $H_0 | W^s_{\mathrm{loc}}(\mathscr{A}_0)$ exit in the direction of W^{u+} and trajectories with energies lower than $H_0 | W^s_{\mathrm{loc}}(\mathscr{A}_0)$ exit in the direction of W^{u-}. This propety of σ is clearly preserved for small perturbations, as we see by comparing the energy of a trajectory to $H | W^s_{\mathrm{loc}}(\mathscr{A}_\varepsilon)$ near the point where the trajectory enters U_{δ_0}. Also, σ has the same meaning for the passage of trajectories that enter U_{δ_0} near $W^{s-} \equiv W^s_{\mathrm{loc}}(\mathscr{A}_0) \cap W_0^-$.

Using the sign constant σ we now associate sign sequences to internal orbits of the reduced Hamiltonian $\mathscr{H}$.

Definition 3.3. Let γ be an internal orbit of the reduced Hamiltonian $\mathscr{H}$ and suppose that $N(\gamma) = N$. Then the *positive sign sequence* $\chi^+(\gamma) = \{\chi_k^+(\gamma)\}_{k=1}^N$ of γ is defined as

$$\chi_1^+(\gamma) = +1, \quad \chi_{k+1}^+(\gamma) = \sigma \operatorname{sign}(\Delta^k \mathscr{H}|\gamma)\chi_k^+(\gamma), \quad k = 1, \ldots, N-1. \quad (3.34)$$

The *negative sign sequence* of γ is defined as $\chi^-(\gamma) = -\chi^+(\gamma)$.

Note that the assumption $N(\gamma) = N$ is important for the sign sequences to be well defined because it implies that the continuous function $\Delta^k\mathscr{H}$ has a constant sign on γ for $k = 1, \ldots, N-1$.

The following theorem establishes the existence of jumping N-pulse homoclinic orbits to the slow manifold $\mathscr{A}_\varepsilon$ based on the sign sequences of internal orbits.

Theorem 3.3. *Assume that hypotheses* (H1′), (H2b), *and* (H3) *hold. Suppose that for an internal orbit $\gamma_0^- \subset A$ of the reduced Hamiltonian $\mathscr{H}$, the assumptions* (A1) *and* (A2) *of Theorem 3.1 are satisfied. Then for ε sufficiently small there exists a jumping N-pulse orbit y_ε^{N+} with jump sequence $j(y_\varepsilon^{N+}) = \chi^+(\gamma_0^-)$ and a jumping N-pulse orbit y_ε^{N-} with jump sequence $j(y_\varepsilon^{N-}) = \chi^-(\gamma_0^-)$. Both y_ε^{N+} and y_ε^{N-} have the properties described in statements* (i) *and* (ii) *of Theorem 3.1.*

Proof. The first part of the proof is the application of the proof of Theorem 3.1 to each of the perturbations of W_0^+ and W_0^-. In this way we obtain the existence of an N-pulse orbit y_ε^{N+}, which makes its first pulse in the direction of W_0^+, and another orbit y_ε^{N-}, which makes its first pulse in the direction of W_0^-. This time, however, we do not need to keep the N-pulse orbits in a neighborhood of the same unperturbed homoclinic structure: After their passages near the slow manifold $\mathscr{A}_\varepsilon$ they are allowed to exit in the direction of either W_0^+ or W_0^-. We only have to show that the sign sequences defined in Definition 3.3 indeed keep track of the exit directions correctly, i.e., they are equal to the jump sequences of y_ε^{N+} and y_ε^{N-}, respectively. We only show by induction that $j(y_\varepsilon^{N+}) = \chi^+(\gamma_0^-)$, because $j(y_\varepsilon^{N-}) = \chi^-(\gamma_0^-)$ follows in the same way.

Since y_ε^{N+} makes its first pulse in the direction of W_0^+, we have $j_1(y_\varepsilon^{N+}) = \chi_1^+(\gamma_0^-) = +1$. Let us now assume that $j_k(y_\varepsilon^{N+}) = \chi_k^+(\gamma_0^-)$. This means that y_ε^{N+} makes its kth pulse near W_0^+ if $\chi_k^+(\gamma_0^-) > 0$, or near W_0^- if $\chi_k^+(\gamma_0^-) < 0$. As we discussed in the proof of Theorem 3.1, the exit direction of y_ε^{N+} at the beginning of its $(k+1)$st passage depends on the relation of its leading-order energy to the leading-order energy of the orbits in $W_{\text{loc}}^s(\mathscr{A}_\varepsilon)$ near the entry of y_ε^{N+}. Recall that, near the kth entry point of y_ε^{N+} into a U_{δ_0} neighborhood of the slow manifold $\mathscr{A}_\varepsilon$, $W_{\text{loc}}^s(\mathscr{A}_\varepsilon)$ is foliated by local unstable manifolds of slow orbits, whose leading-order energies fall in the range $\varepsilon\mathscr{H}|\mathscr{R}^k(\gamma_0^-)$, whereas the leading-order energy of y_ε^{N+} is $\varepsilon\mathscr{H}|\gamma_0^-$. If sign $(\Delta^k\mathscr{H}|\gamma_0^-) \equiv$ sign $(\mathscr{H}|\mathscr{R}^k(\gamma_0^-) - \mathscr{H}|\gamma_0^-) > 0$, then from (3.34) we have $\chi_{k+1}^+(\gamma_0^-) = \sigma\chi_k^+(\gamma_0^-) = \sigma j_k(y_\varepsilon^{N+})$. On the other hand, since the leading-order

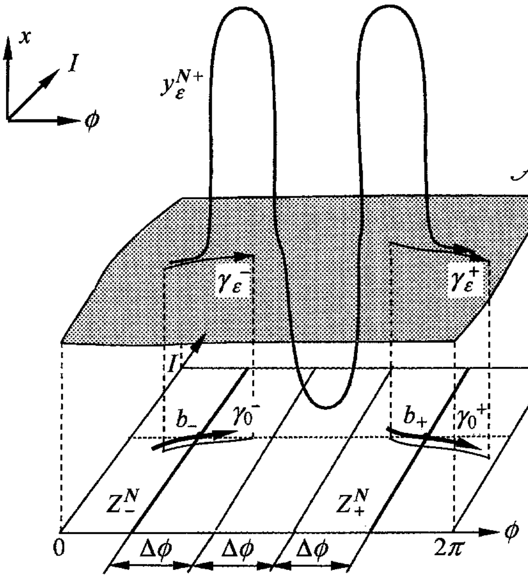

Fig. 12. An example of the statement of Theorem 3.3 for $N = 3$ and jump sequence $\chi_2^+ = -\chi_1^+, \chi_3^+ = -\chi_2^+$.

energy of y_ε^{N+} is lower than the energy of nearby orbits in $W_{\rm loc}^s(\mathcal{A}_\varepsilon)$, Remark 3.4 implies that $j_{k+1}(y_\varepsilon^{N+}) = \sigma j_k(y_\varepsilon^{N+})$; hence we obtain $j_{k+1}(y_\varepsilon^{N+}) = \chi_{k+1}^+(\gamma_0^-)$. Similarly, if sign $(\Delta^k \mathscr{H} | \gamma_0^-) < 0$, then from (3.34) we have $\chi_{k+1}^+(\gamma_0^-) = -\sigma\chi_k^+(\gamma_0^-) = -\sigma j_k(y_\varepsilon^{N+})$. Remark 3.4 implies that $j_{k+1}(y_\varepsilon^{N+1}) = -\sigma j_k(y_\varepsilon^{N+})$, which again gives $j_{k+1}(y_\varepsilon^{N+}) = \chi_{k+1}^+(\gamma_0^-)$. $\square$

An example of the possible cases covered by Theorem 3.3 is sketched in Fig. 12 for $N = 3$ and for the jump sequence $j_1(y_\varepsilon^{N+}) = +1$, $j_2(y_\varepsilon^{N+}) = -1$, $j_3(y_\varepsilon^{N+}) = +1$. (The intersection of the jumping homoclinic orbits with the slow manifold is of course an artifact of the projection from $\mathscr{P}$.)

3.3. *The case of resonance bands*

In this subsection we examine the existence of N-pulse homoclinic orbits in the case covered by hypothesis (H2a). Namely, we assume the presence of an isolated circle of equilibria within the unperturbed normally hyperbolic manifold $\mathcal{A}_0$ and focus on the consequences of the break-up of this circle under perturbation. The key idea in studying this is to blow up the circle into a "thin" manifold of equilibria or a *resonance band* (see KOVAČIČ & WIGGINS [33]). This resonance band appears as a two-dimensional manifold of equilibria for a system which we call the *standard form* (see (3.36)). Consequently, the analysis of N-pulse orbits homoclinic to resonance bands reduces to the application of the more general results of the previous sections. For $N = 1$ the energy-phase method yields the same single-pulse homoclinic orbits as the Melnikov method in HALLER & WIGGINS [19] or KOVAČIČ [34].

First, we restrict the variable I to an ε-dependent neighborhood of the resonant value $I = I_r$ by letting

$$I = I_r + \eta\sqrt{\varepsilon}, \quad \eta \in [-\eta_0, \eta_0],$$

with $\eta_0 > 0$ to be determined later. In the *resonance band*

$$\mathscr{P}_{\sqrt{\varepsilon}} = \{(x, I, \phi) \in \mathscr{P} | I \in [I_r - \sqrt{\varepsilon}\eta_0, I_r + \sqrt{\varepsilon}\eta_0]\} \tag{3.35}$$

we can Taylor-expand the right-hand side of (1.2) to obtain the *standard form*

$$\begin{aligned} \dot{x} &= JD_x[H_0(x, I_r) + \sqrt{\varepsilon}D_I H_0(x, I_r)\eta + \varepsilon(\tfrac{1}{2}D_I^2 H_0(x, I_r)\eta^2 \\ &\qquad + H_1(x, I_r, \phi; 0))] + \mathcal{O}(\varepsilon^{3/2}), \\ \dot{\eta} &= -\sqrt{\varepsilon}D_\phi H_1(x, I_r, \phi; 0) + \mathcal{O}(\varepsilon), \\ \dot{\phi} &= D_1 H_0(x, I_r) + \sqrt{\varepsilon}D_I^2 H_0(x, I_r)\eta + \mathcal{O}(\varepsilon). \end{aligned} \tag{3.36}$$

We now analyze this standard form on the phase space

$$\hat{\mathscr{P}} \subset \mathbb{R}^2 \times [-\eta_0, \eta_0] \times S^1, \tag{3.37}$$

to obtain information about the original system (2.1) near $I = I_r$. Any object in the standard form for $\varepsilon \neq 0$ has its counterpart in system (2.1), which can be found through the inverse of the C^r map

$$\begin{aligned} &\mathscr{B}_\varepsilon : \mathscr{P}_{\sqrt{\varepsilon}} \to \hat{\mathscr{P}}, \\ &(x, I, \phi) \mapsto \left(x, \frac{I - I_r}{\sqrt{\varepsilon}}, \phi\right). \end{aligned} \tag{3.38}$$

To avoid confusion between the two systems, we use a hat ($\hat{\ }$) when referring to objects computed or defined for the standard form.

First note that for $\varepsilon > 0$ the system (3.36) is Hamiltonian on the space $(\hat{\mathscr{P}}, \hat{\omega})$ with

$$\hat{\omega} = dx_1 \wedge dx_2 + \frac{1}{\sqrt{\varepsilon}} d\phi \wedge d\eta$$

and with the corresponding Hamiltonian

$$\hat{H}(x, \eta, \phi; \sqrt{\varepsilon}) = H(x, I_r + \sqrt{\varepsilon}\eta, \phi; \varepsilon) = H_0(x, I_r) + \sqrt{\varepsilon}\hat{H}_1(x, \eta, \phi; \sqrt{\varepsilon}). \tag{3.39}$$

Note that in (3.39) the function

$$\hat{H}_1(x, \eta, \phi; \varepsilon) = D_1 H_0(x, I_r)\eta + \sqrt{\varepsilon}\,[\tfrac{1}{2}D_I^2 H_0(x, I_r)\eta^2 + H_1(x, I_r, \phi; 0)] + \mathcal{O}(\varepsilon)$$

is only in C^{r-1}, and accordingly, the right-hand side of (3.36) is only in C^{r-2}. For $\varepsilon > 0$ we can define the energy surface with energy h for the standard form (3.36) as

$$\hat{E}_{\sqrt{\varepsilon}}(h) = \{(x, \eta, \phi) \in \hat{\mathscr{P}} | \hat{H}(x, \eta, \phi; \sqrt{\varepsilon}) = h\}.$$

Equations (3.36) can be considered as an $\mathcal{O}(\sqrt{\varepsilon})$ perturbation of the system

$$\begin{aligned} \dot{x} &= JD_x H_0(x, I_r), \\ \dot{\eta} &= 0, \\ \dot{\phi} &= D_I H_0(x, I_r), \end{aligned} \tag{3.40}$$

which is not Hamiltonian, but is *integrable* with the two independent integrals $H_0(x, I_r)$ and η. Therefore, for a given h it makes sense to define a (quasi-) energy surface for system (3.40) in the form

$$\hat{E}_0(h) = \{(x, \eta, \phi) \in \hat{\mathscr{P}} | H_0(x, I_r) = \hat{H}(x, \eta, \phi; 0) = h\}.$$

This hypersurface relates in the same way to $\hat{E}_{\sqrt{\varepsilon}}(h)$ as $E_0(h)$ to $E_\varepsilon(h)$ in the previous sections. One also finds that $\hat{E}_0(\hat{h}_0) \supset \hat{\mathscr{A}}_0 \cup \hat{W}_0$ (see (3.41) below), by analogy with the previous sections.

Based on hypothesis (H1), for system (3.40) (or $(3.36)_{\varepsilon=0}$) we again have a normally hyperbolic invariant two-manifold of equilibria given by

$$\hat{\mathscr{A}}_0 = \{(x, \eta, \phi) \in \hat{\mathscr{P}} | x = \bar{x}^0(I_r), \eta \in [-\eta_0, \eta_0], \phi \in S^1\}, \tag{3.41}$$

which is a graph over the annulus

$$\hat{A} = [-\eta_0, \eta_0] \times S^1.$$

Furthermore, under hypothesis (H1′) $\mathscr{A}_0$ has two three-dimensional homoclinic manifolds $\hat{W}_0^+$ and $\hat{W}_0^-$ which contain trajectories of the form

$$\hat{y}_0^\pm(t, \eta, \phi_0) = \left(x^{h\pm}(t, I_r), \eta, \phi_0 + \int_0^t D_I H_0(x^{h\pm}(\tau, I_r), I_r) d\tau \right). \tag{3.42}$$

Again, for $\varepsilon > 0$, (3.36) has a normally hyperbolic manifold $\hat{\mathscr{A}}_\varepsilon$ $(\sqrt{\varepsilon}, C^{r-2})$-close to $\hat{\mathscr{A}}_0$, given by the embedding

$$\begin{aligned} &\hat{g}_\varepsilon : \hat{A} \to \hat{\mathscr{P}}, \\ &(\eta, \phi) \mapsto (\hat{x}^\varepsilon(\eta, \phi), \eta, \phi) = (\bar{x}^0(I_r) + \varepsilon \hat{x}^1(\sqrt{\varepsilon}\eta, \phi; \sqrt{\varepsilon}), \eta, \phi). \end{aligned} \tag{3.43}$$

Also, $(\hat{\mathscr{A}}_\varepsilon, \hat{i}_\varepsilon^* \hat{\omega})$ is a C^{r-2} symplectic manifold with

$$\hat{i}_\varepsilon^* : \hat{\mathscr{A}}_\varepsilon \hookrightarrow \hat{\mathscr{P}},$$

$$\hat{i}_\varepsilon^* \hat{\omega} = \left(\frac{1}{\sqrt{\varepsilon}} + \mathcal{O}(\varepsilon) \right) d\phi \wedge d\eta.$$

As in the case of hypothesis (H2b), we can define the *restricted Hamiltonian*

$$\hat{\mathscr{H}}_\varepsilon = \hat{H} | \hat{\mathscr{A}}_\varepsilon = \hat{i}_\varepsilon^* \hat{H}, \tag{3.44}$$

which generates the restricted Hamiltonian flow on $\hat{\mathscr{A}}_\varepsilon$ satisfying

$$\begin{pmatrix} \dot{\phi} \\ \dot{\eta} \end{pmatrix} = \hat{i}_\varepsilon^* \hat{\omega}^\# (D_{(\varphi, \eta)} \hat{\mathscr{H}}_\varepsilon) = \sqrt{\varepsilon} J D_{(\varphi, \eta)} \hat{\mathscr{H}} + \mathcal{O}(\varepsilon).$$

Here the *reduced Hamiltonian* $\hat{\mathscr{H}}: \hat{A} \to \mathbb{R}$ takes the form

$$\hat{\mathscr{H}}(\eta, \phi) = \tfrac{1}{2} m(I_r)\eta^2 + H_1(\bar{x}^0(I_r), I_r, \phi; 0), \tag{3.45}$$

with $m(I_r)$ defined as in hypothesis (H2a). $\hat{\mathscr{H}}$ is related to the restricted Hamiltonian $\hat{\mathscr{H}}_\varepsilon$ through

$$\hat{\mathscr{H}}_\varepsilon = \hat{h}_0 + \varepsilon \hat{\mathscr{H}} + \mathcal{O}(\varepsilon^{3/2}), \tag{3.46}$$

with

$$\hat{h}_0 = H_0(\bar{x}^0(I_r), I_r).$$

Note that the reduced Hamiltonian of (3.45) is always the sum of kinetic and potential energy-type terms. Any internal orbit $\hat{\gamma}_0 \subset \hat{A}$ of $\hat{\mathscr{H}}$ (defined in analogy with Definition 2.1) gives rise to an internal orbit $\hat{\gamma}_\varepsilon \subset \hat{\mathscr{A}}_\varepsilon$ such that $\hat{\gamma}_0$ and $\hat{g}_\varepsilon^{-1}(\hat{\gamma}_\varepsilon)$ are $(\sqrt{\varepsilon}, C^{r-2})$-close in $\hat{A}$. Also, defining the map

$$\begin{aligned} b_\varepsilon &: A \to \hat{A}, \\ (I, \phi) &\mapsto \left(\frac{I - I_r}{\sqrt{\varepsilon}}, \phi \right), \end{aligned} \tag{3.47}$$

we can use the relation between $\hat{\mathscr{H}}_\varepsilon$ and $\hat{\mathscr{H}}$ to find an orbit $\gamma_\varepsilon \subset \mathscr{A}_\varepsilon$ in the resonance band of the original system (1.2) such that $b_\varepsilon \circ g_\varepsilon^{-1}(\gamma_\varepsilon)$ and $\hat{\gamma}_0$ are $(\sqrt{\varepsilon}, C^{r-2})$-close in $\hat{A}$.

Introducing the tubular set

$$\hat{U}_\delta = \{(x, \eta, \phi) \in \hat{\mathscr{P}} \,|\, |x - \bar{x}^0(I_r)| \leqq \delta, (\eta, \phi) \in \hat{A}\},$$

one can redo the estimates of Section 2 for system (3.36) by substituting η for I, and $r - 2$ for r in all the statements and proofs. Therefore, our main construction of a local map $\hat{L}_\varepsilon^h$ to track trajectories inside $\hat{U}_{\delta(\varepsilon)}$ and a global map $\hat{G}_\varepsilon^h$ to follow them outside $\hat{U}_{\delta(\varepsilon)}$ holds without modification.

As in Section 3.1, we define the nth *order energy-difference function* $\Delta^n \hat{\mathscr{H}}: \hat{A} \to \mathbb{R}$ as

$$\begin{aligned} \Delta^n \hat{\mathscr{H}}(\phi) &= \hat{\mathscr{H}}(\eta, \phi + n\Delta\phi) - \hat{\mathscr{H}}(\eta, \phi) \\ &= H_1(\bar{x}^0(I_r), \mathrm{I}_r, \phi + n\Delta\phi; 0) - H_1(\bar{x}^0(I_r), I_r, \phi; 0). \end{aligned} \tag{3.48}$$

Note that $\Delta^n \hat{\mathscr{H}}$ does not depend on η; hence the corresponding zero sets

$$\begin{aligned} &\hat{V}_-^0 = \emptyset, \quad \hat{V}_-^n = \{(\eta, \phi) \in \hat{A} \,|\, \Delta^n \hat{\mathscr{H}}(\phi) = 0\}, \quad \hat{V}_+^n = \hat{\mathscr{R}}^n(\hat{V}_-^n), \quad n \geqq 1, \\ &\hat{Z}_-^n = \{(\eta, \phi) \in V_-^n \,|\, D_\phi \Delta^n \hat{\mathscr{H}}(\phi) \neq 0\}, \quad \hat{Z}_+^n = \hat{\mathscr{R}}^n(\hat{Z}_-^n), \quad n \geqq 1, \end{aligned} \tag{3.49}$$

generically consist of lines $\phi = \text{const.}$ in the annulus $\hat{A}$. We note that the rotation map

$$\begin{aligned} \hat{\mathscr{R}} &: \hat{A} \to \hat{A}, \\ (\eta, \phi) &\mapsto (\eta, \phi + \Delta\phi) \end{aligned} \tag{3.50}$$

has no explicit η-dependence either. As in (3.6), for any internal orbit $\hat{\gamma} \subset \hat{A}$ of $\hat{\mathscr{H}}$ we define the *pulse number*

$$N(\hat{\gamma}) = \min\{n \geqq 1 \,|\, \hat{V}^k_- \cap \hat{\gamma} = \emptyset, k = 0, \ldots, n-1, \hat{Z}^n_- \pitchfork \hat{\gamma}\}. \tag{3.51}$$

Referring to the discussion in Remark 3.1, we also introduce the resonant pulse number

$$N_R(\hat{\gamma}) = \min\{n \geqq 1 \,|\, \hat{V}^k_- \cap \hat{\gamma} = \emptyset, k = 0, \ldots, n-1, \hat{V}^n \equiv \hat{A}\}. \tag{3.52}$$

Using N_R we shall be able to show the existence of N-pulse orbits for cases when the quotient of the phase shift and 2π is k/N with some integer k. This generically occurs on a dense set of the space of the system parameters and causes the pulse number $N(\hat{\gamma})$ to be undefined for an open set of internal orbits.

We directly formulate our results for jumping N-pulse orbits in the system (1.2). (This of course includes the case of no jumping at all, i.e., when all pulses are made around the same unperturbed homoclinic structure.) The jump sequence $j(y^N_\varepsilon)$ of an N-pulse orbit y^N_ε is defined the same way as in Definition 3.2 (note that in the context of resonance bands the point b_- in Definition 3.2 always lies on the resonant circle of fixed points). Let us suppose that for an internal orbit $\hat{\gamma}$ of the reduced Hamiltonian $\hat{\mathscr{H}}$ either $N(\hat{\gamma}) = N$ or $N_R(\hat{\gamma}) = N$. In either case, we define the *positive and negative sign sequences*, $\{\chi^\pm_k(\hat{\gamma})\}^N_{k=1}$, *of* $\hat{\gamma}$ by analogy with Definition 3.3:

$$\begin{aligned} &\chi^+_1(\hat{\gamma}) = +1, \quad \chi^+_{k+1}(\hat{\gamma}) = \sigma\,\mathrm{sign}(\Delta^k \hat{\mathscr{H}} \,|\, \hat{\gamma})\chi^+_k(\gamma), \quad k = 1, \ldots, N-1, \\ &\chi^-_k(\hat{\gamma}) = -\chi^+_k(\hat{\gamma}), \quad k = 1, \ldots, N-1, \end{aligned} \tag{3.53}$$

with σ defined as in (3.33). Finally, we require the two phase shifts on $\hat{W}^-_0$ and $\hat{W}^+_0$ to be equal at the action value $I = I_r$, i.e.,

(H3′) $$\Delta\phi = \int_{-\infty}^{+\infty} D_I H_0(x^{h+}(t, I_r), I_r)\,dt \equiv \int_{-\infty}^{+\infty} D_I H_0(x^{h-}(t, I_r), I_r)\,dt.$$

This requirement is weaker than (H3) in that it is restricted to the resonant value of I. The assumptions of the following theorem are given in terms of the quantities defined for the standard form (3.36), but the results are stated directly in terms of the dynamics of (2.1).

Theorem 3.4. *Assume that hypotheses* (H1′), (H2a), *and* (H3′) *hold. Suppose that for an internal orbit* $\hat{\gamma}^-_0 \subset \hat{A}$ *of the reduced Hamiltonian* $\hat{\mathscr{H}}$

(A1) $N \equiv N(\hat{\gamma}^-_0)$ *is defined,*

(A2) *Let* $\hat{b}_- \in \hat{Z}^N_- \cap \hat{\gamma}^-_0$ *and* $\hat{b}_+ = \hat{\mathscr{R}}^N(\hat{b}_-)$. *Assume that the orbit* $\hat{\gamma}^+_0 \subset \hat{A}$ *of the reduced Hamiltonian* $\hat{\mathscr{H}}$ *which contains* b_+ *is an internal orbit with* $\hat{Z}^N_+ \pitchfork \hat{\gamma}^+_0$.

Then there exists $\varepsilon_0 > 0$ *such that for* $0 < \varepsilon < \varepsilon_0$,

(i) $\mathscr{A}_\varepsilon$ *has two N-pulse homoclinic orbits,* y^{N+}_ε *and* y^{N-}_ε, *which are positively asymptotic to an internal orbit* $\gamma^+_\varepsilon \subset \mathscr{A}_\varepsilon$ *and negatively asymptotic to an internal orbit* $\gamma^-_\varepsilon \subset \mathscr{A}_\varepsilon$. *Moreover,* $b_\varepsilon \circ g^{-1}_\varepsilon(\gamma^-_\varepsilon)$ *and* $\hat{\gamma}^-_0$ *are* $(\sqrt{\varepsilon}, C^{r-2})$*-close, and* $b_\varepsilon \circ g^{-1}_\varepsilon(\gamma^+_\varepsilon)$ *and* $\hat{\gamma}^+_0$ *are* $(\sqrt{\varepsilon}, C^0)$*-close. If* $\hat{\gamma}^+_0$ *is periodic, this latter*

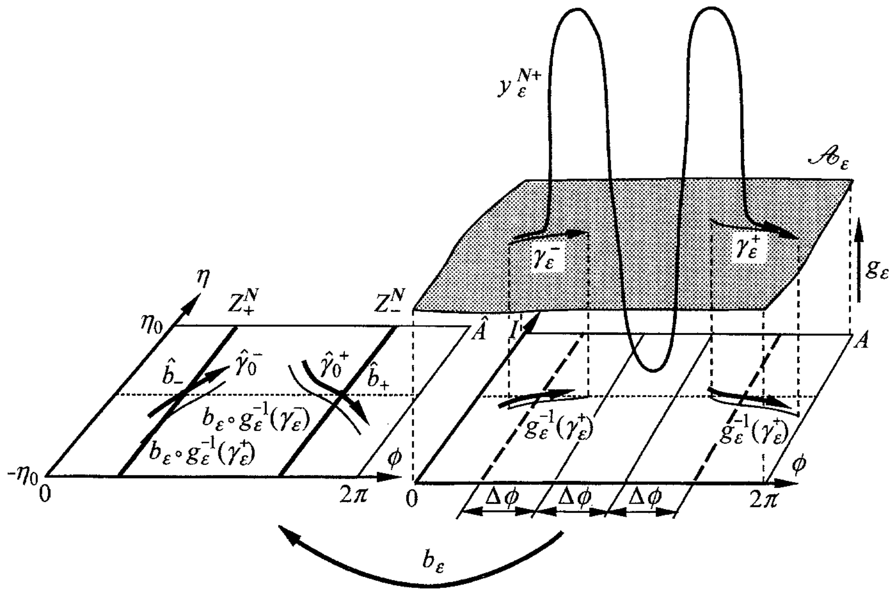

Fig. 13. The geometry of Theorem 5.1 for $N = 3$.

statement can be strengthened by replacing C^0 *with* C^{r-2}. *Furthermore, if* $\hat{\gamma}_0^- = \hat{\gamma}_0^+$, *then* $\gamma_\varepsilon^- = \gamma_\varepsilon^+$.

(ii) y_ε^{N+} *and* y_ε^{N-} *lie in the intersection of* $W^u(\gamma_\varepsilon^-)$ *and* $W^s(\gamma_\varepsilon^+)$, *which is transversal within the energy surface* $E_\varepsilon(h)$ *with* $h = H\,|\,\gamma_\varepsilon^+ = H\,|\,\gamma_\varepsilon^-$.

(iii) *The jump sequences of* y_ε^{N+} *and* y_ε^{N-} *are* $j(y_\varepsilon^{N+}) = \chi^+(\hat{\gamma}_0^-)$ *and* $j(y_\varepsilon^{N-}) = \chi^-(\hat{\gamma}_0^-)$, *respectively.*

Suppose now that assumption (A1) *is replaced with*

(A1′) $N \equiv N_R(\hat{\gamma}_0^-)$ *is defined.*

Then statements (i)–(iii) *still hold with the exception of the transversality of the N-pulse orbits.*

Proof. We first apply Theorem 3.1 to the standard form (3.36) then we relate back the results on system (3.36) to system (2.1) using the map $\mathscr{B}_\varepsilon$. Note that objects of the standard form which are $(\sqrt{\varepsilon}, C^1)$-close in $\hat{\mathscr{P}}$ are mapped under $\mathscr{B}_\varepsilon^{-1}$ into objects of system (1.2) which are $(\sqrt{\varepsilon}, C^1)$-close in $\mathscr{P}$. From this the statements of Theorem 3.4 follow. □

We illustrate the statements of Theorem 3.4 in Fig. 13.

Remark 3.5. Notice in the statement of Theorem 3.4 that we can locate the orbit γ_ε^- only with $\mathscr{O}(\sqrt{\varepsilon})$ precision. However, the I coordinates of the corresponding points of γ_ε^- and the approximating curve $g_\varepsilon \circ b_\varepsilon^{-1}(\hat{\gamma}_0^-)$ are only $\mathscr{O}(\varepsilon)$ apart, as one can see from the definition of b_ε (see (3.47)). As a result, we can guarantee that γ_ε^-

indeed falls in the $\mathcal{O}(\sqrt{\varepsilon})$-thick resonance band. A similar statement holds for the approximation of γ_ε^+ by $g_\varepsilon \circ b_\varepsilon^{-1}(\hat{\gamma}_0^+)$. Finally, for the same reason, the deviation of an N-pulse orbit y_ε^N from the corresponding shadowing set Y_j^N is actually only $\mathcal{O}(\varepsilon)$ in the I coordinate direction; hence y_ε^N also lies entirely in the resonance band $\mathscr{P}_{\sqrt{\varepsilon}}$.

Remark 3.6. By analogy with Remark 3.3, the N-pulse orbits guaranteed by Theorem 3.4 intersect a one-parameter family of unstable fibers whose basepoints form the *N-take-off curve* $B_{\mathrm{u},\varepsilon}^N \subset \mathscr{A}_\varepsilon$. The N-take-off curve now has the property that $b_\varepsilon \circ g_\varepsilon^{-1}(B_{\mathrm{u},\varepsilon}^N)$ is $(\sqrt{\varepsilon}, C^1)$-close to the set

$$\hat{z}_-^N = \{\hat{p} \in \hat{Z}_-^N \mid \exists \hat{\gamma}: N(\hat{\gamma}) = N, \hat{\gamma} \pitchfork \hat{Z}_-^N, \hat{p} \in \hat{\gamma} \cap \hat{Z}_-^N\}. \tag{3.54}$$

Likewise, the *N-landing curve* $B_{\mathrm{s},\varepsilon}^N$ has the property that $b_\varepsilon \circ g_\varepsilon^{-1}(B_{\mathrm{s},\varepsilon}^N)$ is $(\sqrt{\varepsilon}, C^1)$-close to the set

$$\hat{z}_+^N = \hat{\mathscr{R}}^N(\hat{z}_-^N). \tag{3.55}$$

Recall that the take-off and landing curves depend smoothly on the system parameters. We can again define the *take-off point* p_ε and the *landing point* q_ε of $y_\varepsilon^{N\pm}$ as

$$p_\varepsilon = B_{\mathrm{u},\varepsilon}^N \cap \gamma_\varepsilon^-, \quad q_\varepsilon = B_{\mathrm{s},\varepsilon}^N \cap \gamma_\varepsilon^+. \tag{3.56}$$

4. The energy-phase method: dissipative perturbations

In this section we show how the energy-phase method extends to the case which includes the non-Hamiltonian perturbation terms in system (1.2). We work in the context of resonance bands (hypothesis (H2a)), since most dissipative applications, as well as our beam example, fall in this category. The same types of results can be formulated for the case of a two-dimensional resonant manifold (hypothesis (H2b)). Also, we assume that hypotheses (H1′) of Section 3.2, (H2a) of Section 1.3, and (H3′) of Section 3.3 hold, but the results we derive also hold under hypothesis (H1) with obvious modifications.

As in Section 3.3, we apply the transformation (3.38) and a Taylor expansion to (1.2) to obtain the *dissipative standard form*

$$\begin{aligned}
\dot{x} &= JD_x[H_0(x, I_r) + \sqrt{\varepsilon} D_I H_0(x, I_r)\eta \\
&\qquad + \varepsilon(\tfrac{1}{2} D_I^2 H_0(x, I_r)\eta^2 + H_1(x, I_r, \phi; 0))] + \varepsilon g_x(x, I_r, \phi; 0) + \mathcal{O}_{H+D}(\varepsilon^{3/2}), \\
\dot{\eta} &= \sqrt{\varepsilon}[-D_\phi H_1(x, I_r, \phi; 0) + g_I(x, I_r, \phi; 0)] + \mathcal{O}_{H+D}(\varepsilon), \\
\dot{\phi} &= D_I H_0(x, I_r) + \sqrt{\varepsilon} D_I^2 H_0(x, I_r)\eta + \varepsilon g_\phi(x, I_r, \phi; 0) + \mathcal{O}_H(\varepsilon) + \mathcal{O}_D(\sqrt{\varepsilon}).
\end{aligned} \tag{4.1}$$

Note that we separate the Hamiltonian terms in the "tail" of the standard form (with subscript "H") from the dissipative terms (with subscript "D"). The reason for not listing certain Hamiltonian terms explicitly is that they derive from the $\mathcal{O}(\varepsilon)$ tail of the Hamiltonian $\hat{H}$ through the symplectic form $\hat{\omega}$ (see Section 3.3). We note that (4.1) is again an $\mathcal{O}(\sqrt{\varepsilon})$ perturbation of the integrable system (3.40).

4.1. *Tracking multi-pulse solutions*

The main idea of our construction in the dissipative case is the following. We again follow perturbed solutions which lie in the unstable manifolds of invariant sets contained in the slow manifold $\hat{\mathscr{A}}_\varepsilon$. These solutions again leave the neighborhood $\hat{U}_{\delta(\varepsilon)}$ of the slow manifold and then return to the same neighborhood, possibly many times. Since our basic normal form (2.6) near the slow manifold $\hat{\mathscr{A}}_\varepsilon$ does not assume that the perturbation is purely Hamiltonian, we can still use (2.6) to obtain estimates for the change of the η and ϕ coordinates, while the solutions passing near $\hat{\mathscr{A}}_\varepsilon$ stay inside the tube $\hat{U}_{\delta(\varepsilon)}$. More specifically, if the minimal distance condition (2.8) of Lemma 2.3 holds for a solution $w_\varepsilon(t)$ at the entry point $p_\varepsilon \in \hat{U}_{\delta(\varepsilon)}$, and the "entry" energy $\hat{h} = \hat{H}_{p_\varepsilon}$ obeys the maximal distance condition $|\hat{h} - \hat{h}_0| < \kappa\varepsilon$ with $\hat{h}_0 = H(\bar{x}^0(I_r), I_r)$ (see Lemma 2.5), then the map $(\eta_{p_\varepsilon}, \phi_{q_\varepsilon}) \mapsto (\eta_{p_\varepsilon}, I_{q_\varepsilon})$ is again locally $(\sqrt{\varepsilon}, C^1)$-close to the identity map of $\hat{A}$. (Recall that q_ε denotes the point where $w_\varepsilon(t)$ exits from $\hat{U}_{\delta(\varepsilon)}$.) Similarly, the map relating $(\eta_{q_\varepsilon}, \phi_{q_\varepsilon})$ to the (η, ϕ) coordinates of the next intersection point of $w_\varepsilon(t)$ with $\hat{U}_{\delta(\varepsilon)}$ is $(\sqrt{\varepsilon}, C^1)$-close to the rotation map $\hat{\mathscr{R}}$ defined in (3.50). This time, however, tracking the (η, ϕ) coordinates of the solution $w_\varepsilon(t)$ is not enough to establish its intersection with $W^{\mathrm{s}}_{\mathrm{loc}}(\hat{\mathscr{A}}_\varepsilon)$. The reason is that the Hamiltonian $\hat{H}$ is not constant on $w_\varepsilon(t)$ any more. As a result, we do not know a priori what energy $\hat{h}$ to choose in order to ensure that the Poincaré section $\hat{\Sigma}^{\mathrm{s}}_\varepsilon(\hat{h}) \subset E_\varepsilon(\hat{h}) \cap \hat{U}_{\delta(\varepsilon)}$ is intersected by $w_\varepsilon(t)$ upon its nth return. Another problem is that we do not know a priori the location of the base points of the stable fibers which intersect this particular Poincaré section, the reason being again that the energy $\hat{H}$ is not conserved on stable fibers of the dissipative system.

4.2. *Energy estimates*

Based on the above argument, our strategy is as follows. We consider a solution $w_\varepsilon(t)$ which intersects an unstable fiber $\hat{f}^{\mathrm{u}}_\varepsilon(b_0) \subset W^{\mathrm{u}}_{\mathrm{loc}}(\hat{\mathscr{A}}_\varepsilon)$ at a point $q_0 \in \partial\hat{U}_{\delta(\varepsilon)}$ and hence backward asymptotes to the slow manifold $\hat{\mathscr{A}}_\varepsilon$. We derive estimates for the change of energy $\Delta\hat{H}$ along $w_\varepsilon(t)$ as it leaves and reenters the tube $\hat{U}_{\delta(\varepsilon)}$ n times, such that between two pulses it passes near the slow manifold $\hat{\mathscr{A}}_\varepsilon$ outside a minimal distance from $\hat{\mathscr{A}}_\varepsilon$. We let $p_n \in \hat{U}_{\delta(\varepsilon)}$ be the intersection point of $w_\varepsilon(t)$ with the tube $\hat{U}_{\delta(\varepsilon)}$ upon its nth return. We also let b_n be the basepoint of the stable fiber $\hat{f}^{\mathrm{s}}_\varepsilon(b_n) \subset W^{\mathrm{s}}_{\mathrm{loc}}(\hat{\mathscr{A}}_\varepsilon)$ which intersects the tube $\hat{U}_{\delta(\varepsilon)}$ in a point s_n with the same (η, ϕ) coordinates as those of p_n. We then compare the two energies $\hat{H}(p_n)$ and $\hat{H}(s_n)$. If, for some appropriate choice of the basepoint b_0, $\hat{H}(p_n) = \hat{H}(s_n) = \hat{h}$ holds, then both p_n and s_n lie on the same two-dimensional Poincaré section $\hat{\Sigma}^{\mathrm{s}}_\varepsilon(\hat{h})$. Since both of these points have the same (η, ϕ) coordinates and, by Lemma 2.4, $\hat{\Sigma}_\varepsilon^{\mathrm{s}}(\hat{h})$ is a graph over the annulus $\hat{A}$, we conclude that the solution $w_\varepsilon(t)$ intersects the stable fiber $\hat{f}_\varepsilon^{\mathrm{s}}(b_n)$ and hence forward asymptotes to the slow manifold. If, however, we find that $\hat{H}(p_n) \neq \hat{H}(s_n)$, then we show that $|\hat{H}(p_n) - \hat{H}(s_n)| = \mathcal{O}(\varepsilon)$. Then, using Lemmas 2.3 and 2.5, we track the solution $w_\varepsilon(t)$ as it passes near $\hat{\mathscr{A}}_\varepsilon$ to return for the $(n+1)$st time, when we repeat the above energy measurement again.

We start by estimating the energy $\hat{H}(p_n)$ with the point p_n defined as above for the solution $w_\varepsilon(t)$.

Lemma 4.1. *Let $w_\varepsilon(t) = (x(t), \eta(t), \phi(t))$ be a solution of (4.1) which intersects an unstable fiber $\hat{f}_\varepsilon^{\mathrm{u}}(b_0)$ at a point $q_0 \in \partial\hat{U}_{\delta(\varepsilon)}$. Assume that $w_\varepsilon(t)$ returns and enters $\hat{U}_{\delta(\varepsilon)}$ n times at the points $p_1, \ldots, p_n \in \partial\hat{U}_{\delta(\varepsilon)}$ such that for $k = 1, \ldots, n-1$,*

$$d(p_k, W_{\mathrm{loc}}^{\mathrm{s}}(\hat{\mathscr{A}}_\varepsilon)) > K\sqrt{\varepsilon} \tag{4.2}$$

for some $0 < K < \vartheta$. Then, for any small $\delta_0 > 0$, there exists $\varepsilon_0 > 0$ such that for all $0 < \varepsilon < \varepsilon_0$,

$$\hat{H}(p_n) = H_0(\bar{x}^0(I_r), I_r) + \varepsilon\left[\hat{\mathscr{H}}(\eta_{b_0}, \phi_{b_0}) + \sum_{i=1}^{n} \int_{-\infty}^{+\infty} \langle DH_0, g\rangle|_{y^i(t)}\, dt\right]$$
$$+ \mathcal{O}(\delta_0\varepsilon, \varepsilon^{11/10}). \tag{4.3}$$

Here the unperturbed solution $y^i(t)$ of $(1.2)_{\varepsilon=0}$ is a heteroclinic orbit between the two points $(\bar{x}^0(I_r), 0, \phi_{b_0} + (i-1)\Delta(\phi))$ and $(\bar{x}^0(I_r), 0, \phi_{b_0} + i\Delta(\phi))$. Furthermore, $\hat{H}(p_n)$ is a C^1 function in the variables (η_{b_0}, ϕ_{b_0}).

Proof. We start by splitting the quantity $\hat{H}(p_n)$ into parts which we estimate separately. We can write

$$\hat{H}(p_n) = \hat{H}(b_0) + [\hat{H}(q_0) - \hat{H}(b_0)] + \sum_{i=1}^{n} [\hat{H}(p_i) - \hat{H}(q_{i-1})]$$
$$+ \sum_{i=1}^{n-1} [\hat{H}(q_i) - \hat{H}(p_i)], \tag{4.4}$$

where the first sum is the total change of energy incurred outside $\hat{U}_{\delta(\varepsilon)}$, and the second sum is the total change of energy during local passages within $\hat{U}_{\delta(\varepsilon)}$.

Considering the first term on the right-hand side of (4.4), we can use the expressions (3.44) and (3.46) to obtain

$$\hat{H}(b_0) = H_0(\bar{x}^0(I_r), I_r) + \varepsilon\hat{\mathscr{H}}(\eta_{b_0}, \phi_{b_0}) + \mathcal{O}(\varepsilon^{3/2}). \tag{4.5}$$

To estimate the magnitude of the second term on the right-hand side of (4.4) we define the point q_h to be the intersection of $\hat{U}_{\delta(\varepsilon)}$ with the *Hamiltonian fiber* $\hat{f}_\varepsilon^{\mathrm{u}}(b_h)$ (i.e., a fiber for $g \equiv 0$) with $(\eta_{b_h}, \phi_{b_h}) = (\eta_{b_0}, \phi_{b_0})$. Using the fact that $\hat{H}(q_h) = \hat{H}(b_h)$ and applying the mean value inequality, we have

$$|\hat{H}(q_0) - \hat{H}(b_0)| \leqq |\hat{H}(q_0) - \hat{H}(q_h)| + |\hat{H}(b_h) - \hat{H}(b_0)| < |D\hat{H}|_{p^*}|q_0 - q_h| + c_1\varepsilon \tag{4.6}$$

with the point p^* lying on the connecting q_0 and q_h. (To obtain the estimate on the second term on the right-hand side we used the fact that $\hat{H}$ is continuous and that $\hat{\mathscr{A}}_\varepsilon$ is deformed by an amount of $\mathcal{O}(\varepsilon)$ under the effect of the dissipative perturbation, so b_h and b_0 are $\mathcal{O}(\varepsilon)$ close.) Looking at the form of $\hat{H}$ defined in (3.39) and using the fact that $|D_I H_0(x, I_r, \phi)| = \mathcal{O}(\sqrt{\varepsilon})$ within $\hat{U}_{\delta(\varepsilon)}$, we obtain from (4.6) that

$$\begin{aligned}|\hat{H}(q_0) - \hat{H}(b_0)| &< |D_x\hat{H}|_{p^*}|x_{q_0} - x_{q_h}| + |D_\eta\hat{H}|_{p^*}|\eta_{q_0} - \eta_{q_h}| \\ &\quad + |D_\phi\hat{H}|_{p^*}|\phi_{q_0} - \phi_{q_h}| + c_1\varepsilon \\ &< c_2\sqrt{\varepsilon}\varepsilon + c_3\varepsilon\sqrt{\varepsilon} + c_4\sqrt{\varepsilon}\varepsilon + c_1\varepsilon < c_5\varepsilon^{3/2}, \qquad (4.7)\end{aligned}$$

for appropriate constants c_i. (Here we used the fact that q_0 and q_h are $\mathcal{O}(\varepsilon)$-close in the (x, I, ϕ) coordinates since the unstable fibers are C^r functions of ε.)

We now estimate the third term on the right-hand side of (4.4). We select some small constant $\delta_0 > 0$ and choose $\varepsilon > 0$ small enough, so that the tube $\hat{U}_{\delta_0}$ contains $\hat{U}_{\delta(\varepsilon)}$. Let $q_i^0 \in \partial\hat{U}_{\delta_0}$ denote the next intersection of $w_\varepsilon(t)$ with the boundary of $\hat{U}_{\delta_0}$ after it leaves $\hat{U}_{\delta(\varepsilon)}$ at the point q_i. Similarly, let $p_i^0 \in \partial\hat{U}_{\delta_0}$ denote the intersection of $w_\varepsilon(t)$ with the boundary of $\hat{U}_{\delta_0}$ before it reaches $\hat{U}_{\delta(\varepsilon)}$ at the point p_i. Let us define the intersection times T_{i-1}^-, T_{i-1}^{0-}, T_i^+, and T_i^{0+} through the equations

$$w_\varepsilon(T_{i-1}^-) = q_{i-1}, \quad w_\varepsilon(T_{i-1}^{0-}) = q_{i-1}^0, \quad w_\varepsilon(T_i^{0+}) = p_i^0, \quad w_\varepsilon(T_i^+) = p_i \qquad (4.8)$$

for $i = 0, \ldots, n$. We then have

$$\begin{aligned}\sum_{i=1}^n \hat{H}(p_i) - \hat{H}(q_{i-1}) &= \sum_{i=1}^n \int_{T_{i-1}^-}^{T_{i-1}^{0-}} \dot{\hat{H}}(w_\varepsilon(t))\,dt + \sum_{i=1}^n \int_{T_{i-1}^{0-}}^{T_i^{0+}} \dot{\hat{H}}(w_\varepsilon(t))\,dt \\ &\quad + \sum_{i=1}^n \int_{T_i^{0+}}^{T_i^+} \dot{\hat{H}}(w_\varepsilon(t))\,dt. \qquad (4.9)\end{aligned}$$

To estimate these integrals, we first simplify the integrands by noting that

$$\begin{aligned}\dot{\hat{H}}(w_\varepsilon(t)) &= [\langle D_x\hat{H}, \varepsilon g_x\rangle + D_\eta\hat{H}(\sqrt{\varepsilon}g_I + \mathcal{O}(\varepsilon^{3/2})) + D_\phi\hat{H}\varepsilon g_\phi]|_{w_\varepsilon(t)} \\ &= \varepsilon\langle DH_0(x, I_r), g(x, I_r, \phi; 0)\rangle|_{w_\varepsilon(t)} + \mathcal{O}(\varepsilon^{3/2}), \qquad (4.10)\end{aligned}$$

where we used the expression for $\hat{H}$ from (3.39). We also need the estimate

$$\frac{4}{5\lambda}\log\frac{\delta_0}{c_7\sqrt{\varepsilon}} < |T_i^+ - T_i^{0+}| < \frac{6}{5\lambda}\log\frac{\delta_0}{c_7\sqrt{\varepsilon}}, \qquad (4.11)$$

which follows, for ε, δ_0 sufficiently small, by standard Gronwall estimates from the "almost linear" local normal form (2.6).

Since $DH_0(\bar{x}^0(I_r), I_r) = 0$, the same argument that led to (2.19) shows that

$$DH_0(x, I_r) = \bar{M}(x)(x - x^0(I_r)), \qquad (4.12)$$

where $\bar{M}$ is a 2×4 matrix of C^{r-1} functions of x, and its norm obeys the estimate $\|\bar{M}\| < K_{\bar{M}}$ in a fixed neighborhood of $\hat{\mathscr{A}}_0$ containing $\hat{U}_{\delta_0}$. We use a linear change of variables to pass from (x_1, x_2) to the coordinates (y_1, y_2) such that $y_1 = 0$ and $y_2 = 0$ are the stable and unstable subspaces, respectively, for the linearized flow along $\hat{\mathscr{A}}_0$. From the local normal form (2.6) we obtain that, in a fixed small neighborhood of $\hat{\mathscr{A}}_\varepsilon$, the time evolution of the norms of these new coordinates obeys the estimates

$$|y_1(t)| < |y_{10}| e^{6\lambda(t-t_0)/5}, \quad |y_2(t)| < |y_{20}| e^{-4\lambda(t-t_0)/5}, \tag{4.13}$$

where y_{10} and y_{20} are the values of y_1 and y_2 at $t = t_0$.

Now from (4.10)–(4.13) we see that the last sum of integrals in (4.9) can be estimated as

$$\begin{aligned} \left| \sum_{i=1}^{n} \int_{T_i^{0+}}^{T_i^+} \dot{\hat{H}}(w_\varepsilon(t))\, dt \right| &< \sum_{i=1}^{n} \int_{T_i^{0+}}^{T_i^+} |\langle DH_0(x, I_r), g(x, I_r, \phi; 0)\rangle|_{w_\varepsilon(t)}\, dt + \mathcal{O}\left(\varepsilon^{3/2} \log \frac{\delta_0}{\sqrt{\varepsilon}}\right) \\ &< \varepsilon n K_{\bar{M}} K_g \int_0^{\frac{6}{5\lambda}\log\frac{\delta_0}{c_7\sqrt{\varepsilon}}} (c_8 |y_{10}| e^{6\lambda t/5} + c_9 |y_{20}| e^{-4\lambda t/5})\, dt + c_{10}\varepsilon^{5/4}, \end{aligned} \tag{4.14}$$

where K_g is a uniform bound on $|g|$ in a neighborhood of $\hat{\mathscr{A}}_0$. Since the solution of $w_\varepsilon(t)$ is assumed to intersect $\hat{U}_{\delta(\varepsilon)}$ at the times T_i^+, we can use (4.11) and (4.13) to obtain the "backward" estimates

$$|y_{10}| \equiv |y_1(T_i^{0+})| < c_{11} \frac{1}{\delta_0} \varepsilon^{41/50}, \quad |y_{20}| \equiv |y_2(T_i^{0+})| < c_{12}\delta_0, \tag{4.15}$$

where the second inequality follows from the definition of the intersection time T_i^{0+}. Then (4.14) and (4.15) imply that, for small but fixed $\delta_0 > 0$ and $\varepsilon > 0$ sufficiently small, the last sum on the right-hand side of (4.9) can be estimated as

$$\begin{aligned} \left| \sum_{i=1}^{n} \int_{T_i^{0+}}^{T_i^+} \dot{\hat{H}}(w_\varepsilon(t))\, dt \right| &< \varepsilon n K_{\bar{M}} K_g \left[\frac{5 c_8 c_{11} \varepsilon^{41/50}}{6\delta_0 \lambda} \left(\exp\left(\frac{36}{25} \log \frac{\delta_0}{c_7\sqrt{\varepsilon}} \right) - 1 \right) \right. \\ &\quad \left. + \frac{5 c_9 c_{12} \delta_0}{4\lambda} \left(1 - \exp\left(-\frac{24}{25} \log \frac{\delta_0}{c_7\sqrt{\varepsilon}} \right) \right) \right] + c_{10}\varepsilon^{5/4} \\ &< \varepsilon (c_{13}\varepsilon^{1/10} + c_{14}\delta_0 + c_{10}\varepsilon^{5/4}). \end{aligned} \tag{4.16}$$

By reversing time, we can estimate the first sum on the right-hand side of (4.9) in a completely analogous way, so it remains to study the second sum.

Recall from the discussion of Section 4.1 that condition (4.2) ensures that the solution $w_\varepsilon(t)$ stays close to a set of unperturbed solutions of the form $\hat{y}^i(t)$ outside $\hat{U}_{\delta_0}$. Then, using (4.10), we can rewrite the second term in (4.9) as

$$\sum_{i=1}^{n} \int_{T_{i-1}^{0-}}^{T_i^{0+}} \dot{\hat{H}}(w_\varepsilon(t))\, dt = \varepsilon \sum_{i=1}^{n} \int_{T_{i-1}^{0-}}^{T_i^{0+}} [\langle DH_0(x, I_r), g(x, I_r, \phi; 0)\rangle|_{\hat{y}^i(t)} + \mathcal{O}(\sqrt{\varepsilon})]\, dt. \tag{4.17}$$

Note that the integrand in (4.17) does not depend on the coordinate η, so we can replace the solution $\hat{y}^i(t)$ of the unperturbed dissipative standard form $(4.1)_{\varepsilon=0}$ with the solution $y^i(t)$ of the original unperturbed system $(1.2)_{\varepsilon=0}$ with the properties described in the statement of this lemma. Also note that, by the exponential decay of DH_0 on the solutions $y^i(t)$ for $t \to \pm\infty$, one can replace the definite integral of $\langle DH_0(x, I_r), g(x, I_r, \phi; 0)\rangle|_{y^i(t)}$ with an improper integral from $-\infty$ to $+\infty$ plus an error term of order $\mathcal{O}(\delta_0)$. Hence we obtain

$$\sum_{i=1}^{n} \int_{T_{i-1}^{0-}}^{T_i^{0+}} \dot{\hat{H}}(w_\varepsilon(t))\,dt = \varepsilon \sum_{i=1}^{n} \int_{-\infty}^{+\infty} \langle DH_0(x, I_r), g(x, I_r, \phi; 0)\rangle|_{y^i(t)}dt$$
$$+ \mathcal{O}(\varepsilon\delta_0) + \mathcal{O}(\varepsilon^{3/2}). \tag{4.18}$$

Then, from (4.16) along with an analogous estimate for the first sum in (4.9), and from (4.18), we obtain that

$$\sum_{i=1}^{n} \hat{H}(p_i) - \hat{H}(q_{i-1}) = \varepsilon \sum_{i=1}^{n} \int_{-\infty}^{+\infty} \langle DH_0(x, I_r), g(x, I_r, \phi; 0)\rangle|_{y^i(t)}dt + \mathcal{O}(\varepsilon\delta_0, \varepsilon^{11/10}), \tag{4.19}$$

which gives an estimate for the third term on the right-hand side of (4.4).

To complete the proof of the lemma, we now estimate the last term on the right-hand side of (4.4). Using the local normal form (2.6), we obtain that the time $t_\varepsilon = T_i^- - T_i^+$ that the solution spends in the tube $\hat{U}_{\delta(\varepsilon)}$ during its ith passage near the slow manifold is again uniformly bounded by a constant as $\varepsilon \to 0$ (see (2.16) and condition (4.2)). Then, using (4.10) and (4.12), we can write

$$\left|\sum_{i=1}^{n-1} \hat{H}(q_i) - \hat{H}(p_i)\right| < \sum_{i=1}^{n-1} \int_{T_i^+}^{T_i^-} |\dot{\hat{H}}(w_\varepsilon(t))|\,dt < (n-1)\varepsilon K_{\bar{M}} K_g t_\varepsilon + c_{14}\varepsilon^{3/2} < c_{15}\varepsilon^{3/2}. \tag{4.20}$$

But (4.4), (4.5), (4.7), (4.19), and (4.20) together prove the first statement of the lemma. The differentiability of $\hat{H}(p_n)$ with respect to η_{b_0} and ϕ_{b_0} follows from the differentiability of the local and global tracking maps (see Section 4.1). □

As we outlined at the beginning of Section 4.2, we now give an estimate for the energy of the intersection of the stable fiber $\hat{f}_\varepsilon^s(b_n)$ with the set $\partial\hat{U}_{\delta(\varepsilon)}$.

Lemma 4.2. *Let $w_\varepsilon(t)$ be a solution of (4.1) with the same properties as in Lemma 4.1. Let $b_n \in \hat{\mathcal{A}}_\varepsilon$ be the base point of the stable fiber $\hat{f}_\varepsilon^s(b_n)$, such that for the point $s_n = \hat{f}_\varepsilon^s(b_n) \cap \partial\hat{U}_{\delta(\varepsilon)}$, $(\eta_{s_n}, \phi_{s_n}) = (\eta_{p_n}, \phi_{p_n})$. Then, for $\delta_0 > 0$ small enough, and for all $\varepsilon < \varepsilon_0$,*

$$\hat{H}(s_n) = H_0(\bar{x}^0(I_r), I_r) + \varepsilon\mathscr{H}(\eta_{b_0}, \phi_{b_0} + n\Delta\phi) + \mathcal{O}(\varepsilon^{3/2}), \tag{4.21}$$

where $\hat{H}(s_n)$ is a C^1 function of the variables (η_{b_0}, ϕ_{b_0}).

Proof. An estimate analogous to (4.7) immediately gives

$$\hat{H}(s_n) = \hat{H}(b_n) + \mathcal{O}(\varepsilon^{3/2}). \tag{4.22}$$

Then, from our discussion in Section 4.1 and from (3.44) and (3.46), we obtain that

$$\begin{aligned}\hat{H}(b_n) &= \hat{\mathscr{H}}_\varepsilon(\eta_{b_n}, \phi_{b_n}) = \hat{\mathscr{H}}_\varepsilon(\eta_{b_0} + \mathcal{O}(\sqrt{\varepsilon}), \phi_{b_0} + n\Delta\phi + \mathcal{O}(\sqrt{\varepsilon}))\\ &= H_0(\bar{x}^0(I_r), I_r) + \varepsilon\hat{\mathscr{H}}(\eta_{b_0}, \phi_{b_0} + n\Delta\phi) + \mathcal{O}(\varepsilon^{3/2}),\end{aligned}$$

as claimed. The differentiability of $\hat{H}(s_n)$ follows the same way as in the previous lemma. □

From Lemmas 4.1 and 4.2 we obtain the following result:

Proposition 4.3. *Let $w_\varepsilon(t)$ be a solution of (4.1) with the same properties as in Lemma 4.1, and let (η_{b_0}, ϕ_{b_0}) be a transverse zero of the function*

$$\Delta^n \hat{\mathscr{H}}(\eta, \phi) - \sum_{i=1}^{n} \int_{-\infty}^{+\infty} \langle DH_0, g\rangle|_{y^i(t)}\, dt \tag{4.23}$$

with $y^i(t)$ defined as in Lemma 4.1, and $\Delta^n\hat{\mathscr{H}}$ defined as in (3.48). Then, for any $\delta_0 > 0$, there exists $\varepsilon_0 > 0$ such that for all $0 < \varepsilon < \varepsilon_0$, system (4.1) has an n-pulse orbit $\hat{y}_\varepsilon^n$ homoclinic to the manifold $\hat{\mathscr{A}}_\varepsilon$. The orbit $\hat{y}_\varepsilon^n$ intersects an unstable fiber of the form $\hat{f}_\varepsilon^u(b_0 + \mathcal{O}(\delta_0))$ and a stable fiber of the form $\hat{f}_\varepsilon^s(b_n + \mathcal{O}(\delta_0))$.

Proof. As we discussed earlier, the existence of an orbit $\hat{y}_\varepsilon^n$ with the properties above follows from the condition (4.2) if the equation $\hat{H}(p_n) = \hat{H}(s_n)$ admits a solution for all sufficiently small $\varepsilon > 0$. From Lemmas 4.1 and 4.2 we directly obtain that this condition is equivalent to the solvability of the equation

$$\Delta^n \hat{\mathscr{H}}(\eta, \phi) - \sum_{i=1}^{n} \int_{-\infty}^{+\infty} \langle DH_0, g\rangle|_{y^i(t)}\, dt + \delta_0 h_1(\eta_{b_0}, \phi_{b_0}; \varepsilon) + \varepsilon^{1/10} h_2(\eta_{b_0}, \phi_{b_0}; \varepsilon) = 0, \tag{4.24}$$

where $\Delta^n\hat{\mathscr{H}}(\phi)$ is defined in (3.48), and h_1 and h_2 are C^1 functions of (η_{b_0}, ϕ_{b_0}) and C^0 functions of ε. By assumption, (η_{b_0}, ϕ_{b_0}) satisfies this equation for $\delta_0 = \varepsilon = 0$, so the implicit function theorem guarantees a nearby solution for $\delta_0 > 0$ and $\varepsilon = 0$. If δ_0 is small enough and fixed, then this nearby solution is also transverse. Therefore, a second application of the implicit function theorem guarantees a solution for (4.24) for $\varepsilon > 0$ small enough. □

4.3. The existence of N-pulse orbits

We have seen that under certain assumptions, one can establish the existence of multi-pulse orbits homoclinic to $\hat{\mathscr{A}}_\varepsilon$ in the dissipative system (4.1). This directly implies the presence of similar orbits homoclinic to $\mathscr{A}_\varepsilon$ in the original system (1.2). Proposition 4.3 provides us with a dissipative version of the energy-difference function we used earlier. So far, however, our existence result depends on detailed knowledge of a perturbed solution $w_\varepsilon(t)$. In particular, we require information of the form (4.2) about the local passages of $w_\varepsilon(t)$ near the slow manifold $\hat{\mathscr{A}}_\varepsilon$. We now remove this condition and give expressions for the pulse numbers of existing homoclinic orbits depending on their limit sets. We also identify the asymptotics and the jump sequences of these homoclinic orbits. (Note that so far we have left this question open by assuming that the unperturbed solutions $y^i(t)$, which "shadow" the n-pulse orbit, are given.)

To study the asymptotic behavior of orbits homoclinic to the slow manifold $\hat{\mathscr{A}}_\varepsilon$, we first note that on $\hat{\mathscr{A}}_\varepsilon$ the dynamics is now described by the *dissipative restricted system*

$$\begin{aligned} \dot{\eta} &= \sqrt{\varepsilon}[-D_\phi \hat{\mathscr{H}}(\eta, \phi) + g_I(\bar{x}^0(I_r), I_r, \phi; 0)] \\ &\quad + \varepsilon D_I g_I(\bar{x}^0(I_r), I_r, \phi; 0)\eta + \mathcal{O}_D(\varepsilon^{3/2}) + \mathcal{O}_H(\varepsilon), \\ \dot{\phi} &= \sqrt{\varepsilon} D_\eta \hat{\mathscr{H}}(\eta, \phi) + \varepsilon g_\phi(\bar{x}^0(I_r), I_r, \phi; 0) + \mathcal{O}_D(\varepsilon^{3/2}) + \mathcal{O}_H(\varepsilon). \end{aligned} \tag{4.25}$$

The $\mathcal{O}_H(\varepsilon)$ terms in (4.25) only smoothly deform the nonsingular level curves of the reduced Hamiltonian $\hat{\mathscr{H}}$ by an amount of $\mathcal{O}(\sqrt{\varepsilon})$, but do not change the asymptotic behavior of the corresponding solutions. Therefore, to understand the effect of dissipation on nonsingular Hamiltonian orbits it suffices to study the *dissipative reduced system*

$$\begin{aligned} \dot{\eta} &= -D_\phi \hat{\mathscr{H}}(\eta, \phi) + g_I(\bar{x}^0(I_r), I_r, \phi; 0) + \sqrt{\varepsilon} D_I g_I(\bar{x}^0(I_r), I_r, \phi; 0)\eta, \\ \dot{\phi} &= D_\eta \hat{\mathscr{H}}(\eta, \phi) + \sqrt{\varepsilon} g_\phi(\bar{x}^0(I_r), I_r, \phi; 0). \end{aligned} \tag{4.26}$$

Note that we rescaled time by $\sqrt{\varepsilon}$ to obtain these equations. In order to obtain information about the limit sets of (4.26), we want it to be non-Hamiltonian. This is satisfied if

(H4) $$D_I g_I(\bar{x}^0(I_r), I_r, \phi; 0) + D_\phi g_\phi(\bar{x}^0(I_r), I_r, \phi; 0) \not\equiv 0,$$

in which case the relation between the orbits of the dissipative restricted and reduced systems is similar to that of Section 3.3: If $\hat{\gamma}_0 \subset \hat{A}$ is a structurally stable orbit of the dissipative reduced system, then for small ε the dissipative restricted system has an orbit $\hat{\gamma}_\varepsilon \subset \hat{\mathscr{A}}_\varepsilon$ such that $\hat{\gamma}_0$ and $\hat{g}_\varepsilon^{-1}(\hat{\gamma}_\varepsilon)$ are $(\sqrt{\varepsilon}, C^{r-2})$-close on appropriate compact subsets of $\hat{A}$.

It is important to note that the reduced system (4.26) is *locally* Hamiltonian for $\varepsilon = 0$. This means that, if we change the angular variable ϕ to a variable $v \in \mathbb{R}$ and if we define the set

$$\hat{A}_D = [-\eta_0, \eta_0] \times C, \tag{4.27}$$

where $C \subset R$ is a suitable compact interval, then $(4.26)_{\varepsilon=0}$ on $\hat{A}_D$ derives from the *reduced Hamiltonian*

$$\hat{\mathscr{H}}_D(\eta, v) = \hat{\mathscr{H}}(\eta, v) - \int_0^v g_I(\bar{x}^0(I_r), I_r, u; 0)\, du. \tag{4.28}$$

Here $\hat{\mathscr{H}}$ is the same as in (3.45).

Definition 4.1. We call a non-equilibrium orbit $\hat{\gamma} \subset \hat{A}$ of the reduced system $(4.26)_{\varepsilon=0}$ an *internal orbit* if it is structurally stable with respect to locally Hamiltonian perturbations.

For what follows we assume that

(H5) For any two unperturbed solutions $y_0^+(t, I_r, \phi_0^+)$ and $y_0^-(t, I_r, \phi_0^-)$ of $(1.2)_{\varepsilon=0}$ with $y_0^+(t, I_r, \phi_0^+) \in W_0^+$ and $y_0^-(t, I_r, \phi_0^-) \in W_0^-$ for all $t \in \mathbb{R}$ and with

$$\lim_{t \to -\infty} y_0^+(t, I_r, \phi_0^+) = \lim_{t \to -\infty} y_0^-(t, I_r, \phi_0^-),$$

the following is satisfied:

$$\int_{-\infty}^{+\infty} \langle DH_0, g \rangle|_{y_0^+(t, I_r, \phi_0^+)}\, dt = \int_{-\infty}^{+\infty} \langle DH_0, g \rangle|_{y_0^-(t, I_r, \phi_0^-)}\, dt.$$

Just as in hypothesis (H3), this hypothesis simplifies the formulation of the upcoming results and holds for all applications we know of (see Section 1.3). (H5) implies that the improper integrals in (4.38) do not depend on which of the two unperturbed homoclinic manifolds the particular solution $y^i(t)$ belongs to. This enables us to remove the implicit assumption in Lemma 4.1 and Proposition 4.3, that we know the "shape" (i.e., .the jump sequence) of the solution $w_\varepsilon(t)$. Then, letting $y^i(t)$ be any of the two unperturbed heteroclinic solutions of system $(1.2)_{\varepsilon=0}$ connecting the points $(\bar{x}^0(I_r), I_r, \phi + (i-1)\Delta\phi)$ and $(\bar{x}^0(I_r), I_r, \phi + i\Delta\phi)$, we define the *dissipative nth order energy-difference function*

$$\Delta^n \hat{\mathscr{H}}_D(\phi) = \Delta^n \hat{\mathscr{H}}(\phi) - \sum_{i=1}^{n} \int_{-\infty}^{+\infty} \langle DH_0, g \rangle|_{y^i(t)} dt. \tag{4.29}$$

We again define the zero sets

$$\begin{gathered} \hat{V}_-^0 = \emptyset, \quad \hat{V}_-^n = \{(\eta, \phi) \in \hat{A} \,|\, \Delta^n \hat{\mathscr{H}}_D(\phi) = 0\}, \quad \hat{V}_+^n = \hat{\mathscr{R}}^n(\hat{V}_-^n), \\ \hat{Z}_-^n = \{(\eta, \phi) \in V_-^n \,|\, D_\phi \Delta^n \hat{\mathscr{H}}_D(\phi) \neq 0\}, \quad Z_+^n = \hat{\mathscr{R}}(\hat{Z}_-^n), \quad n \geqq 1. \end{gathered} \tag{4.30}$$

For any internal orbit $\hat{\gamma}$ of the locally Hamiltonian system $(4.26)_{\varepsilon=0}$ we again introduce the *pulse number*

$$N(\hat{\gamma}) = \min\{n \geqq 1 \,|\, \hat{V}_-^k \cap \hat{\gamma} = \emptyset,\ k = 0, \ldots, n-1,\ \hat{Z}_-^n \pitchfork \hat{\gamma}\}. \tag{4.31}$$

Definition 4.2. Suppose that for an internal orbit $\hat{\gamma}$ of the reduced system $(4.26)_{\varepsilon=0}$, $N(\hat{\gamma}) \equiv N$ is defined. Then the *positive and negative sign sequences* $\{\chi^\pm(\hat{\gamma})\}_{k=1}^N$ *of*

$\hat{\gamma}$ are defined as

$$\chi_1^+(\hat{\gamma}) = +1, \quad \chi_{k+1}^+(\hat{\gamma}) = \sigma\,\mathrm{sign}(\Delta^k \hat{\mathscr{H}} \,|\, \hat{\gamma})\chi_k^+(\gamma), \quad k = 1, \ldots, N-1,$$

$$\chi_k^-(\hat{\gamma}) = -\chi_k^+(\hat{\gamma}), \quad k = 1, \ldots, N-1,$$

with σ defined in (3.33).

Before we formulate our main result for the dissipative case we note that in a general dissipative system of the form (1.2) there may be no orbits other than fixed points, which are isolated from $\partial \hat{A}$. This observation is related to the fact that for non-Hamiltonian perturbations, $\mathscr{A}_0$ usually perturbs into an overflowing or inflowing invariant manifold $\mathscr{A}_\varepsilon$ whose stable and unstable manifolds are only locally invariant. As a result, when we speak about *N-pulse orbits* in this section, we mean orbits which leave and reenter a neighborhood of $\mathscr{A}_\varepsilon$ N-times, and which, before the first and after the last pulse, follow orbits in $\mathscr{A}_\varepsilon$ in backward and forward time, respectively, as long as these latter orbits stay in the resonance band $\mathscr{P}_{\sqrt{\varepsilon}}$ (see (3.35)). This property can most conveniently be described in terms of the stable and unstable foliations discussed in Proposition 2.1.

Definition 4.3. We say that an N-pulse orbit y_ε^N of the dissipative system (1.2) *positively approaches* an orbit $\gamma_\varepsilon^+ \subset \mathscr{A}_\varepsilon$, if y_ε^N intersects a stable fiber $f_\varepsilon^s(q) \subset W_{\mathrm{loc}}^s(\mathscr{A}_\varepsilon)$ with basepoint $q \in \gamma_\varepsilon^+$. Similarly, we say that y_ε^N *negatively approaches* a slow orbit $\gamma_\varepsilon^- \subset \mathscr{A}_\varepsilon$ if y_ε^N intersects an unstable fiber $f_\varepsilon^u(p) \subset W_{\mathrm{loc}}^u(\mathscr{A}_\varepsilon)$ with base point $p \in \gamma_\varepsilon^-$.

An example of an N-pulse orbit positively approaching a slow orbit is shown in Fig. 14.

Theorem 4.4. *Assume that hypotheses* (H1′), (H2a), (H3′), (H4) *and* (H5) *are satisfied. Suppose that for an internal orbit $\hat{\gamma}_0^- \subset \hat{A}$ of the reduced system* $(4.26)_{\varepsilon=0}$,

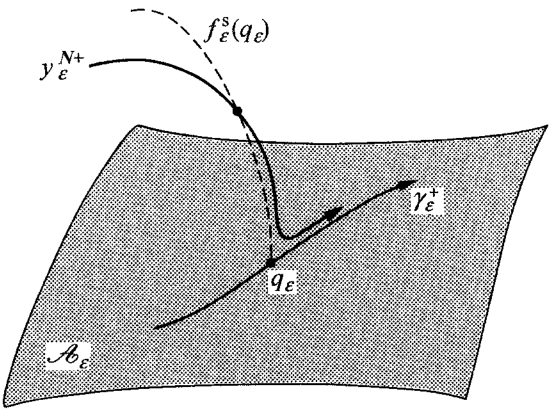

Fig. 14. An N-pulse orbit y_ε^N positively aproaching γ_ε^+.

(A1) $N \equiv N(\hat{\gamma}_0^-)$ *is defined.*

(A2) *Let* $\hat{b}_- \in \hat{Z}_-^N \cap \hat{\gamma}_0^-$ *and* $\hat{b}_+ = \hat{\mathscr{R}}^N(\hat{b}_-)$. *Assume that the orbit* $\hat{\gamma}_0^+ \subset \hat{A}$ *of system* $(4.26)_{\varepsilon=0}$ *which contains* $\hat{b}_+$ *is an internal orbit with* $\hat{Z}_+^N \pitchfork \hat{\gamma}_0^+$.

Then for each of the two jump sequences $\{\chi_k^\pm\}$, *there exists* $\varepsilon_0 > 0$ *such that for* $0 < \varepsilon < \varepsilon_0$, *the dissipative system* (1.2) *has an N-pulse homoclinic orbit* y_ε^N *with jump sequence* $\{\chi_k^\pm\}$ *which positively approaches a slow orbit* $\gamma_\varepsilon^+ \subset \mathscr{A}_\varepsilon$ *and negatively approaches a slow orbit* $\gamma_\varepsilon^- \subset \mathscr{A}_\varepsilon$. *Moreover, the orbits* $b_\varepsilon \circ g_\varepsilon^{-1}(\gamma_\varepsilon^+)$ *and* $\hat{\gamma}_0^+$ *are* $(\sqrt{\varepsilon}, C^1)$*-close near* $\hat{b}_-$, *and* $b_\varepsilon \circ g_\varepsilon^{-1}(\gamma_\varepsilon^+)$ *and* $\hat{\gamma}_0^+$ *are* $(\sqrt{\varepsilon}, C^1)$*-close near* $\hat{b}_+$.

Proof. In view of our discussion in Section 4.1, Proposition 4.3, and the arguments we used to prove the analogous theorems for purely Hamiltonian perturbations, we only have to show that under the assumptions of this theorem any solution $w_\varepsilon(t)$ lying in the unstable manifold $W^{\mathrm{u}}(\hat{\gamma}_\varepsilon)$ of an orbit $\hat{\gamma}_\varepsilon$ of the dissipative restricted system (4.25) satisfies the minimal distance condition (4.2) for $k = 1, \ldots, n = N$, as well as the energy-type maximal distance condition in the statement of Lemma 2.5. These two conditions ensure that our construction in Section 4.1 for tracking dissipative orbits is indeed valid. Then the asymptotic behavior of the multi-pulse orbit follows from the fact that the N-take-off and N-landing curves of system (4.1) perturb smoothly in the parameter $\sqrt{\varepsilon}$ from the respective curves obtained for purely Hamiltonian perturbations. Indeed, the set of all N-pulse orbits positively and negatively approach orbits on $\mathscr{A}_\varepsilon$ that intersect B_{u}^N and B_{s}^N, which project down to the annulus $\hat{A}$ close to $\hat{z}_-^N$ and $\hat{z}_+^N$, respectively (see (3.54), (3.55)). But the projections of slow orbits on the annulus $\hat{A}$ under the map $b_\varepsilon \circ g_\varepsilon^{-1}$ are locally C^1-close to the orbits of the system $(4.26)_{\varepsilon=0}$.

To verify the minimal and maximal distance conditions, we first note that for any $k < N(\hat{\gamma}_0^-)$, we have $\Delta^k \hat{\mathscr{H}}_D \,|\, \hat{\gamma}_0^- \neq 0$, by the definition of the pulse number. Since the closure of $\hat{\gamma}_0^-$ is compact and $\Delta^k \hat{\mathscr{H}}_D$ is continuous, this implies the existence of $h_1, h_2 > 0$ such that

$$h_1 < |\Delta^k \hat{\mathscr{H}}_D \,|\, \hat{\gamma}_0^-| < h_2, \quad k = 1, \ldots, N-1. \tag{4.32}$$

Assume now that the condition (4.2) holds for some $n - 1 < N - 1$ with $n \geqq 1$. Then, by (4.3) and (4.21), we obtain that for $\varepsilon > 0$ sufficiently small

$$|\hat{H}(p_n) - \hat{H}(s_n)| > \tfrac{1}{2}\varepsilon h_1. \tag{4.33}$$

Then (4.12) and the mean value inequality applied to (4.33) imply

$$|p_n - s_n| > \frac{h_1}{2K_{\bar{M}}}\sqrt{\varepsilon}. \tag{4.34}$$

If s_n is the point in $W_{\mathrm{loc}}^{\mathrm{s}}(\hat{\mathscr{A}}_\varepsilon)$ which is the closest to p_n, then (4.34) shows that (4.2) also holds for n. This, by induction, implies that the minimal-distance condition (4.2) holds for all $k = 1, \ldots, N - 1$ for any solution $w_\varepsilon(t)$ in $W^{\mathrm{u}}(\hat{\gamma}_\varepsilon)$. If s_n is not the closest point to p_n in $W_{\mathrm{loc}}^{\mathrm{s}}(\hat{\mathscr{A}}_\varepsilon)$, then the actual closest point $r_n \in W_{\mathrm{loc}}^{\mathrm{s}}(\hat{\mathscr{A}}_\varepsilon)$ must satisfy $|\eta_{r_n} - \eta_{s_n}| + |\phi_{r_n} - \phi_{s_n}| < K^* \sqrt{\varepsilon}$; otherwise it would be farther away from

p_n than s_n. Combining this fact with the same type of fiber-argument leading to (4.6), we obtain that $|\hat{H}(s_n) - \hat{H}(r_n)| < c_{16}\varepsilon^{3/2}$. This, together with (4.33), implies that

$$|\hat{H}(p_n) - \hat{H}(r_n)| = \left| |\hat{H}(p_n) - \hat{H}(s_n)| - |\hat{H}(s_n) - \hat{H}(r_n)| \right| > \frac{h_1}{2}\varepsilon - c_{16}\varepsilon^{3/2} > \frac{h_1}{4}\varepsilon \tag{4.35}$$

for $\varepsilon > 0$ sufficiently small. The same mean value inequality that we applied to the left-hand side of (4.33) now gives

$$|p_n - r_n| > \frac{h_1}{4K_{\bar{M}}}\sqrt{\varepsilon}, \tag{4.36}$$

and the same induction argument gives that the required minimal distance condition (4.2) holds for all $k = 1, \ldots, N-1$. The maximal distance condition required in Lemma 2.5 follows from (4.3), which shows that

$$|\hat{H}(p_n) - \hat{h}_0| < 2\varepsilon h_2 \tag{4.37}$$

with $\hat{h}_0 = H_0(\bar{x}^0(I_r), I_r)$. This concludes the proof of the theorem. □

Remark 4.1. In applications it is sometimes easier to use an equivalent formula for the second term in the expression for $\Delta^n \hat{\mathscr{H}}_D(\phi)$ in (4.29). Using Green's theorem we can write this term as

$$\begin{aligned}\sum_{i=1}^{n} \int_{-\infty}^{+\infty} \langle D_x H, g\rangle|_{y^i(t)}\, dt &= \sum_{i=1}^{n} \int_{-\infty}^{+\infty} \langle(-J\dot{x}, \dot{\phi}, 0), g(x, I_r, \phi; 0)\rangle|_{y^i(t)}\, dt \\ &= \sum_{i=1}^{n} \int_{y^i} g_{x_2} dx_1 - g_{x_1} dx_2 + g_I d\phi \\ &= \sum_{i=1}^{n} \Bigg[\sigma \int_{A_i} \nabla_x \cdot g_x(x, I_r, \phi; 0)\, dx_1\, dx_2 \\ &\qquad + \int_{\partial A_i} g_I(x(\phi), I_r, \phi; 0)\, d\phi\Bigg],\end{aligned}$$

where A_i denotes the region in the (x_1, x_2) plane which is enclosed by the x-component of the solution $y^i(t)$, and the constant σ (defined in (3.33)) enters the formula to ensure the correct orientation on ∂A_i for the application of Green's theorem. The integral of $\nabla_x \cdot g_x$ on A_i is independent of i, so we can, say, choose $A_i \equiv A_r = \mathrm{Int}(\mathscr{L}^+(I_r))$ (see (3.32)). In that case (4.29) takes the form

$$\begin{aligned}\Delta^n \hat{\mathscr{H}}_D(\phi) = \Delta^n \hat{\mathscr{H}}(\phi) &- n\sigma \int_{A_r} \nabla_x \cdot g_x(x, I_r, \phi; 0)\, dx_1\, dx_2 \\ &- \sum_{i=1}^{n} \int_{\partial A_r} g_I(x(\phi), I_r, \phi; 0)\, d\phi.\end{aligned} \tag{4.38}$$

Some applications we mentioned earlier arise in modal truncations of systems with mode-independent damping (see, e.g., our beam example to be studied in Section 5). In such systems the function g_I usually has no expllicit x- and ϕ-dependence, so it is constant on unperturbed orbits. In such cases (4.38) further simplifies to

$$\Delta^n \hat{\mathscr{H}}_D(\phi) = \Delta^n \hat{\mathscr{H}}(\phi) - n\sigma \int_{A_r} \nabla_x \cdot g_x(x, I_r, \phi; 0)\, dx_1\, dx_2 - n g_I(I_r; 0)\Delta\phi. \quad (4.39)$$

The advantage of this formulation is that one does not have to solve the unperturbed integrable problem explicitly to obtain the solutions $y^i(t)$.

4.4. Codimension-one N-pulse orbits

In the previous sections we proved the existence of N-pulse orbits based on pulse numbers for non-equilibrium orbits which approximated the α-limit sets of the N-pulse orbits. There are, however, important types of homoclinic orbits which emanate from and possibly return to equilibria. Such orbits are, e.g., orbits homoclinic to a saddle-center in the purely Hamiltonian case and Šilnikov-type orbits homoclinic to a saddle-focus in the dissipative case. In their vicinities both of these structures may create chaotic invariant sets, which survive small changes in the system parameters even though the underlying homoclinic connection generically breaks (because these homoclinic orbits are not transverse). We now extend the energy-phase method to such cases: We give conditions for the existence of N-pulse orbits negatively asymptotic to a fixed point on the slow manifold. We again restrict the discussion to resonance bands subject to Hamiltonian and dissipative perturbations so that we can apply the results directly to our beam example in the next section. Similar results hold for all other cases considered earlier.

Theorem 4.5. *Let hypotheses* (H1′), (H2a), (H3′), (H4), *and* (H5) *be satisfied for system* (1.2) *which is now assumed to depend on a vector* $\mu \in \mathbb{R}^p$ *of system parameters. Assume further that*

(A1) $M \subset W$ *is an open set of* $\mathbb{R}^p$ *such that for any* $\mu \in M$ *the system* $(4.26)_{\varepsilon=0}$ *has a nondegenerate equilibrium* $\hat{c}_0(\mu) = (\eta_{\hat{c}_0}(\mu), \phi_{\hat{c}_0}(\mu)) \in \hat{A}$ *(i.e.,* $JD^2_{(\eta,v)}\hat{\mathscr{H}}_D \,|\, \hat{c}_0(\mu)$ *has no zero eigenvalues).*

(A2) *For some integer* $N \geqq 1$, $\hat{c}_0(\mu_0) \in \hat{Z}^N_-$ *with* $\hat{Z}^N_-$ *defined in* (4.30).

(A3) $D_\mu \Delta^n \hat{\mathscr{H}}_D(\phi_{\hat{c}_0}(\mu); \mu)|_{\mu_0} \neq 0 \in \mathbb{R}^p$ *with* $\Delta^N \hat{\mathscr{H}}_D$ *defined in* (4.29).

Then, for any small $\delta_0 > 0$, *there exists* $\varepsilon_0 > 0$ *and for* $0 < \varepsilon < \varepsilon_0$ *there exists a codimension-one surface* $C_N^+ \subset M \times \mathbb{R}$ *near* $(\mu_0, 0)$ *such that for any* $(\mu, \varepsilon) \in C_N^+$ *the following hold*:

(i) $\mathscr{A}_\varepsilon$ *has an N-pulse homoclinic orbit* y_ε^{N+} *which is negatively asymptotic to an equilibrium* $c_\varepsilon(\mu) \in \mathscr{A}_\varepsilon$ *such that* $b_\varepsilon \circ g_\varepsilon^{-1}(c_\varepsilon(\mu))$ *and* $\hat{c}_0(\mu_0)$ *are* $\mathcal{O}(\sqrt{\varepsilon})$*-close in* $\hat{A}$. *Furthermore,* y_ε^{N+} *positively approaches a slow orbit* γ_ε^+ *such that* $b_\varepsilon \circ g_\varepsilon^{-1}(\gamma_\varepsilon^+)$ *and* $\mathscr{R}^N(\hat{c}_0(\mu_0))$ *are* $\mathcal{O}(\delta_0)$*-close.*

(ii) *For the jump sequence* y_ε^{N+}, $j(y_\varepsilon^{N+}) = \chi^+(\hat{c}_0(\mu_0))$, *where* $\chi^+(\hat{c}_0(\mu_0))$ *is obtained by substituting* $\hat{c}_0(\mu_0)$ *for* $\hat{\gamma}$ *and using the integer* N *from* (A2) *in Definition 4.2.*

There also exists a codimension-one surface $C_N^- \subset M \times \mathbb{R}$ near $(\mu_0, 0)$ yielding homoclinic orbits y_ε^{N-} with properties similar to those of y_ε^{N+}, but with the jump sequence $j(y_\varepsilon^{N-}) = \chi^-(\hat{c}_0(\mu_0))$.

Proof. Let $\hat{c}_\varepsilon(\mu)$ be the equilibrium of the dissipative restricted system which perturbs from $\hat{c}_0(\mu_0)$. In view of our earlier results, we only have to show that there exists a codimension-one surface C_N^+ (see above) in the space of the parameters (μ, ε) such that $\hat{c}_\varepsilon(\mu) \in b_\varepsilon \circ g_\varepsilon^{-1}(B_{\mathrm{u},\varepsilon}^N)$ for parameter values taken from C_N^+, where $B_{\mathrm{u},\varepsilon}^N$ is the N-take-off curve of the system (1.2) described in Theorem 4.4. Since $b_\varepsilon \circ g_\varepsilon^{-1}(B_{\mathrm{u},\varepsilon}^N)$ is $(\sqrt{\varepsilon}, C^1)$-close to a subset $\hat{z}_-^N$ of $\hat{Z}_-^N$ (see Remark 3.6), in a neighborhood of the point $\hat{c}_\varepsilon(\mu)$, $b_\varepsilon \circ g_\varepsilon^{-1}(B_{\mathrm{u},\varepsilon}^N)$ satisfies

$$\Delta^N \mathscr{H}_D(\phi; \mu) + \sqrt{\varepsilon}\tilde{\mathscr{H}}(\eta, \phi; \mu, \sqrt{\varepsilon}) = 0,$$

with some C^{r-2} function $\tilde{\mathscr{H}}$. Hence, the requirement that $\hat{c}_\varepsilon(\mu) \in b_\varepsilon \circ g_\varepsilon^{-1}(B_{\mathrm{u},\varepsilon}^N)$ can be expressed as

$$\Delta^N \mathscr{H}_D(\phi_{\hat{c}_\varepsilon}(\mu); \mu) + \sqrt{\varepsilon}\tilde{\mathscr{H}}(\eta_{\hat{c}_\varepsilon}(\mu), \phi_{\hat{c}_\varepsilon}(\mu); \mu, \sqrt{\varepsilon}) = 0.$$

Note that by assumption (A2), this equation is satisfied by $(\mu, \varepsilon) = (\mu_0, 0)$ for all $\mu_0 \in M$. But then, using assumption (A3) we conclude from the implicit function theorem the local existence of the hypersurface C_N^+ within the set $M \times \mathbb{R}$ of the parameter space. The existence of C_N^- follows in the same way. $\square$

5. An example: N-pulse orbits and horseshoes in the beam model

In this section we apply our results to the two-mode model of the forced inextensional beam introduced in Section 1.2. In Section 5.1 below we consider the system (1.1) with pure forcing ($d = 0$), and in Section 5.2 we also include the effect of damping ($d > 0$).

5.1. *The forced beam without dissipation* ($d = 0$)

5.1.1. Set-up. Note that for $d = 0$ the equations in (1.1) are of the form (2.1) with the Hamiltonians

$$\begin{aligned} H_0(x, I) &= -(b + x_2^2)(x_1^2 + x_2^2) + I(2x_2^2 + b + s - \delta I), \\ H_1(x, I, \phi) &= \Gamma[(I - x_2^2)\cos 2\phi + x_1 x_2 \sin 2\phi]. \end{aligned} \tag{5.1}$$

It is simple to verify that $(1.1)_{\varepsilon=0}^x$ has a hyperbolic fixed point at $\bar{x}_0(I) = (0, 0)$ with a symmetric pair of homoclinic orbits for any $I > b/2$. The phase portrait of $(1.1)_{\varepsilon=0}^x$ for such an I value is shown in Fig. 15. (For more details on the unperturbed geometry see FENG & SETHNA [14], where a very similar system arising in the study of parametrically forced thin plates was considered.) In Fig. 15 we also indicate the

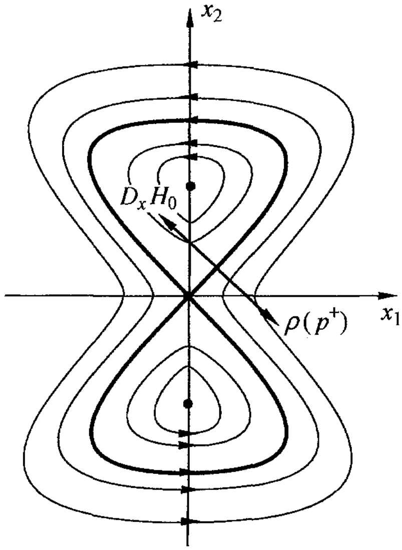

Fig. 15. The phase portrait of $(1.1)^x_{\varepsilon=0}$.

direction of the vector $\rho(p^+)$ (defined in relation with (3.33)) and the gradient D_xH_0 on the homoclinic loop $\mathscr{L}^+(I)$. Using (3.33) we immediately obtain

$$\sigma = -1. \tag{5.2}$$

As we discussed in Section 1.3, these features of $(1.1)_{\varepsilon=0}$ imply that in the phase space

$$\mathscr{P} = \{(x, I, \phi) \in \mathbb{R}^2 \times \mathbb{R}^+ \times S^1 \,|\, x_1^2 + x_2^2 \leqq 2I\}$$

there exists a normally hyperbolic invariant two-manifold

$$\mathscr{A}_0 = \{(x, I, \phi) \in \mathscr{P} \,|\, x = \bar{x}^0(I) = (0, 0), I \in [I_1, I_2]\},$$

with

$$0 < \frac{b}{2} < I_1 < \frac{b+s}{2\delta} < I_2 \tag{5.3}$$

chosen so that $\mathscr{A}_0$ includes the circle of fixed points

$$\mathscr{C}_r = \left\{(x, I, \phi) \in \mathscr{P} \,|\, x = (0, 0), I = I_r = \frac{b+s}{2\delta}\right\}.$$

Hence hypothesis (H2a) is satisfied for the unperturbed system $(1.1)_{\varepsilon=0}$. As a result of the symmetry (1.1) under $x \mapsto -x$, the invariant manifold $\mathscr{A}_0 \equiv \mathscr{A}_\varepsilon$ survives the perturbation unchanged, even for $d > 0$. This gives

$$g_0(I, \phi) \equiv g_\varepsilon(I, \phi) = (0, 0, I, \phi)$$

for the embeddings defined in (1.5) and (1.7). We also recall that the presence of the pair of homoclinic orbits in Fig. 15 gives rise to two three-dimensional homoclinic manifolds, W_0^+ and W_0^-. For any solution homoclinic to the circle $\mathscr{C}_r$, the phase shift in hypothesis (H3′) can be computed to equal

$$\Delta\phi = \cos^{-1}\left[\frac{b(2\delta - 1) - s}{b + s}\right] \in [0, \pi], \tag{5.4}$$

where we again use the calculations of FENG & SETHNA [14]. We conclude that the unperturbed beam equations satisfy hypothesis (H3′). It is interesting to note that the phase shift can be calculated without explicit expressions for the homoclinic solutions.

5.1.2. Energy-difference functions and their zeros. As we saw in Section 3.3, a first-order approximation for the orbits on the slow manifold $\hat{\mathscr{A}}_\varepsilon = \mathscr{B}_\varepsilon(\mathscr{A}_\varepsilon \cap \mathscr{P}_{\sqrt{\varepsilon}})$ of the standard form is given by the level curves of the reduced Hamiltonian $\hat{\mathscr{H}}$ defined in (3.45). For our example we easily obtain that

$$\hat{\mathscr{H}}(\eta, \phi) = -\delta\eta^2 + \Gamma\frac{b + s}{2\delta}\cos 2\phi. \tag{5.5}$$

$\hat{\mathscr{H}}$ is defined on $(\hat{A}, \hat{\omega})$ for some fixed

$$\eta_0 > 2\sqrt{\Gamma\frac{b + s}{2\delta}}.$$

The phase portrait of $\hat{\mathscr{H}}$ is shown in Fig. 16. We denote by $\hat{S}_0^a$ and $\hat{S}_0^b$ the two open domains in this figure that are enclosed by heteroclinic cycles. By the presence of

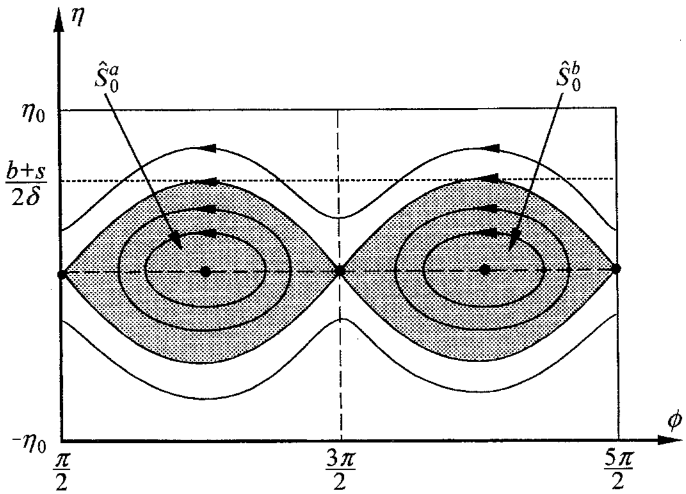

Fig. 16. The phase portrait of the reduced Hamiltonian $\hat{\mathscr{H}}$.

the symmetry $\phi \mapsto \phi + \pi$ in (1.1), both the reduced Hamiltonian and the restricted Hamiltonian $\hat{\mathscr{H}}_\varepsilon$ (see (3.44)) have phase portraits symmetric with respect to $\phi = \pi$. This fact will enable us to restrict our consideration to the domain $\hat{S}_0^a$ in our upcoming calculations. This figure also explains our choice of η_0 to include all internal orbits (see Definition 2.1) associated with the presence of the resonance at $\eta = 0$. Note that the symmetry $\phi \mapsto \phi + \pi$ of the Hamiltonian perturbation terms in the system (1.1) implies that the separatrices are structurally stable, so they are also internal orbits.

Using (3.48) and (5.5) we obtain the nth order energy-difference function

$$\Delta^n \hat{\mathscr{H}}(\phi) = \Gamma \frac{b+s}{2\delta}[\cos 2(\phi + n\Delta\phi) - \cos 2\phi]. \tag{5.6}$$

As a result of the symmetry mentioned above, it is enough to look for zeros of the energy-difference functions in the domain $[\frac{\pi}{2}, \frac{3\pi}{2}]$, because a translation by π gives the zeros in $[\frac{3\pi}{2}, \frac{5\pi}{2}]$. From (5.6) we obtain that for any n satisfying

$$n\Delta\phi \neq 2l\pi, \quad l \in \mathbb{Z}, \tag{5.7}$$

the zeros of $\Delta^n \hat{\mathscr{H}}$ in $[\frac{\pi}{2}, \frac{3\pi}{2}]$ are

$$\phi^n_{-,1} = \frac{3\pi}{2} - \frac{n\Delta\phi}{2} \bmod \pi, \quad \phi^n_{-,2} = \frac{3\pi}{2} - \left[\frac{\pi}{2} + \frac{n\Delta\phi}{2}\right] \bmod \pi. \tag{5.8}$$

Both zeros are transverse under the condition (5.7). We now introduce the two additional angles

$$\phi^n_{+,1} = [\phi^n_{-,1} + n\Delta\phi] \bmod 2\pi, \quad \phi^n_{+,2} = [\phi^n_{-,2} + n\Delta\phi] \bmod 2\pi, \tag{5.9}$$

which may or may not fall in $[\frac{\pi}{2}, \frac{3\pi}{2}]$. If they do, then $\phi^n_{+,i}$ and $\phi^n_{-,i}$ are symmetric with respect to π. (This has the important consequence that $\gamma_0^- = \gamma_0^+$ for a periodic orbit γ_0^- satisfying the assumptions of Theorem 3.4, leading to *homoclinic* N-pulse orbits.) Using the definitions of the zero sets in (3.49) we obtain

$$\begin{aligned} \hat{V}^n_- = \hat{Z}^n_- &= \{(\eta, \phi) \in \hat{S}^a_0 \mid \phi \in \{\phi^n_{-,1}, \phi^n_{-,2}\}\}, \\ \hat{V}^n_+ = \hat{Z}^n_+ &= \{(\eta, \phi) \in \hat{A} \mid \phi \in \{\phi^n_{+,1}, \phi^n_{+,2}\}\}. \end{aligned} \tag{5.10}$$

5.1.3. Pulse numbers. Note that under (5.7) all internal orbits outside $\hat{S}^a_0 \cup \hat{S}^a_0$ (periodic orbits and separatrices) intersect $\hat{Z}^1_-$ transversally. Hence, for any periodic or heteroclinic orbit $\hat{\gamma}$ outside $\hat{S}^a_0 \cup \hat{S}^a_0$ we have $N(\hat{\gamma}) = 1$ (see the definition in (3.51)). We now classify the periodic orbits in $\hat{S}^a_0$ based on their pulse numbers. An identical classification follows for the periodic orbits inside $\hat{S}^b_0$. Let us start by defining the energy sequence

$$\hat{h}_0 = -\Gamma \frac{b+s}{2\delta}, \quad \hat{h}_n = \max(\hat{\mathscr{H}}(0, \phi^n_{-,1}), \hat{\mathscr{H}}(0, \phi^n_{-,2})) \tag{5.11}$$

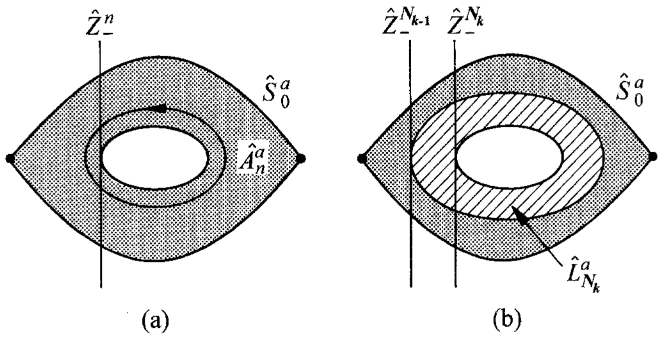

Fig. 17. The construction of the layer sequence.

and the sequence of sets

$$\hat{A}_0^a = \emptyset, \quad \hat{A}_n^a = \{(\eta, \phi) \in \hat{S}_0^a \,|\, \mathscr{H}(\eta, \phi) < \hat{h}_n\}, \quad n \geqq 1. \tag{5.12}$$

For $n \geqq 1$, $\hat{A}_n^a$ has a simple meaning: It is the open set of internal orbits in $\hat{S}_0^a$ which intersect at least one component of $\hat{Z}_-^n$ transversally (see Fig. 17a). Note that the element $\hat{h}_n$ of the energy sequence in (5.11) gives the reduced energy of the periodic orbit $\hat{\gamma}_n$, which is the inner boundary of $\hat{A}_n^a$. Next we define the *pulse sequence*

$$N_1 = 1, \quad N_k = \min\{n \in \mathbb{Z}^+ \,|\, n > N_{k-1}, \hat{h}_n > \hat{h}_{N_{k-1}}\}, \quad k \geqq 2. \tag{5.13}$$

Since the energy of the periodic orbits in $\hat{S}_0^a$ increases monotonically as the orbits shrink to the center, we necessarily have

$$\hat{A}_{N_1}^a \subset \hat{A}_{N_2}^a \subset \ldots \subset \hat{A}_{N_k}^a \subset \ldots.$$

This sequence of sets is infinite if the condition (5.7) is satisfied for all $n \in \mathbb{Z}$. Otherwise, if m is the minimal index such that $N_m \Delta\phi = 2l\pi$ for some integer l, then the pulse sequence and the set sequence $\{\hat{A}_{N_k}^a\}$ are finite and have exactly m elements, with $\hat{A}_{N_m}^a \equiv \hat{S}_0^a$. In any case, we can define the finite or infinite *layer sequence*

$$\hat{L}_{N_k}^a = \mathrm{Int}(\hat{A}_{N_k}^a \backslash \hat{A}_{N_{k-1}}^a), \tag{5.14}$$

where $\mathrm{Int}(\cdot)$ refers to the interior of a set. The construction of the layer sequence is shown in Fig. 17b. Note that $\hat{L}_{N_k}^a$ is an open set and that its inner boundary is the unique periodic orbit $\hat{\gamma}_{N_k}$ in $\hat{S}_0^a$ with

$$\mathscr{H} \,|\, \hat{\gamma}_{N_k} = \hat{h}_{N_k}. \tag{5.15}$$

In addition, we observe that if the pulse sequence is infinite, then no periodic orbit $\hat{\gamma} \subset L_{N_k}^a$ intersects $\hat{V}_-^n = \hat{Z}_-^n$ for $n < N_k$, but all intersect $\hat{Z}_-^{N_k}$ transversally. If the pulse sequence is finite, i.e., if it terminates at an index $m \geqq 1$, then this observation holds for any $k < m$. Since in this case the nonresonance condition (5.7) is violated for $n = N_m$, we obtain $\hat{V}_-^{N_m} \equiv \hat{A}$. To summarize, using the definitions in (3.51) and (3.52) we obtain the following:

- If condition (5.7) holds for all $n \geqq 1$ (i.e., if the pulse sequence is infinite), then for any periodic orbit $\hat{\gamma} \subset \hat{L}^a_{N_k}$ we have $N(\hat{\gamma}) = N_k$. Furthermore, the approximate take-off and landing curves of N_k-pulse orbits (defined in (3.54) and (3.55)) can be written as

$$\hat{z}_-^{N_k} = \hat{Z}_-^{N_k} \cap \hat{L}^a_{N_k}, \quad \hat{z}_+^{N_k} = \hat{Z}_+^{N_k} \cap (\hat{L}^a_{N_k} \cup \hat{L}^b_{N_k}), \tag{5.16}$$

  where $\hat{L}^b_{N_k}$ is the analogous layer sequence defined for $\hat{S}^b_0$.
- If $\bar{n} \geqq 1$ is the smallest integer which violates (5.7) (i.e., if the pulse sequence terminates at $N_m = \bar{n}$), then for any periodic orbit $\hat{\gamma} \subset \hat{L}^a_{N_k}$, $k < m$, we have $N(\hat{\gamma}) = N_k$, and $\hat{z}_\pm^{N_k}$ is defined as above. Furthermore, for any periodic orbit $\hat{\gamma} \subset \hat{L}^a_{N_m}$ we have $N_R(\hat{\gamma}) = N_m = \bar{n}$.

Notice that this way we have formally computed the pulse number or resonant pulse number for any periodic orbit in $\hat{S}^a_0$ for which one of these numbers is defined. The orbits for which neither the pulse number nor the resonant pulse number is defined are exactly the periodic orbits $\hat{\gamma}_{N_k}$ appearing in (5.15), and the center itself.

The recursion defining the pulse sequence can be computed by hand up to a reasonable index, but of course it is best to implement this simple algorithm on a computer. The elements of $\{N_k\}$ obtained this way are shown in Fig. 18 as a function of the phase shift $\Delta\phi$ for $N_k < 100$. The horizontal line segments at each level N indicate that an infinity of N-pulse orbits exist for all values of the phase shift in the interval below that line. The diagram shows a fairly stable pulse distribution for low pulses and increasing sensitivity to small changes in the parameters for higher pulses. The structure and bifurcation of the layer sequence

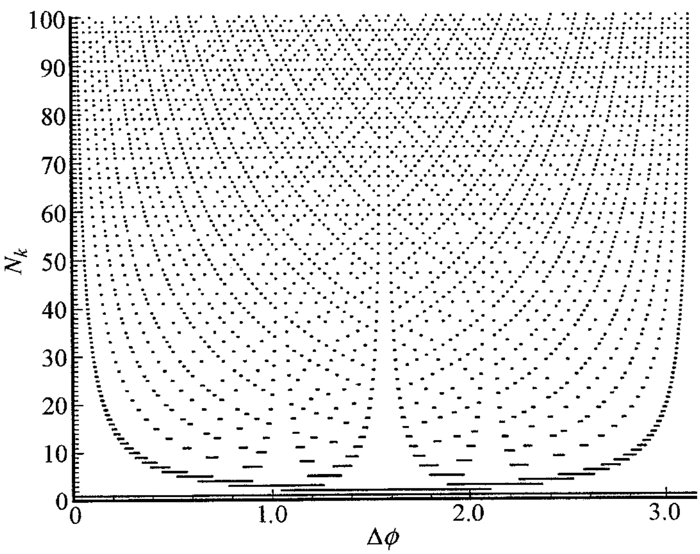

Fig. 18. The pulse sequence as a function of the phase shift.

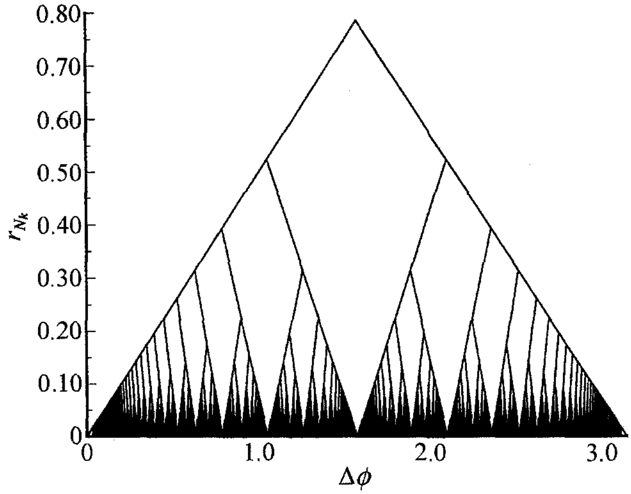

Fig. 19. The layer radius sequence as a function of the phase shift.

$\{\hat{L}^a_{N_k}\}$ is shown in Fig. 19, where we plot the corresponding inner angular radii

$$r_{N_k} = \min(|\pi - \phi^{N_k}_{-,1}|, |\pi - \phi^{N_k}_{-,2}|) \tag{5.17}$$

of the layers in the layer sequence. The diagram for the layer radii also has a secondary meaning: For fixed $\Delta\phi$, $\{r_{N_k}\}$ gives the angular distance of the take-off curves $B^{N_k}_{u,\varepsilon}$ from the nearest center on the manifold $\mathscr{A}_\varepsilon$ with an error of $\mathscr{O}(\sqrt{\varepsilon})$ (see Remark 3.6). This observation will be important in interpreting similar diagrams in Section 5.2.3.

The diagram in Fig. 19 has a self-similar structure as $\{N_k\}$ is allowed to go to infinity. Based on Theorem 3.4, each non-branching point in this *homoclinic tree* indicates the existence of a layer of slow periodic orbits on $\mathscr{A}_\varepsilon$ which have transverse N-pulse homoclinic orbits with the same N (the corresponding pulse numbers are shown in Fig. 18). At the branching points, one of the layers bifurcates to two new layers with different pulse numbers. The set of values of $\Delta\phi$ for which such a bifurcation occurs appears to admit a fractal structure in the interval $[0, \pi]$. These homoclinic bifurcations do not necessarily double or triple the value of N: Fig. 18 shows a variety of ways in which N can change. The homoclinic tree intersects the $\Delta\phi$ axis at the values of $\Delta\phi$ where condition (5.7) is violated for some n and l. These points indicate a degenerate layer of slow periodic orbits for which only the resonant pulse number is defined. The inner boundary of these layers degenerates into the center in $\hat{S}^a_0$, and for small N_R they usually occupy a substantial portion of $\hat{A}$.

5.1.4. Jump sequences. Consider an internal orbit $\hat{\gamma}_0^- \subset \hat{S}^a_0$ and suppose that $N(\hat{\gamma}_0^-) \equiv N > 1$ is defined. Then from (3.51) we obtain that for $k = 1, \ldots, N-1$, $\hat{\mathscr{R}}^k(\hat{\gamma}_0^-)$ does not intersect any orbit with reduced energy $\mathscr{H} \,|\, \hat{\gamma}_0^-$. In particular, it intersects neither $\hat{\gamma}_0^-$ nor the identical $\hat{\gamma}_0^{-*}$ in $\hat{S}_0^b$. Since $\hat{\mathscr{R}}$ preserves area and since all internal orbits encircled by $\hat{\gamma}_0^-$ and $\hat{\gamma}_0^{-*}$ have energies higher than $\hat{\mathscr{H}}\,|\,\hat{\gamma}_0^-$, we conclude that for $k = 1, \ldots, N-1$, $\hat{\mathscr{R}}^k(\hat{\gamma}_0^-)$ only intersects internal orbits with energies lower than $\hat{\mathscr{H}}\,|\,\hat{\gamma}_0^-$, i.e.,

$$\operatorname{sign}(\Delta^k \hat{\mathscr{H}}\,|\,\hat{\gamma}_0^-) = \operatorname{sign}(\hat{\mathscr{H}}\,|\,\hat{\mathscr{R}}^k(\hat{\gamma}_0^-) - \hat{\mathscr{H}}\,|\,\hat{\gamma}_0^-) = -1, \quad k = 1, \ldots, N-1.$$

Using this, (5.2), and the definition of the positive and negative sign sequences in (3.53) we obtain

$$\chi^+(\hat{\gamma}_0^-) = \{+1\}_{k=1}^N, \quad \chi^-(\hat{\gamma}_0^-) = \{-1\}_{k=1}^N. \tag{5.18}$$

According to (iii) of Theorem 3.4, this means that the multi-pulse orbits constructed above always stay near the same unperturbed homoclinic structure, i.e., their jump sequences are sign-preserving. The same argument shows that for $N = N_R$ the jump sequences are again sign-preserving.

5.1.5. Homoclinic orbits, heteroclinic orbits, and horseshoes. For any element N_k of the pulse sequence which satisfies the nonresonance condition (5.7), we can guarantee the existence of transverse N_k-pulse orbits doubly asymptotic to the manifold $\mathscr{A}_\varepsilon$. These orbits are homoclinic to a slow periodic solution if the approximate landing curve $\hat{z}_+^{N_k}$ computed in (5.16) intersects $\hat{S}_0^a$. In this case the transformation $\phi \mapsto \phi + \pi$ yields an identical slow periodic solution with an identical transverse N-pulse homoclinic orbit. If, instead, $\hat{z}_+^{N_k}$ intersects $\hat{S}_0^b$, then we deduce the existence of two transverse N_k-pulse heteroclinic orbits connecting slow periodic orbits (one for each jump sequence). Again, the discrete symmetry of the full system implies the existence of another pair of similar heteroclinic connections between the two slow periodic orbits, so that the two pairs form two transverse heteroclinic cycles. Hence, by Theorem 3.4 we always obtain horseshoes with their associated chaotic dynamics on the energy surfaces containing the N_k-pulse orbits, independently of the location of $\hat{z}_+^{N_k}$. Since, as mentioned in Section 5.1.3, the pulse number of the separatrices forming $\partial\hat{S}_0^a$ is 1, Theorem 3.4 also implies the existence of either transverse 1-pulse orbits homoclinic to the two saddle-saddle fixed points, or transverse 1-pulse heteroclinic cycles between these two equilibria. Such structures do not seem to admit horseshoes in the case of resonance bands (see the example in HALLER & WIGGINS [19]). We now summarize our main results for the forced beam model in the following theorem.

Theorem 5.1. *For some fixed value of the parameters* (b, s, Γ) *consider the pulse sequence defined in* (5.13) *and plotted as a function of* $\Delta\phi$ *in Fig. 18. Then for any element* N_k *of this sequence satisfying* (5.7) *there exists* $\varepsilon_0(\mu, N_k) > 0$ *such that for* $0 < \varepsilon < \varepsilon_0(N_k)$,

(i) *System* $(1.1)_{d=0}$ *has an infinite number of transverse* N_k*-pulse orbits homoclinic to the manifold* $\mathscr{A}_\varepsilon$. *These orbits are homoclinic to slow periodic* *solutions in the resonance band* $\mathcal{P}_{\sqrt{\varepsilon}}$ *if* $\hat{z}_+^{N_k} \cap \hat{S}_0^b = \emptyset$, *or form heteroclinic cycles between slow periodic orbits if* $\hat{z}_+^{N_k} \cap \hat{S}_0^a = \emptyset$ *(see* (5.16)). *Accordingly, there exist Smale horseshoes on the energy levels containing these orbits. Each such slow periodic orbit in these level sets has in fact two transverse* N_k*-pulse homoclinic orbits or heteroclinic cycles with the jump sequence* $+1, +1, \ldots$ *and two with the jump sequence* $-1, -1, \ldots$.

(ii) *The slow periodic orbits with transverse* N_k*-pulse orbits form two smooth layers on* $\mathcal{A}_\varepsilon$ *which are* $(\sqrt{\varepsilon}, C^1)$*-close to* $g_\varepsilon \circ b_\varepsilon^{-1}(\hat{L}_{N_k}^a)$ *and* $g_\varepsilon \circ b_\varepsilon^{-1}(\hat{L}_{N_k}^b)$, *respectively.*

(iii) *For* $N_k = 1$ *there also exist either eight transverse* 1*-pulse transverse homoclinic orbits to, or four transverse heteroclinic cycles between, the two saddle-saddle-type equilibria on the manifold* $\mathcal{A}_\varepsilon$.

If N_k *does not satisfy condition* (5.7), *then these statements still hold with the exception of transversality and the existence of Smale horseshoes.*

Proof. The statements follow from our earlier observations. For the number of N_k-pulse orbits for individual slow orbits, it is enough to note that if a periodic orbit in $\hat{S}_0^a$ intersects $\hat{Z}_-^n$ transversally, then the intersection contains at least two distinct points. Furthermore, the separatrices of the reduced Hamiltonian intersect both components of $\hat{Z}_-^n$ transversally, which proves statement (iii). □

We remark that the statement (iii) of this theorem establishes the existence of single-pulse connections doubly asymptotic to two unstable nonlinear normal modes in the beam model. More importantly, from the statement (i) we obtain the existence of transverse orbits with arbitrarily high pulses which connect unstable quasiperiodic oscillations near two other nonlinear normal modes.

To illustrate the statements of Theorem 5.1 numerically, we select the parameter values $b = 1.0$, $s = 7.0$, $\Gamma = 1.0$. In this case the resonant circle $\mathcal{C}_r$ is located at $I_r = 0.8319$ and the phase shift in (5.4) is $\Delta\phi = 1.3664$. As one can verify from the pulse diagram in Fig. 18, for this value of the phase shift the first four elements of the pulse sequence are $N_1 = 1$, $N_2 = 2$, $N_3 = 7$, and $N_4 = 16$. The corresponding inner angular radii for the first four elements of the layer sequence in (5.14) are computed to be $r_1 = 0.6832$, $r_2 = 0.2044$, $r_7 = 0.0701$, and $r_6 = 0.0642$ (see also (5.17)). From the magnitude of r_2 and $2\Delta\phi$, it follows that the zero set $\hat{Z}_+^2$ intersects $\hat{S}_0^b$. Hence, based on (i), (ii) of Theorem 5.1, there exist two smooth layers of slow periodic orbits on $\mathcal{A}_\varepsilon$, $L_{2,\varepsilon}^a$ and $L_{2,\varepsilon}^b$, such that each periodic orbit in $L_{2,\varepsilon}^a$ is connected through two transverse 2-pulse heteroclinic cycles to a periodic orbit in $L_{2,\varepsilon}^b$. We select two periodic orbits $\hat{\gamma}_0^-$ and $\hat{\gamma}_0^+$ of $\hat{\mathcal{H}}$, as shown in the upper right-hand corner of Fig. 20. The figure also shows the location of the zero sets $\hat{Z}_-^2$ and $\hat{Z}_+^2$ in $\hat{A}$. We then locate two slow periodic orbits on $\mathcal{A}_\varepsilon$, γ_ε^- and γ_ε^+, which are $(\sqrt{\varepsilon}, C^1)$-close to $g_\varepsilon \circ b_\varepsilon^{-1}(\hat{\gamma}_0^-)$ and $g_\varepsilon \circ b_\varepsilon^{-1}(\hat{\gamma}_0^+)$, respectively, and so they must fall in $L_{2,\varepsilon}^a$ and $L_{2,\varepsilon}^b$, respectively. We iterate the components of the unstable manifold of γ_ε^- and the local stable manifold of γ_ε^+, which lie near the unperturbed homoclinic manifold W_0^+. The results are projected on the (x_2, η, ϕ)-coordinate space. As Fig. 20 shows, the two invariant manifolds do intersect in a fashion

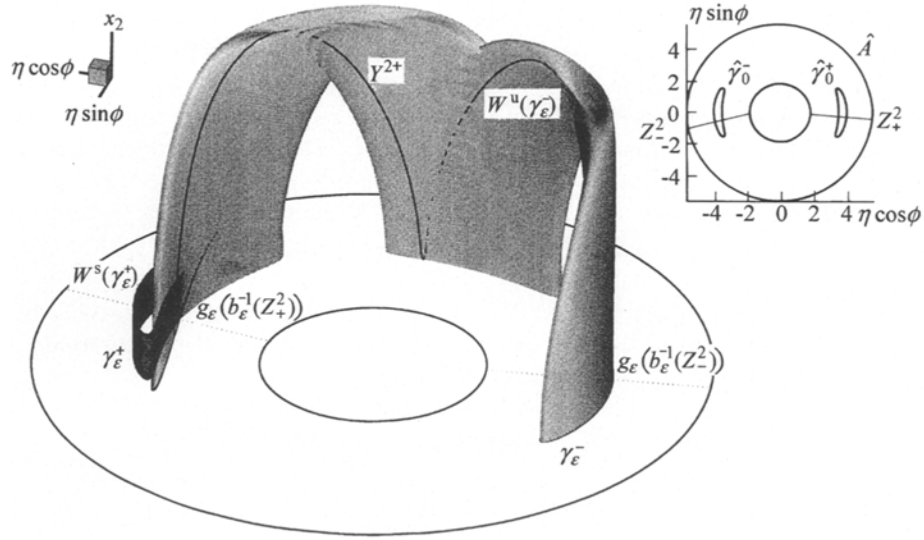

Fig. 20. The intersection of invariant manifolds ($\varepsilon = 10^{-4}$, step size $= 5 \times 10^{-2}$, integration time $= 10.5$).

predicted by Theorem 5.1, giving rise to two transverse double-pulse heteroclinic orbits. By the symmetry under $\phi \mapsto \phi + \pi$, this fact implies the existence of another similar heteroclinic orbit completing the two heteroclinic cycles. The other discrete symmetry $x \mapsto -x$ of the system implies the existence of two more symmetric cycles. This figure also shows the shadowing set Y_j^2 with $j = \{+1, +1\}$ for one of the heteroclinic orbits (see Definition 3.2). We finally note that the transverse intersection of the two invariant manifolds indicated by the projection is real, since $D_{x_1} H \neq 0$ on a fixed U_δ tube around $\mathscr{A}_\varepsilon$. Hence the energy surface is locally a graph over the (x_2, η, ϕ) variables.

5.2. *The forced-damped beam* $(d > 0)$

In this section we study the multi-pulse behavior in system (1.2) including the effect of damping. Using the general form (1.2) we find that the dissipative terms for the beam equation (1.1) are

$$g_{x_1} = -dx_1, \quad g_{x_2} = -dx_2, \quad g_I = -2dI, \quad g_\phi \equiv 0. \tag{5.19}$$

Before proceeding with the application of the results of Section 4, we want to verify the two major hypothesis of that section. From (5.19) we obtain by direct calculation that

$$D_I g_I(\bar{x}^0(I_r), I_r, \phi; 0) + D_\phi g_\phi(\bar{x}^0(I_r), I_r, \phi; 0) = -\frac{d(b+s)}{2\delta} < 0,$$

where we used (5.3) and the fact that $d > 0$. Therefore, hypothesis (H4) in Section 4.3 is satisfied. To verify hypothesis (H5) of the same section, we use (5.1) and (5.19) to obtain

$$\langle DH_0, g\rangle|_{I=I_r} = 2d[(b+2x_2^2)(x_1^2+x_2^2) - I_r(2x_2^2+b+s+2\delta I_r)]. \quad (5.20)$$

For any two solutions $y_0^+(t, I_r, \phi^+0)$ and $y_0^-(t, I_r, \phi^-0)$ with the properties described in (H5), one can select $\phi_0 = \phi_0^+ = \phi_0^-$. Then, by the discrete symmetry of system $(1.1)_{\varepsilon=0}$ under $x \mapsto -x$, we can choose the initial time $t = t_0$ such that

$$x_0^+(t, I_r, \phi_0) = -x_0^-(t, I_r, \phi_0).$$

Since from (5.20) we see that $\langle DH_0, g\rangle|_{I=I_r}$ is quadratic in x, this last relation implies that condition (H5) holds for our example.

5.2.1. The reduced dynamics. As we have seen in Section 4.2, the first step in the analysis of dissipative perturbations is to understand the phase portrait of the system $(4.26)_{\varepsilon=0}$. Direct substitution into (4.26) shows that for the forced damped beam the dissipative reduced system is of the form

$$\begin{aligned}\dot{\eta} &= \frac{b+s}{\delta}(\Gamma \sin 2\phi + d) - \sqrt{\varepsilon}2d\eta,\\ \dot{\phi} &= -2\delta\eta. \end{aligned}\qquad (5.21)$$

Setting $\varepsilon = 0$ we obtain the locally Hamiltonian part of this system, which on the set $\hat{A}_D$ (defined in (4.27)) derives from the Hamiltonian

$$\hat{\mathscr{H}}_D(v;\mu) = -\delta\eta^2 + \Gamma\frac{b+s}{2\delta}\cos 2v + d\frac{b+s}{\delta}v. \qquad (5.22)$$

Here $\mu = (b, s, \Gamma, d)$ is the vector of system parameters. For $d/\Gamma < 1$, this Hamiltonian generates the phase portrait of a pendulum subject to a constant torque in the domains $\phi \in [\frac{\pi}{2}, \frac{3\pi}{2}]$ and $\phi \in [\frac{3\pi}{2}, \frac{5\pi}{2}]$ (see Fig. 21). There are two centers at $\hat{c}_a(\zeta) = (0, \phi_c^a(\zeta))$ and $\hat{c}_b(\zeta) = (0, \phi_c^b(\zeta))$ with

$$\phi_c^a(\zeta) = \pi + \tfrac{1}{2}\sin^{-1}\zeta, \quad \phi_c^b(\zeta) = 2\pi + \tfrac{1}{2}\sin\zeta, \quad \zeta = \frac{d}{\Gamma}. \qquad (5.23)$$

There are also two saddles $\hat{s}_a(\zeta) = (0, \phi_s^a(\zeta))$ and $\hat{s}_b(\zeta) = (0, \phi_s^b(\zeta))$, with single homoclinic loops at

$$\phi_s^a(\zeta) = \tfrac{3\pi}{2} - \tfrac{1}{2}\sin^{-1}\zeta, \quad \phi_s^b(\zeta) = \tfrac{5\pi}{2} - \tfrac{1}{2}\sin\zeta. \qquad (5.24)$$

By analogy with the previous sections, we define the two sets $\hat{S}_0^a$ and $\hat{S}_0^b$ to be the open regions bounded by the two homoclinic loops (see Fig. 21). Again, the symmetry of the flow on $\hat{A}$ makes it possible to restrict the calculations to the subset $[-\eta_0, \eta_0] \times [\frac{\pi}{2}, \frac{3\pi}{2}]$ of the annulus.

5.2.2. Energy-difference functions and their zeros. We see from (5.19) that the function g_I does not depend on the variable ϕ, so we can use the form (4.39) of

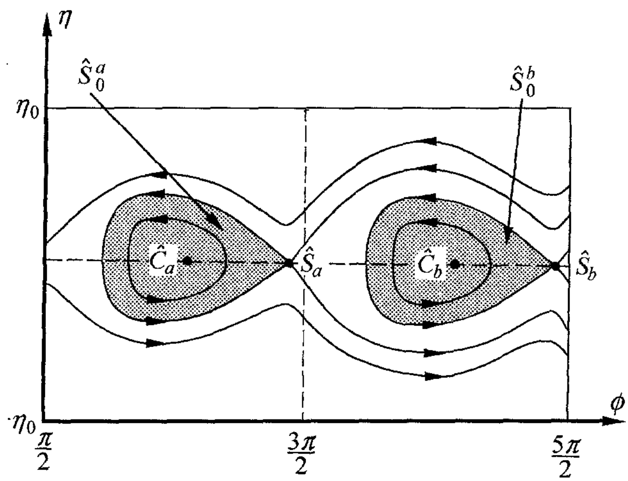

Fig. 21. The phase portrait of the reduced system $(5.21)_{\varepsilon=0}$.

$\Delta^n \hat{\mathscr{H}}_D$. The first term in that expression is just $\Delta^n \hat{\mathscr{H}}$, which we computed already in (5.6). Using (5.2) and (5.19), we can write the second term in (4.39) as

$$n\sigma \int_{A_r} V_x \cdot g_x(x, I_r, \phi; 0)\, dx_1\, dx_2 = 2nd \int_{A_r} dx_1\, dx_2. \tag{5.25}$$

To evaluate this expression we need to compute the area of the region A_r enclosed by the unperturbed homoclinic orbit $x^{h+}(t, I_r)$ of $(1.1)^x_{\varepsilon=0}$. This area is preserved under symplectic changes of variables, so, following FENG & SETHNA [14], we introduce the new variables (P, Q) by letting

$$x_1 = \sqrt{2P}\sin Q, \quad x_2 = \sqrt{2P}\cos Q,$$

and evaluate the corresponding area using these new coordinates. As is shown by FENG & SETHNA [14], in the (Q, P) variables the homoclinic orbits of $(1.1)^x_{\varepsilon=0}$ become heteroclinic orbits of the form

$$P = I_r - \frac{b}{1 + \cos 2Q} = I_r - \frac{b}{2\cos^2 Q}$$

connecting the two equilibria $(Q, P) = (-\Delta\phi/2, 0)$ and $(Q, P) = (\Delta\phi/2, 0)$. Therefore, we can compute (5.25) to obtain

$$n\sigma \int_{A_r} V_x \cdot g_x(x, I_r, \phi; 0)\, dx_1\, dx_2 = 2nd \int_{-(\Delta\phi)/2}^{\Delta\phi/2} I_r - \frac{b}{2\cos^2 Q}\, dQ$$

$$= 2ndI_r\Delta\phi - 2ndb\tan\frac{\Delta\phi}{2}.$$

When substituted into (4.39), this expression together with $ng_I(I_r;0)\Delta\phi = -2ndI_r\Delta\phi$ gives the dissipative nth order energy-difference function

$$\Delta^n \hat{\mathscr{H}}_D(\phi;\mu) = \frac{b+s}{2\delta}\Gamma[\cos 2(\phi + n\Delta\phi) - \cos 2\phi] + 2ndb\tan\frac{\Delta\phi}{2}. \quad (5.26)$$

Using the identity for the difference of the cosines of two angles and assuming that

$$|\zeta| < \frac{(b+s)}{nb\delta}\left|\cos\frac{n\Delta\phi}{2}\right|, \quad (5.27)$$

with the dissipation factor ζ defined in (5.23), we find the transverse zeros of $\Delta^n\hat{\mathscr{H}}(\phi;\mu)$ in the interval $[\frac{\pi}{2},\frac{3\pi}{2}]$:

$$\begin{aligned} \phi^n_{-,1} &= \frac{3\pi}{2} - \left[\frac{n\Delta\phi}{2} + \frac{1}{2}\sin^{-1}\frac{\zeta nb}{2I_r\cos\frac{n\Delta\phi}{2}}\right] \bmod \pi, \\ \phi^n_{-,2} &= \frac{3\pi}{2} - \left[\frac{\pi}{2} + \frac{n\Delta\phi}{2} - \frac{1}{2}\sin^{-1}\frac{\zeta nb}{2I_r\cos\frac{n\Delta\phi}{2}}\right] \bmod \pi. \end{aligned} \quad (5.28)$$

We again introduce the two angles

$$\phi^n_{+,1} = [\phi^n_{-,1} + n\Delta\phi] \bmod 2\pi, \qquad \phi^n_{+,2} = [\phi^n_{-,2} + n\Delta\phi] \bmod 2\pi, \quad (5.29)$$

and use them to obtain the zero sets from (4.30) in the form

$$\begin{aligned} \hat{V}^n_- = \hat{Z}^n_- &= \{(\eta,\phi)\in \hat{S}^a_0 \mid \phi\in\{\phi^n_{-,1},\phi^n_{-,2}\}\}, \quad n \geqq 1, \\ \hat{V}^n_+ = \hat{Z}^n_+ &= \{(\eta,\phi)\in \hat{A} \mid \phi\in\{\phi^n_{+,1},\phi^n_{+,2}\}\}, \quad n \geqq 1. \end{aligned} \quad (5.30)$$

5.2.3. Pulse numbers. First we note that from (5.27) we obtain the following upper bound on the pulse numbers:

$$n < \frac{b+s}{|\zeta| b\delta}, \quad (5.31)$$

which shows that even for arbitrarily small dissipation, the infinite homoclinic tree found in Section 5.1.3 breaks into a finite tree.

Following Section 5.1.3, we easily see that the pulse number of any internal orbit outside $\hat{S}^a_0 \cup \hat{S}^b_0$ is 1. For the orbits inside $\hat{S}^a_0 \cup \hat{S}^b_0$ we can carry out the same construction as in Section 5.1.3 to classify the periodic orbits based on their pulse numbers. Namely, we can again define the energy sequence

$$\hat{h}_0 = \hat{\mathscr{H}}_D(0,\phi^a_s;\mu), \quad \hat{h}_n = \max(\hat{\mathscr{H}}_D(0,\phi^n_{-,1};\mu), \hat{\mathscr{H}}_D(0,\phi^n_{-,2};\mu)). \quad (5.32)$$

Then the definitions of $\{\hat{A}^a_n\}$, the pulse sequence $\{N_k\}$, and the layer sequences $\{\hat{L}^a_{N_k}\}$ and $\{\hat{L}^b_{N_k}\}$ are the same as in the undamped case (see Figs. 22a, b). However, all these sequences are now finite by (5.31). As earlier, we obtain that for any periodic orbit $\hat{\gamma} \subset \hat{L}^a_{N_k} \cup \hat{L}^b_{N_k}$, the pulse number is $N(\hat{\gamma}) = N_k$.

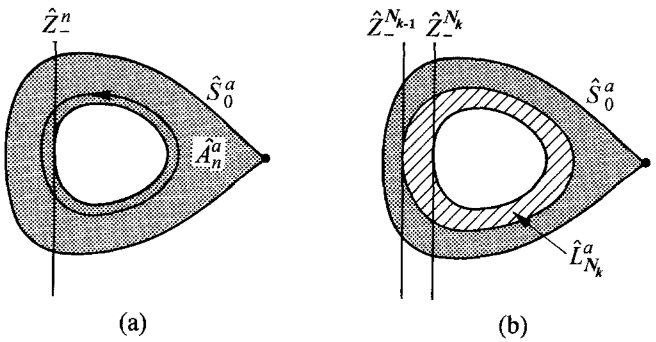

Fig. 22. The construction of the layer sequence for $(5.21)_{\varepsilon=0}$.

The result of the recursive construction of pulse numbers and layers can be plotted in the same way as in Section 5.1.3. For some values of the dissipation factor ζ we show the corresponding pulse diagrams and layer radius diagrams in Figs. 23a, b (we fixed $\frac{b}{2I_r} = 1$). Here the layer radii are defined as

$$r_{N_k} = \min(|\phi_c^a - \phi_{-,1}^{N_k}|, |\phi_c^a - \phi_{-,2}^{N_k}|). \tag{5.33}$$

As we might expect, these diagrams show a gradual break-up of the homoclinic tree in the intermediate system as the dissipation is increased relative to the forcing. It is interesting to note that the number of low-pulse orbits temporarily increases (see the case $\zeta = 10^{-4}$), then again decreases with increasing ζ. Finally, at $\zeta = 1$ all multi-pulse orbits disappear. Since N_R is not defined, the resonant "tips" of the homoclinic tree must necessarily disappear for nonzero ζ. One can indeed notice this for larger values of ζ in the diagrams, together with the formation of cusps near the resonant tips. We finally recall that all these diagrams refer to multi-pulse behavior in the locally Hamiltonian intermediate system, but they also have a direct meaning for the full dissipative system (1.1). We discuss this in Section 5.2.5.

5.2.4. Jump sequences. The argument we gave in Section 5.1.4 is not valid here and there exist N-pulse orbits with jump sequences that do not preserve sign. Here we do not deal with the classification of all the possible jump sequences.

5.2.5. Homoclinic and heteroclinic orbits. Since the pulse numbers of internal orbits outside $\hat{S}_0^a \cup \hat{S}_0^b$ are 1, all multi-pulse orbits in the intermediate system (1.1) are necessarily asymptotic to slow periodic orbits in backward time. However, their forward asymptotics can be quite different. As we discussed in Section 4.2.3, the asymptotics of multi-pulse connections in the full dissipative system (1.1) can be inferred from the dissipative reduced system (4.26). It is easy to verify that the locations of the equilibria for this system are independent of ε. However, while the saddles remain saddles, the centers turn into sinks for $\varepsilon > 0$ (see Fig. 24). Accordingly, some types of multi-pulse orbits for the dissipative system (1.1) are shown in Fig. 25. All these connections exist on open sets in the parameter space. For brevity, we do not give a full classification of the possibilities as the parameters are varied; see HALLER & WIGGINS [22] for this classification in a similar problem. However, without their detailed asymptotics, we have obtained the existence of multi-pulse orbits with pulse numbers belonging to the pulse sequence constructed above (see Theorem 4.4). The pulse diagrams shown in Figs. 23a, b show the distribution of pulses as a function of the phase shift. The layer radius diagrams now do not refer to layers of periodic orbits, but their secondary meaning remains valid for the full dissipative system (1.1): They show the approximate distances of the take-off curves of multi-pulse orbits from the sinks on $\mathscr{A}_\varepsilon$ (see the discussion after (5.17) and the formula (5.33)). We summarize these facts in the following theorem.

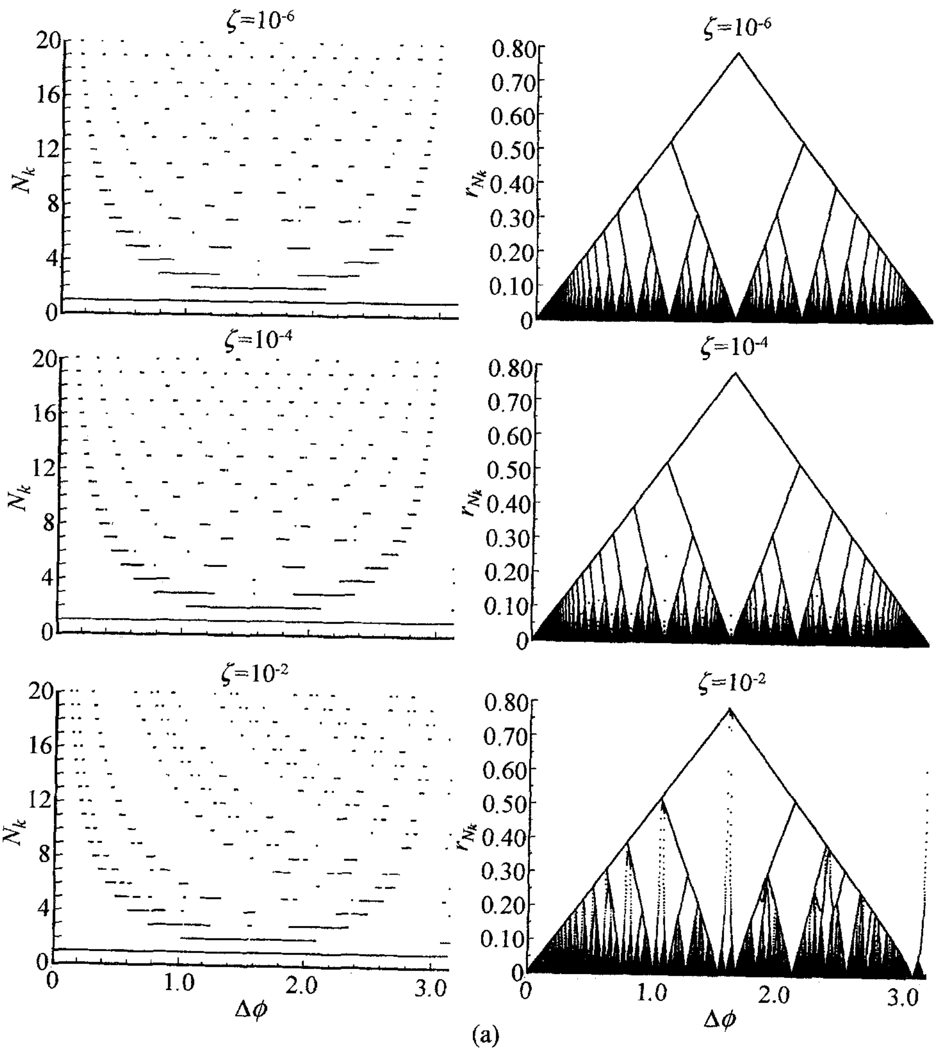

Fig. 23a

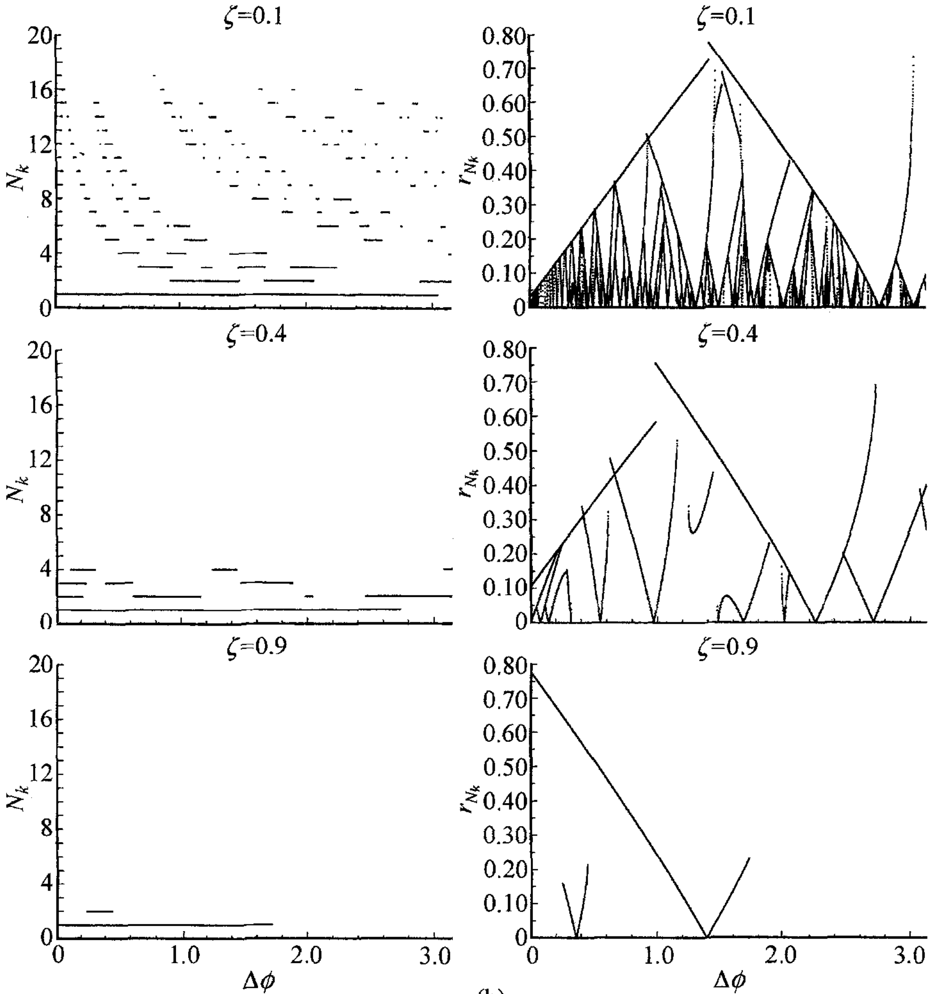

(b)

Fig. 23a, b. The pulse sequence and the layer radius sequence as a function of the phase shift in the dissipative case ($b/I_r = 1$).

Theorem 5.2. *For some fixed value of the parameter* $\mu = (b, s, \Gamma, d)$, *consider the pulse sequence defined in Section 5.2.3 and plotted as a function of* $\Delta\phi$ *in Figs. 23a, b for some values of* $\zeta = d/\Gamma$. *Then, for any element* N_k *of this sequence and for any small* $\delta_0 > 0$, *there exists* $\varepsilon_0(\mu, N_k, \delta_0) > 0$ *such that for* $0 < \varepsilon < \varepsilon_0(\mu, N_k, \delta_0)$:

(i) *The system* (1.1) *has an infinite number of structurally stable* N_k*-pulse orbits homoclinic to* $\mathscr{A}_\varepsilon$.

(ii) *The distance of the* N_k*-take-off curve* $B_{\mathrm{u},\varepsilon}^{N_k}$ *from the nearest sink on* $\mathscr{A}_\varepsilon$ *is* $\mathcal{O}(\delta_0)$*-close to* r_{N_k}, *where* r_{N_k} *is defined in* (5.33), *and plotted in Figs. 23a, b.*

Proof. The theorem is a direct application of Theorem 4.4. □

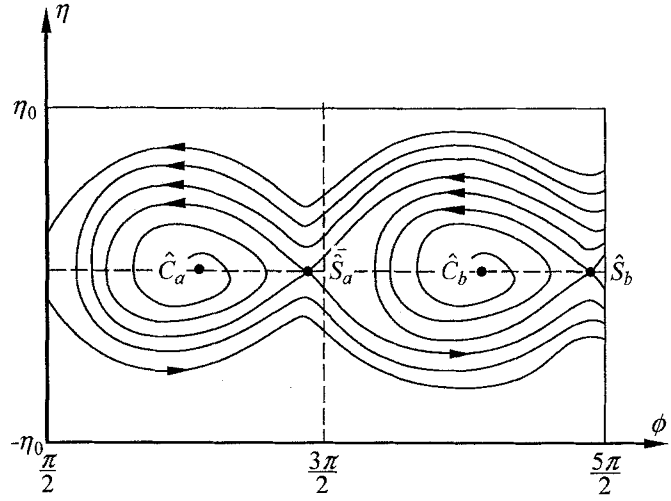

Fig. 24. The phase portrait of the dissipative reduced system (5.21).

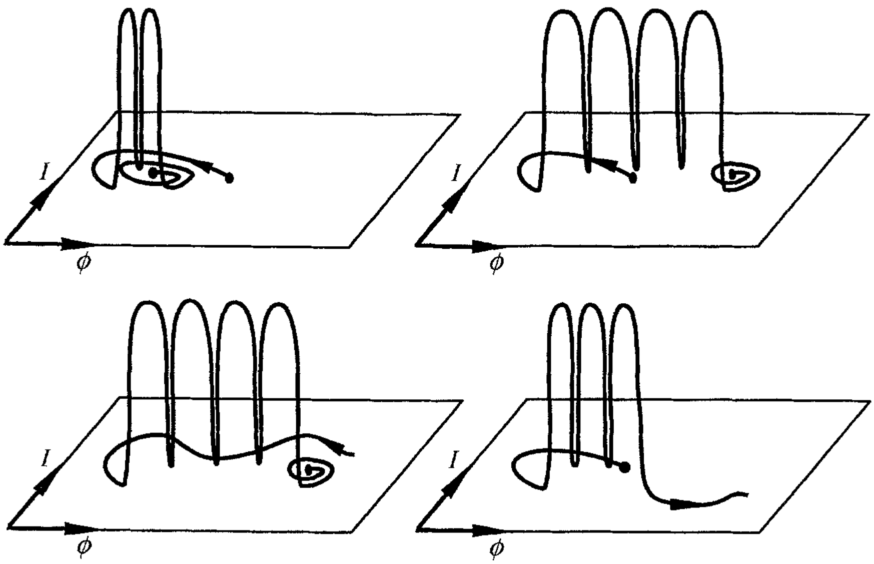

Fig. 25. Structurally stable multi-pulse connections in the dissipative system (1.1).

5.2.6. N-pulse Šilnikov orbits and Šilnikov cycles. In this last part of our study of the forced-beam model, we prove the existence of chaotic dynamics for nonzero damping. This dynamics is the result of the presence of multi-pulse Šilnikov orbits or Šilnikov cycles in the phase space, and exists on an open neighborhood of a complicated codimension-one set of the parameter space (see below). We show the existence of Šilnikov orbits and cycles by applying Theorem 4.5 to the sinks of the reduced system (5.21).

To simplify the calculations we pass to the parameter $\bar{\mu} = (b, s, \zeta) \in \mathbb{R}^3$ and assume that $0 < \zeta < 1$ (which means that $\Gamma > 0$). Codimension-one sets in the $\bar{\mu}$-space correspond to codimension-one sets in the full parameter space of $\mu = (b, s, \Gamma, d)$. We note that for $\varepsilon = 0$ the sinks of (5.21) change into the centers of $(5.21)_{\varepsilon=0}$; hence they satisfy assumption (A1) of Theorem 4.5. To satisfy assumption (A2) of the same theorem, we must find values $(\zeta, \Delta\phi, N)$ for which the center

$$\hat{c}_a(\zeta) = (0, \pi + \tfrac{1}{2}\sin^{-1}\zeta)$$

falls in the zero set $\hat{Z}^N_-$ defined in (5.30). This means finding solutions of

$$\Delta^N \hat{\mathscr{H}}_D(\phi_{\hat{c}_a}(\zeta); \mu) = 0,$$

or, equivalently, of

$$\cos 2(\pi + \tfrac{1}{2}\sin^{-1}\zeta + N\Delta\phi) - \cos(\sin^{-1}\zeta) + \frac{2b\zeta N}{I_r}\tan\frac{\Delta\phi}{2} = 0.$$

After some elementary algebra, this equation yields the relation

$$\sqrt{1-\zeta^2}(1 - \cos 2N\Delta\phi) = \zeta\left(\frac{2bN}{I_r}\tan\frac{\Delta\phi}{2} - \sin 2N\Delta\phi\right), \tag{5.34}$$

which gives

$$\zeta = \frac{1 - \cos 2N\Delta\phi}{\sqrt{(1 - \cos 2N\Delta\phi)\bigcup\left(\frac{2b}{I_r}\tan\frac{\Delta\phi}{2} - \sin 2N\Delta\phi\right)^2}}. \tag{5.35}$$

For any positive integer N this last expression defines a surface in the $\bar{\mu}$-space. However, it is only meaningful for positive ζ values, i.e., for

$$\Delta\phi \neq \frac{k\pi}{N}, \quad k \in \mathbb{Z}^+. \tag{5.36}$$

To show the structure of the set defined by (5.35), we fix the parameter ratio $b/I_r = 1$, and plot ζ as a function of $\Delta\phi$ for $N = 1, \ldots, 50$. Two intersecting curves on this plot show a bifurcation of Šilnikov orbits, and any intersection of the curves with the $\Delta\phi$-axis shows a value of $\Delta\phi$ for which the condition (5.36) is violated. In order to verify assumption (A3) of Theorem 4.5, we shall show that

$$D_\zeta\left[\cos 2\left(\pi + \frac{1}{2}\sin^{-1}\zeta + N\Delta\phi\right) - \cos(\sin^{-1}\zeta) + \frac{2b\zeta N}{I_r}\tan\frac{\Delta\phi}{2}\right] \neq 0, \tag{5.37}$$

whenever (5.35) and (5.36) hold. Carrying out the differentiations in this expression, we obtain that (5.37) fails to be satisfied when

$$\sqrt{1-\zeta^2}\left(\sin 2N\Delta\phi - \frac{2bN}{I_r}\tan\frac{\Delta\phi}{2}\right) = \zeta(1 - \cos 2N\Delta\phi). \tag{5.38}$$

But it is easy to see that, under condition (5.36), the equations (5.34) and (5.38) cannot hold simultaneously. Therefore, assumption (A3) of Theorem 4.5 is satisfied whenever $0 < \zeta < 1$. Hence, for any integer N and on a codimension-one set near that described by (5.35) and (5.36), we obtain the existence of N-pulse orbits that are backward asymptotic to a saddle-sink equilibrium. We now have to give conditions for the slow orbit γ_ε^+ in (i) of Theorem 4.5 to fall in the domain of attraction of a sink on $\mathscr{A}_\varepsilon$. For this purpose we introduce the angle

$$\phi_*^N(\bar{\mu}) = \phi_s^a(\zeta) - \pi + [\phi_c^a(\zeta) + N\,\Delta\phi - (\phi_s^a(\zeta) - \pi)] \bmod \pi, \tag{5.39}$$

which gives the approximate location of the projection of the landing points q_ε in the interval $[\frac{\pi}{2}, \frac{3\pi}{2}]$. We require that

$$\hat{\mathscr{H}}_D(0, \phi_*^N(\bar{\mu}); \mu) > \hat{\mathscr{H}}_D(0, \phi_s^a(\zeta); \mu),$$

or, equivalently, that

$$\cos 2\phi_*^N(\bar{\mu}) - \cos \phi_s^a(\zeta) > 2\zeta(\phi_s^a(\zeta) - \phi_*^N(\bar{\mu})), \tag{5.40}$$

to ensure that the projected landing points fall in the homoclinic loop contained in the subset $[-\eta_0, \eta_0] \times [\frac{\pi}{2}, \frac{3\pi}{2}]$ of the annulus. Clearly, by the relation of $(5.21)_{\varepsilon=0}$ to (5.21), this implies that the projection of q_ε falls in the domain of attraction of one of the sinks for $\varepsilon > 0$ sufficiently small. The calculations in this section lead to the following theorem.

Theorem 5.3. *For any integer $N \geqq 1$ there exists a positive number $\varepsilon_0(N) > 0$ and a finite union C_N of codimension-one surfaces in the $(b, s, \Gamma, d, \varepsilon)$ parameter space near the set satisfying $0 < \zeta < 1$, (5.35), and (5.40), such that for any $(b, s, \Gamma, d, \varepsilon) \in C_N$ and $0 < \varepsilon < \varepsilon_0(N)$ the following hold:*

(i) *If the integer*

$$Q = \mathrm{INT}\left(\frac{1}{2} + \frac{N\,\Delta\phi + \sin^{-1}\zeta}{\pi}\right)$$

is even, then each of the two saddle-focus-type equilibria contained in the manifold $\mathscr{A}_\varepsilon$ admits two Šilnikov-type homoclinic orbits. If Q is odd, then there exist two cycles of Šilnikov-type heteroclinic orbits connecting the two saddle-foci to each other. In both cases the N-pulse orbits form pairs which are symmetric with respect to the subspace $x = 0$.

(ii) *There exists an open set of parameter values containing C_N for which* (1.1) *admits Smale horseshoes in its dynamics. In the $(\Delta\phi, \zeta)$ parameter space, for $b = I_r$, the parameter values leading to horseshoes fall in an open neighborhood of the set plotted in Fig. 26.*

Proof. Based on our earlier observations, we only note that the integer

$$Q = \mathrm{INT}\left(\frac{\phi_c^a(\zeta) + N\,\Delta\phi - (\phi_s^a(\zeta) - \pi)}{\pi}\right)$$

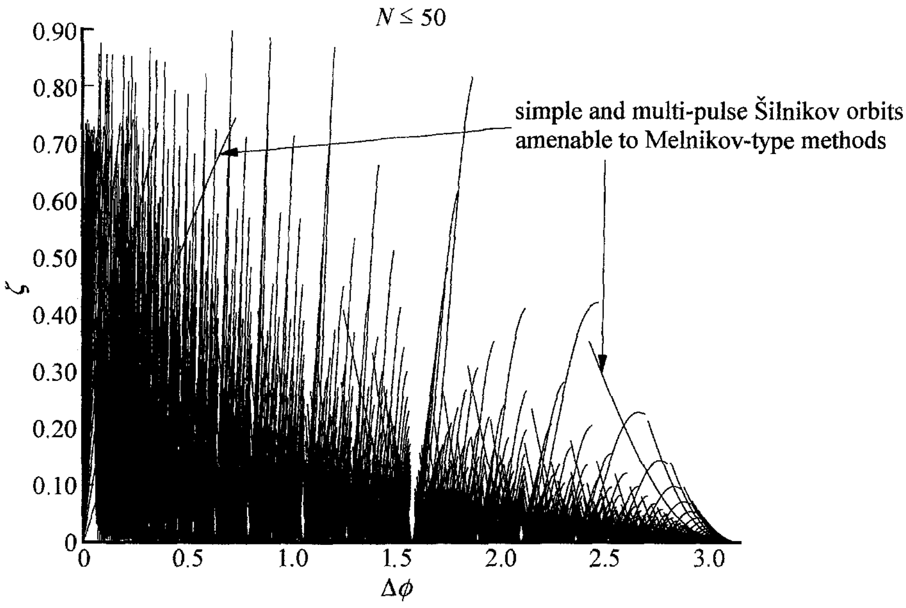

Fig. 26. The approximate parameter set for which single- and multi-pulse Šilnikov orbits or cycles exist ($2b/I_r = 0.5$).

is even if the projection of q_ε on the annulus $\hat{A}$ falls in $\hat{S}_0^a$, and is odd if this projection falls in $\hat{S}_0^b$. The existence of Šilnikov cycles follow from the symmetry of the system under $\phi \mapsto \phi + \pi$. The existence of a symmetric counterpart for each of the Šilnikov orbits follows from the symmetry under $x \mapsto -x$. The existence of horseshoes follows from the fact that the divergence of the right-hand side of the dissipative system (1.1) equals $-4d < 0$. Hence the real eigenvalues of the saddle-foci cannot be equal and the corresponding theorem of Šilnikov [40] applies (see also Wiggins [45]). □

In terms of the beam model, these results again indicate the existence of multi-pulse connections between two nonlinear normal modes of the forced beam. These motions have three different time scales: the fast pulses, the slower intermediate passages near the slow manifold and the final very slow approach to a saddle-focus.

In Fig. 26 we plot the parts of the curves in (5.35) which satisfy (5.40) for some $N \leqq 50$. As N increases, this "web" of curves becomes denser and denser near the two coordinate axes. The diagram indicates the two approximate curves of one-pulse Šilnikov orbits, which can also be obtained by applying the results of Kovačič & Wiggins [33]. The approximate parameter set for secondary multi-pulse Šilnikov orbits obtained from the results of Kaper & Kovačič [30] is also this single curve, since one needs the presence of single-pulse Šilnikov orbits for their methods to apply. Therefore, the energy-phase method finds horseshoes and predicts chaotic dynamics on a much larger set of parameter values than for other existing global perturbation methods.

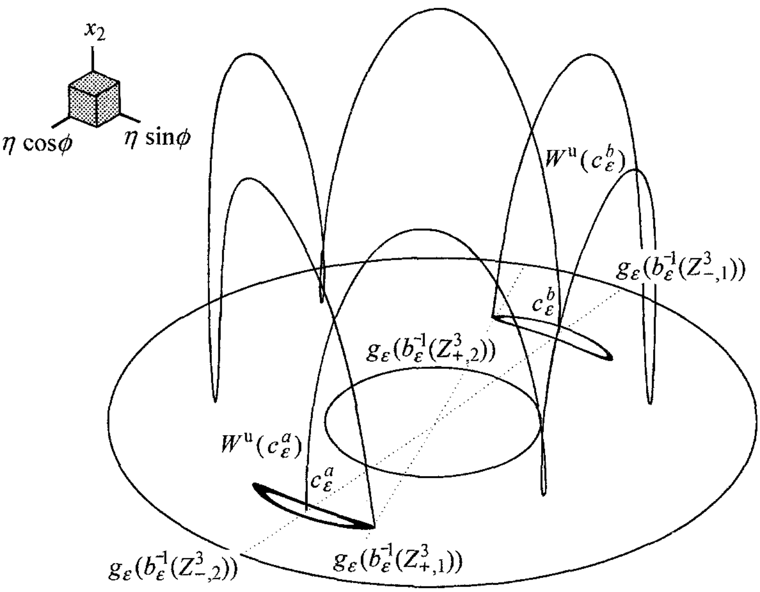

Fig. 27. Šilnikov-like 3-pulse cycle for the damped-forced beam model (step size $= 2 \times 10^{-5}$, integration time $= 40$).

Even if we knew the exact location of the codimension-one surface C_N, it would be a delicate matter to verify the existence of the codimension-one multi-pulse Šilnikov orbits and cycles numerically. After the Nth pulse it takes a time of order $\mathcal{O}(1/\sqrt{\varepsilon})$ for the Šilnikov-type orbits to reach the corresponding saddle-focus. During this long period of time the unstable eigenvalues of magnitude $\mathcal{O}(1)$ in the hyperbolic splitting along $\mathcal{A}_\varepsilon$ inevitably amplify any finite numerical error, and drive the solution away from the slow manifold to follow subsequent pulses. In fact, these numerically induced "bursts" occur in much shorter time scales, usually of the order $\mathcal{O}(1)$. This is exactly the difficulty one successively encounters in the iteration of multi-pulse orbits constructed by other methods (see Kaper & Kovačič [30]). For the orbits obtained by the energy-phase method, the numerical problem of long passage only occurs after the last pulse.

For a numerical illustration of Theorem 5.3, we select the parameter values $b = 1$, $s = 6$, $\Gamma = 1$, for which the value of the phase shift at $I = I_r = 0.7274$ is $\Delta\phi = 1.1866$. We select the pulse number $N = 3$, because the errors near the three near-saddle passages almost seem to cancel out for odd pulse numbers. Then (5.35) gives $\zeta = d = 6.8288 \times 10^{-2}$, and the statement (i) of Theorem 5.3 gives $Q = 2$; hence the corresponding nearby Šilnikov-type orbits form double-pulse heteroclinic cycles. We finally select $\varepsilon = 10^{-3}$ for the strength of the perturbation. To avoid the final artificial numerical burst, we adopt the rule: If the iterated orbit approaches the slow manifold within a distance less than 10ε, then we "freeze" the motion in the unstable x-direction and speed up the dynamics by a factor of $1/\sqrt{\varepsilon}$ in the directions tangent to the slow manifold. The unstable manifolds of the saddle-foci c_ε^a and c_ε^b computed in this way are shown in Fig. 27, where we again project the results in the coordinate space (x_2, η, ϕ). We also indicate the location of the two saddle-foci as well as the lift of the two components of the zero sets $\hat{Z}^3_\pm$ to the slow manifold through the map $g_\varepsilon \circ b_\varepsilon$. The minimal distances of the orbits from the slow manifold at the near-saddle passages are 51.06ε, 40.78ε, and $8.72\varepsilon < 10\varepsilon$. The sharp decrease in the passage distance after the third pulse is a good numerical indication of an actual nearby Šilnikov cycle, since numerical errors usually lead to increasing passage distances for typical trajectories. One can expect to follow the heteroclinic-like orbits for longer times by employing integration methods more involved than the ordinary four-point Runge–Kutta scheme, which we used mainly for illustration. Also, a more sophisticated shooting algorithm (e.g., the one in McLaughlin, Overman, Wiggins, & Xiong [35]) could be used to identify the exact location of the codimension-one surface C_N guaranteed by Theorem 5.3.

6. Conclusions

In this paper we have presented an analytical method which can be used to find families of multi-pulse orbits doubly asymptotic to slow manifolds in a class of two-degree-of-freedom Hamiltonian systems. While the various steps in the justification of the method involve long and subtle arguments, the result is a simple criterion, the energy-phase method, which is easy to use in practice. Indeed, solving for the zeros of the nth order energy-difference function for the purely Hamiltonian case usually involves elementary trigonometry, as opposed to the evaluation of improper integrals required by Melnikov-type methods. Even more importantly, for the case of Hamiltonian resonance bands, one can locate the zeros and identify their dependence on the parameters qualitatively by sketching the graph of the "potential part" of the reduced Hamiltonian $\hat{\mathscr{H}}$ or $\hat{\mathscr{H}}_D$, and by looking for isoenergetic level curves that are a distance $N\Delta\phi$ apart.

Most of the literature on multi-pulse orbits deals with the existence of orbits homoclinic to fixed points (see, e.g., Glendinning [18], Kokubu [32], Chow, Deng, & Fiedler [9], Mielke, Holmes, & O'Reilly [36], Kisaka, Kokubu, & Oka [31], Champneys & Toland [8] and the references therein). Similar methods have been used to establish the existence of multi-pulse orbits for certain semilinear parabolic partial differential equations, whose travelling wave solutions can be studied with ordinary differential equations (see, e.g., Evans, Fenichel, & Feroe [10], Hastings [24], Alexander & Jones [1], and the references therein). Multi-pulse orbits homoclinic to periodic solutions in the vicinity of a reversible saddle-center were recently obtained by Camassa [6] in the study of an atmospheric model system. Rom-Kedar [39] studied the creation of secondary orbits homoclinic to periodic solutions in a class of periodically forced planar Hamiltonian systems. Kaper & Kovačič [30] constructed multi-pulse orbits homoclinic to resonance bands near single-pulse orbits by using the Melnikov method and singular perturbation theory (see Sections 1.4 and 5.2.6 for a comparison with our results). In contrast to all these methods, the energy-phase method can be used to detect orbits homoclinic to a two-dimensional slow manifold, with the case of resonance bands being a specific application. Furthermore, our method does not require solving variational equations or verifying involved transversality conditions. As a result, one can obtain simple recursive formulas describing the structure of multi-pulse solutions and their bifurcations. Finally, as our damped-forced beam example shows (see Fig. 26), the energy-phase method detects complicated or chaotic dynamics on much larger parameter regions than other perturbation methods for simple or multi-pulse homoclinic orbits.

Applying our method to the forced-beam model (1.1) without damping, we obtained the homoclinic tree shown in Fig. 19. It is important to observe that this object is *universal* in the same sense as the pendulum-type equations are universal as first-order approximations for near-resonance dynamics (see, e.g., ARNOLD, KOZLOV, & NEISHTADT [4]). Hence, in other applications one typically obtains a finite union of smooth deformations of the structure we found for the forced inextensional beam. For example, in a two-mode model of the forced nonlinear Schrödinger equation one finds the same homoclinic tree shown in Fig. 19 over the interval $\Delta\phi \in [0, 2\pi]$ (see HALLER & WIGGINS [22]). We also note that by identifying the possible range of the phase shift in a given problem, one can construct the homoclinic tree without actually computing how $\Delta\phi$ depends on the system parameters.

Other applications of the energy-phase method involve those we listed in Section 1.3. An application to the study of partially slow manifolds (see Section 1.1) in three-degree-of-freedom Hamiltonian systems will appear in HALLER & WIGGINS [23]. There we also give extensions of the result of the present paper for unequal phase shifts and for heteroclinic unperturbed manifolds. Generalizations to higher-dimensional slow and partially slow manifolds along the lines of the present paper are also possible and will appear elsewhere.

Acknowledgment. This work was supported by an NSF Presidential Young Investigator Award and ONR Grant No. N00014-89-J-3023. We thank CHRIS JONES, TASSO KAPER, and SIU-KEI TIN for stimulating conversations and explanations of their results, and PHIL HOLMES for several very useful comments and suggestions. A part of this work was carried out while G. HALLER was a visiting member of the Courant Institute of Mathematical Sciences.

References

1. ALEXANDER, J. C. & JONES, C. K. R. T, Existence of asymptotically oscillatory triple pulses, *Z. Angew. Math. Phys.* **44** (1993) 189–200.
2. ARNOLD, V. I. & AVEZ, A., *Ergodic Theory of Dynamical Systems*, Benjamin-Cummings, Reading, Mass. (1968).
3. ARNOLD, V. I., *Mathematical Methods of Classical Mechanics*, Springer-Verlag, New York (1978).
4. ARNOLD, V. I., KOZLOV, V. V., & NEISHTADT, A. I., *Mathematical Aspects of Classical and Celestial Mechanics* in *Dynamical Systems III*, V. I. ARNOLD (ed.), Springer-Verlag, New York (1988).
5. BISHOP, A. R., FOREST, M. G., MCLAUGHLIN, D. W., & OVERMANN, E. A., A modal representation of chaotic attractors for the driven, damped pendulum chain, *Phys. Lett. A* **144** (1990) 17–25.
6. CAMASSA, R., On the geometry of an atmospheric slow manifold, to appear in *Physica D* (1994).

7. CASCON, A. & KOILLER, J., Bifurcations of mode equations: spin waves, *Physica D* **54** (1991) 98–124.
8. CHAMPNEYS, A. R. & TOLAND, J. F., Bifurcation of a plethora of multimodal homoclinic orbits for autonomous Hamiltonian systems, *Nonlinearity* **6** (1993) 665–721.
9. CHOW, S. N., DENG, B., & FIEDLER, B., Homoclinic bifurcations at resonant eigenvalues, *J. Dyn. Diff. Eqs.* **2** (1990) 177–244.
10. EVANS, J. W., FENICHEL, J. W., & FEROE, J. A., Double impulse solutions in nerve axon equations, *SIAM J. Appl. Math.* **42** (1982) 219–234.
11. FENG, Z. C. & LEAL, L. G., Symmetries of the amplitude equations of an inextensional beam with internal resonance, submitted to *J. Appl. Mech.* (1993).
12. FENG, Z. C. & SETHNA, P. R., Symmetry breaking bifurcations in resonant surface waves, *J. Fluid Mech.* **199** (1989) 495–518.
13. FENG, Z. C. & SETHNA, P. R., Global bifurcation and chaos in parametrically forced systems with one-one resonance, *Dynamics and Stability of Systems* **5** (1990) 201–225.
14. FENG, Z. C. & SETHNA, P. R., Global bifurcations in the motion of parametrically excited thin plates, *Nonlin. Dyn.* **4** (1993) 389–408.
15. FENG, Z. C. & WIGGINS, S., On the existence of chaos in a class of two-degree-of-freedom, damped, strongly parametrically forced mechanical systems with broken $O(2)$ symmetry, *Z. Angew. Math. Phys.* **44** (1993) 201–248.
16. FENICHEL, N., Persistence and smoothness of invariant manifolds for flows, *Indiana Univ. Math. J.* **21** (1971) 193–225.
17. FENICHEL, N., Geometric singular perturbation theory for ordinary differential equations, *J. Diff. Eqs.* **31** (1979) 53–98.
18. GLENDINNING, P., Subsidiary bifurcations near bifocal homoclinic orbits, *Math. Proc. Cambridge Phil. Soc.* **105** (1989) 597–605.
19. HALLER, G. & WIGGINS, S., Orbits homoclinic to resonances: the Hamiltonian case, *Physica D* **66** (1993) 298–346.
20. HALLER, G., *Multi-pulse homoclinic phenomena in resonant Hamiltonian systems*, Ph.D. Thesis, California Institute of Technology (1993).
21. HALLER, G. & WIGGINS, S., Whiskered tori and chaos in resonant Hamiltonian normal forms, to appear in *Normal Forms and Homoclinic Chaos*, Fields Institute Publications (1994).
22. HALLER, G. & WIGGINS, S., Multi-pulse jumping orbits and homoclinic trees in a modal truncation of the damped-forced nonlinear Schrödinger equation, submitted to *Physica D* (1994).
23. HALLER, G. & WIGGINS, S., Geometry and chaos near resonant equilibria of 3DOF Hamiltonian systems: I. Theory, submitted to *Physica D* (1994).
24. HASTINGS, S. P., Single and multiple pulse waves for the Fitzhugh-Nagumo equations, *SIAM J. Appl. Math.* **42** (1982) 247–260.
25. HIRSCH, M. W., PUGH, C. C., & SHUB, M., *Invariant Manifolds*, Lect. Notes in Math., Vol. 583, Springer-Verlag, New York (1977).
26. HOLMES, P. & MARSDEN, J., Horseshoes in perturbations of Hamiltonian systems with two degrees of freedom, *Comm. Math. Phys.* **82** (1982) 523–544.
27. HOLMES, P., Chaotic motion in a weakly nonlinear model for surface waves, *J. Fluid Mech.* **162** (1986) 365–388.
28. JONES, C. K. R. T. & KOPELL, N., Tracking invariant manifolds with differential forms in singularly perturbed systems, *J. Diff. Eqs.* **108** (1994) 64–88.
29. JONES, C. K. R. T., KAPER, T. J., & KOPELL, N., Tracking invariant manifolds up to exponentially small errors, preprint (1993).

30. KAPER, T. J. & KOVAČIČ, G., Multi-bump orbits homoclinic to resonance bands, preprint (1993).
31. KISAKA, M., KOKUBU, H., & OKA, H., Bifurcations to N-homoclinic orbits and N-periodic orbits in vector fields, *J. Diff. Eqs.* **5** (1993) 305–357.
32. KOKUBU, H., Homoclinic and heteroclinic bifurcations of vector fields, *Jap. J. Appl. Math.* **5** (1988) 455–501.
33. KOVAČIČ, G. & WIGGINS, S., Orbits homoclinic to resonances, with an application to chaos in the damped and forced Sine-Gordon equation, *Physica D* **57** (1992) 185–225.
34. KOVAČIČ, G., Singular perturbation theory for homoclinic orbits in a class of near-integrable Hamiltonian systems, *J. Dyn. and Diff. Eqs.* **5** (1993) 559–597.
35. MCLAUGHLIN, D., OVERMAN, E. A. II., WIGGINS, S., & XIONG, C., Homoclinic orbits in a four dimensional model of a perturbed NLS equation: a geometric singular perturbation study, submitted to *Dynamics Reported* (1993).
36. MIELKE, A., HOLMES, P., & O'REILLY, O., Cascades of homoclinic orbits to, and chaos near, a Hamiltonian saddle-center, *J. Dyn. Diff. Eqs.* **4** (1992) 95–126.
37. MOSER, J., *Stable and Random Motions in Dynamical Systems*, Princeton University Press, Princeton (1973).
38. NAYFEH, A. H. & PAI, P. F., Non-linear, non-planar parametric responses of an inextensional beam, *Int. J. Non-Lin. Mech.* **24** (1989) 139–158.
39. ROM-KEDAR, V., Secondary homoclinic bifurcation theorems, to appear in *Chaos* (1994).
40. ŠILNIKOV, L. P., A contribution to the problem of the structure of an extended neighborhood of a rough equilibrium state of saddle-focus type, *Math. USSR Sbornik* **10** (1970) 91–102.
41. SMALE, S., Diffeomorphisms with many periodic points, in *Differential and Combinatorial Topology*, S. S. CAIRNS (ed.), Princeton Univ. Press, Princeton (1963) 63–80.
42. TIEN, W. M. & NAMACHCHIVAYA, N. S., Nonlinear dynamics of a shallow arch under periodic excitation, part II: 1:1 internal resonance, submitted to the *Int. J. Non-Lin. Mech.* (1992).
43. TIN, S. K., *On the dynamics of tangent spaces near a normally hyperbolic invariant manifold*, Ph.D. Thesis, Brown University (1993).
44. TRESHCHEV, D. V., The mechanism of destruction of resonance tori of Hamiltonian systems, *Math. USSR Sbornik* **68** (1991) 181–203.
45. WIGGINS, S., *Global Bifurcations and Chaos – Analytical Methods*, Springer-Verlag, New York (1988).
46. WIGGINS, S., *Normally Hyperbolic Invariant Manifolds in Dynamical Systems*, Springer-Verlag, New York (1994).
47. YANG, X. L. & SETHNA, P. R., Non-linear phenomena in forced vibrations of a nearly square plate: antisymmetric case, *J. Sound Vib.* **155** (1992) 413–441.

Division of Applied Mathematics
Brown University
Providence, Rhode Island 02912

and

Department of Applied Mechanics
California Institute of Technology
Pasadena, California 91125

(Accepted August 24, 1994)